Title
In vivo whole cell measurements of sound-evoked synaptic excitation and inhibition in auditory cortex neurons

Author
Tan, Andrew Yong-Yi

Publication Date
2006

Peer reviewed|Thesis/dissertation

In vivo whole cell measurements of sound-evoked synaptic excitation and inhibition in auditory cortex neurons

by

Andrew Yong-Yi Tan

DISSERTATION

Submitted in partial satisfaction of the requirements for the degree of

DOCTOR OF PHILOSOPHY

in

Neuroscience

in the

GRADUATE DIVISION

of the

UNIVERSITY OF CALIFORNIA, SAN FRANCISCO

Date University Librarian

Degree Conferred:.....

Acknowledgments

Remember your creator in the days of your youth, before the days of trouble come, and the years draw near when you will say, "I have no pleasure in them"; before the sun and the light and the moon and the stars are darkened and the clouds return with the rain; in the day when the guards of the house tremble, and the strong men are bent, and the women who grind cease working because they are few, and those who look through the windows see dimly.

Ecclesiastes 12:1-3

Abstract

In vivo whole cell measurements of sound-evoked synaptic excitation and inhibition in auditory cortex neurons

Andrew Yong-Yi Tan

In vivo whole cell recordings from auditory cortex neurons were used to measure the synaptic excitation and inhibition evoked by tones, frequency-modulated (FM) sweeps and noise bursts. Tones evoked synaptic excitation, followed by synaptic inhibition. Synaptic excitation and inhibition could account for the gross time course of the typical membrane potential response. Synaptic excitation and inhibition had the same frequency tuning. As tone intensity increased, the amplitudes of synaptic excitation and inhibition increased, and the latency of synaptic excitation decreasesd.

FM sweeps evoked synaptic excitation and inhibition that were direction selective. Synaptic excitation and inhibition had the same preferred direction. Synaptic inhibition enhanced direction selectivity by suppressing the synaptic excitation of the non-preferred direction more than that of the preferred. The spectral asymmetry of tonal receptive fields covaried with direction selectivity, and suggested a mechanism for direction selectivity.

Intensity-tuned neurons were probed with noise bursts of various intensities. In some intensity neurons, intensity-tuning was created solely through disproportionally large synaptic inhibition at high intensities, without any intensity-tuned synaptic excitation. Since synaptic inhibition is essentially cortical in origin, such neurons provide examples of auditory feature-selectivity arising de novo at the cortex.

Table of Contents

Acknowledgments....iii

Abstract....iv

Table of Contents....v

List of Tables....vi

List of Figures....vii

Chapter 1: Introduction....1

Chapter 2: Topography and synaptic shaping of direction selectivity in primary auditory cortex....18

Chapter 3: Tone-evoked excitatory and inhibitory synaptic conductances of primary auditory cortex neurons....40

Chapter 4: Unbalanced synaptic inhibition can create intensity-tuned auditory cortex neurons....86

Chapter 5: Conclusion....115

List of Tables

Table 3.1 84

List of Figures

Figure 2.1.....30

Figure 2.2.....32

Figure 2.3.....34

Figure 2.4.....36

Figure 2.5.....38

Figure 3.1.....70

Figure 3.2.....72

Figure 3.3.....74

Figure 3.4.....76

Figure 3.5.....78

Figure 3.6.....80

Figure 3.7.....82

Figure 4.1.....105

Figure 4.2.....107

Figure 4.3.....109

Figure 4.4.....111

Figure 4.5.....113

Chapter 1

Introduction

The responses of neurons of the primary auditory cortex to simple sounds such as tones and frequency sweeps have been well studied. However, we do not have a good understanding of how these responses differ from those in the thalamus or other subcortical stations. Nor can we predict the responses of primary auditory cortex neurons to complex sounds. This work presents intracellular measurements of the total synaptic excitation and total synaptic inhibition evoked in auditory cortex neurons by pure tones (Chapters 2,3), frequency sweeps (Chapter 2), and noise bursts (Chapter 4); and reveals the roles of excitation and inhibition in frequency tuning and adaptation (Chapters 2,3), frequency sweep direction selectivity (Chapter 2), and intensity tuning (Chapter 4). These experiments address the auditory thalamocortical transformation, and will help the construction of a model for auditory cortex receptive fields that is based on synaptic organization.

Neurons of the primary auditory cortex respond well to tones. In response to a tone of appropriate frequency and intensity, a primary auditory cortex neuron typically emits one or a few spikes that mark the tone onset. There is rapid adaptation, with the duration and end of the tone usually not indicated by spiking. Increasing tone intensity at any particular frequency generally causes an increase in spike rate and a decrease in spike latency. At the lowest tone intensity at which spiking can be evoked, only tone

frequencies within a very narrow range evoke spiking; the mean of this range is the neuron's characteristic frequency. As tone intensity increases, the range of frequencies which evokes spiking increases. The primary auditory cortex is tonotopic: in the rat, characteristic frequency increases caudorostrally (Brugge et al 1969; Merzenich et al 1975; Sally and Kelly 1988; Heil 1997a,b).

Frequency tuning and tonotopy begin in the cochlea (von Békésy 1961, Rhode 1971, Robles et al 1976), and are found in the cochlear nucleus (Rose et al 1959), the inferior colliculus (Rose et al 1963, Hind et al 1963), and the medial geniculate body (Aitkin and Webster 1971, 1972, Imig and Morel 1985). Responses which mark the tone onset more strongly than the rest of the tone are also present in the cochlear nucleus (Godfrey et al 1975a,b; Rhode and Smith 1986), the inferior colliculus (Rose et al 1963, Hind et al 1963, Bock et al 1972; Ehret and Moffat 1985), and the medial geniculate body (Rouiller et al 1979). Cortical responses to tones are thus not qualitatively different from those found subcortically.

Frequency sweeps also evoke spikes from primary auditory cortex neurons, usually only if they sweep through the neuron's spike tonal receptive field. Some neurons show selectivity for the direction of frequency modulation (Heil 1992a,b; Mendelson et al 1993; Shamma 1993; Gaese and Ostwald 1995, Nelken and Versnel 2000). The spike tonal receptive field alone is insufficient to explain direction selectivity: appropriate inhibition is also necessary. Such inhibition may suppress spontaneous spiking. Spontaneous spiking in the auditory cortex is, however, usually too low to be much further suppressed. In order to observe the inhibition produced by a tone, a second tone which by itself evokes spiking, is played after the first tone. The extent to which the

spike response to the second tone is reduced when it is played after the first, compared to when it is played by itself, is a measure of the inhibition. By such methods, late, long lasting inhibition has been demonstrated (Calford and Semple 1995; Brosch and Schreiner 1997). The inhibition has been shown to have the right spectral asymmetry and temporal relationship relative to inhibition to produce direction selectivity (Suga 1965, Shamma 1993). Such inhibition need not arise from monosynaptic input onto the cortical neuron, but could arise from synaptic or intrinsic inhibition at any stage up to and including the cortex.

Indeed, selectivity for the direction of frequency modulation has also been demonstrated at the cochlear nucleus (Britt and Starr 1976) and the inferior colliculus (Clopton and Winfield 1974; Poon and Yu 2000). In the inferior colliculus, the inhibition revealed by tones also appears to contribute to direction selectivity (Fuzessery 1994; Fuzessery and Hall 1996). Like cortical responses to tones, direction selectivity in the cortex may therefore arise subcortically.

Another type of feature selectivity that arises centrally is intensity-tuning. Intensity-tuned neurons have nonmonotonic rate-intensity functions. Their spike rate first increases with increasing sound intensity, but then decreases as sound intensity is further increased (Phillips et al 1985; Phillips and Kelly 1989). Intensity-tuning arises centrally, as all neurons of the auditory nerve increase their spike rate with increasing sound intensity (Kiang et al 1965). However, there are intensity-tuned neurons at subcortical auditory stations (Rhode and Smith 1986; Ding and Voigt 1997; Ding et al 1999; Davis and Young 2000; Pollak et al 1978; Ryan and Miller 1978, Palombi and

Caspary 1996a, 1996b; Sivaramakrishnan et al 2004). Intensity-tuning in the cortex may therefore also arise subcortically.

Is it possible that there is no thalamocortical transformation in the auditory system? The bulk of the thalamic input to the auditory cortex is received by cortical layers 3 and 4. These layers send information to the superficial layers, which in turn send information to the deep layers (Matsubara and Phillips 1988; Ojima et al 1991; Wallace et al 1991). Because the cortex receives only excitatory inputs from the thalamus, synaptic inhibition onto a cortical neuron reflects cortical processing (Mitani and Shimokouchi 1985; Mitani et al 1985; Winer and Larue 1988; Winer 1992). The anatomical type and number of inhibitory interneurons are different in each cortical layer. Hendry and Jones (1991) classified inhibitory interneurons according to the calcium-binding proteins they express. They found that the majority of inhibitory neurons in layer 4 expressed parvalbumin; such neurons were rare in layers 2 and 5, and absent in layer 1; Calbindin expressing inhibitory neurons were, on the other hand more common in layers 2 and 6. Prieto et al (1994a, b) distinguished 10 types of inhibitory interneurons according to their morphology, with each layer having a different proportion of each type; most interestingly, they found that there were significantly more inhibitory interneurons in layers 3 and 4 in the central part of the cat primary auditory cortex, along the dorsoventral axis, where physiological studies had shown neurons to be most sharply tuned (Schreiner and Mendelson 1990). In slice, the spontaneous and electrically-evoked inhibitory postsynaptic potentials of regular spiking pyramidal neurons of Layer 5 differ from those of intrinsically bursting pyramidal neurons in the same layer. The well-organized anatomical structure of the primary auditory cortex suggests a systematic

transformation of thalamic input with successive layers via a mechanism in which synaptic inhibition has an important role.

Still, the only known overt difference between the cortex and lower central subcortical stations is in their ability to phase lock to amplitude modulated stimuli. Most neurons in the cortex are able to phase lock up to 20 Hz (Creutzfeldt et al 1980; Schreiner and Urbas 1986, 1988); in contrast, most neurons in the inferior colliculus phase-lock up to 100 Hz (Rees and Møller 1983, 1987; Rees and Palmer 1989). Phase-locking in the thalamus is intermediate between that of the inferior colliculus and the cortex (Creutzfeldt et al 1980, Wehr and Zador 2005). However, this does not mean that the cortical response to all high modulation frequencies is temporally imprecise. The ability of the cortex to maintain precisely timed spiking to transient aural features dominated by high modulation frequencies indicates that there is more to the thalamocortical transformation (Heil 1997a, b; Elhilali et al 2004).

It is possible that the right stimuli for probing the transformation have not been used, but it may also be that the additional processing carried out by the cortex is subtle. The primary auditory cortex processes sound at a time scale at which onsets and timbre interact. The complexity of these perceptual qualities is underlined by the fact that unlike pitch, melody and rhythm, they can only be very approximately notated in musical scores, even though they are musically important (Bregman 1990). In speech, these qualities are notated, and they correspond, for example, to the difference between a 'ba' and a 'pa'. However, models with thousands of free parameters are needed to classify the corresponding sounds in a speaker-independent way in continuous speech (Diehl et al 2004, Kuhl 2004). Hence, we should not expect the thalamocortical transformation to be

obvious. A closer examination of the cortical responses to simple sounds such as tones and frequency sweeps may well reveal aspects of the thalamocortical transformation; this will be borne out in Chapters 2 to 4.

The auditory thalamocortical transformation has been probed by paired extracellular recordings in the thalamus and the cortex. In this method, monosynaptic connectivity between two neurons is assayed using the cross-correlation function of their spike trains. If a thalamic neuron provides input to a cortical neuron, then the cross-correlation function should show that the cortical neuron tends to spike within a few milliseconds after the thalamic neuron spikes. The caveat to this method is that monosynaptic connectivity between the thalamic and cortical neuron is not the only way by which such cross-correlation functions can be produced; it could also be produced by common synaptic input to both neurons. Common monosynaptic input to a thalamic neuron and a cortical neuron is unlikely, because the locally projecting interneurons of the thalamus are not thought to also project to the cortex (Morest 1975). However, common input that is monosynaptic to a thalamic neuron and disynaptic to a cortical neuron cannot be ruled out; an inferior colliculus neuron that diverges onto two thalamic neurons could produce such common input. Although a disynaptic cross-correlation involving an intracortical synapse usually has a broad peak very different from the sharp peak of a monosynaptic cross-correlation, this is not true of all disynaptic cross-correlations; a disynaptic cross-correlation from the retina to the cortex, for example, often has a sharp peak (Alonso and Martinez 1998; Lee at al 1977; Kara and Reid 2003). Furthermore, some locally projecting thalamic interneurons may also project to the cortex (Winer 1984). Paired extracellular recordings in the thalamus and the cortex have shown

that the characteristic frequency of a thalamic neuron is very similar to that of the cortical neuron to which it is connected. The thalamocortical transformation, while preserving characteristic frequency, substantially modifies other properties such as inhibitory subregions, and spectral and temporal modulation preferences (Creutzfeldt el at 1980; Miller et al 2001).

Because the thalamic input onto cortical neurons is entirely excitatory, examining the role of synaptic inhibition in forming cortical responses has provided another way of determining the cortical contribution to auditory processing. Iontophoretic application of a pharmacological blocker of synaptic inhibition usually results in broader frequency tuning and higher spike rates (Foeller et al 2001, Wang et al 2002). This, however, may say nothing about sound-evoked synaptic inhibition, since it can arise from the removal of tonic inhibition. Such studies have also indicated that the removing synaptic inhibition can change a neuron's rate-versus-intensity curve from monotonic into nonmonotonic (Wang et al 2002). These effects are difficult to interpret as they involved the removing synaptic inhibition from multiple neurons in a complex circuit, rather than from just one. Since the removal of synaptic inhibition also increases spike rate, intrinsic voltage-sensitive channels may be activated, resulting in nonmonotonic rate-intensity curves (Sivaramakrishnan 2004).

Intracellular recordings provide a way of examining the synaptic inhibition received by single neurons. Intracellular studies in which sound-evoked hyperpolarizations were interpreted as synaptic inhibition have suggested that tones evoke synaptic excitation followed by synaptic inhibition, with inhibition and excitation co-varying across different tone frequencies and intensities (De Ribaupierre et al 1972;

Volkov and Galazyuk 1991, 1992; Ojima and Murakami 2002). However, the tonal receptive fields obtained by previous studies have been highly incomplete. The full V-shape of the tonal receptive fields, seen in the intracellular recordings presented in Chapters 2 and 3, had long been observed in extracellular recordings, but not in intracellular recordings. The voltage-clamp decomposition of sound-evoked synaptic input into excitation and inhibition presented in Chapters 2 to 4 had also not been previously performed. By providing insight into the role of synaptic inhibition in forming cortical responses, these intracellular recordings further our understanding of auditory cortical processing.

The intracellular recordings presented here will also help the formulation of a receptive field model based on synaptic mechanism. Receptive field studies have usually used models which do not take mechanism into account; such models have, however, had limited success thus far. The most general model used in receptive field studies has been the Volterra series, an infinite series which can describe any system with a finite memory. If the terms of the Volterra series can be determined from experimental data, knowledge of the underlying mechanism is not needed. The Wiener series is a reordering of the terms in the Volterra series such that each term can be independently obtained if white noise is used as the stimulus (Marmeralis and Marmeralis 1978).

Unfortunately, most neurons in the auditory cortex respond so poorly to white noise that it is not possible to acquire enough data even to estimate the first order Wiener term. For this reason, several non-white noise stimuli that do drive auditory cortex neurons have been developed. In the spirit of Wiener the long-time averages of these non-white noise stimuli do have white spectra, although their short-time averages are

non-white (Kowalski et al 1996a, 1996b; deCharms et al 1998; Escabi and Schreiner 2002). Due to the non-white nature of the stimuli, the Wiener series cannot be used, and studies using non-white noise stimuli have usually used a completely linear model, instead of the Wiener series. Unlike the Volterra or Wiener series which is guaranteed to be the correct model for any system with a finite memory, the linear model is guaranteed to fail with almost any system. It is used because it is easy to fit data to, and one might be lucky and have it work. It is important to note that the best-fit linear filter obtained with an arbitrary stimulus is not the linear filter of the Volterra series or the Wiener series. In fact, the best-fit linear filter, or, for that matter, any model that is not completely correct, will generally be stimulus dependent (Theunissen et al 2000; Escabi and Schreiner 2002). It is possible to interpret this stimulus dependence as adaptation (Blake and Merzenich 2002; David et al 2004).

The linear model has proved useful. It can predict the responses of auditory cortex neurons to certain classes of stimuli with high accuracy (Kowalski et al 1996b; deCharms et al 1998). It has been used to examine receptive field differences between thalamic and cortical neurons (Miller et al 2001), and between neurons in different regions of the auditory cortex (Linden et al 2003). It has also been used to examine how auditory cortex receptive fields change depending on the attentional state of the animal (Fritz et al 2003). Furthermore, it can be easily used in conjunction with non-Gaussian stimuli such as 'natural' stimuli, which can be extremely effective at driving neurons (Theunissen et al 1998; Machens et al 2004). However, it is, ultimately, a highly incomplete model. Machens et al (2004) found that if stimuli are not restricted to a well-defined class, then the linear model is capable of predicting only 11% of the response

power. They also concluded that it is not possible to correct the linear model with any static nonlinearity, and that a 'dynamic' nonlinearity was needed. Another receptive field model is clearly needed, perhaps one takes into account the mechanisms underlying receptive fields.

This work describes synaptic aspects of these mechanisms. The following chapters present intracellular measurements of the total synaptic excitation and total synaptic inhibition evoked when the receptive fields of auditory cortex neurons are probed by simple sounds such as pure tones (Chapters 2,3), frequency sweeps (Chapter 2), and noise bursts (Chapter 4). Chapters 2 and 3 have been published (Zhang et al 2003, Tan et al 2004). Chapter 4 has been published in abstract form (Tan et al 2005).

References

Aitkin LM and Webster WR. Tonotopic organization in the medial geniculate body of the cat. Brain Res 26:402-405, 1971.

Aitkin LM and Webster WR. Medial geniculate body of the cat: organization and responses to tonal stimuli of neurons in ventral division. J Neurophysiol 35:365-380, 1972.

Alonso JM and Martinez LM. Functional connectivity between simple cells and complex cells in cat striate cortex. Nat Neurosci 1:395-403, 1998.

Blake DT, Merzenich MM. Changes of AI receptive fields with sound density. J Neurophysiol 88:3409-3420, 2002.

Bock GR, Webster WR, and Aitkin LM. Discharge patterns of single units in inferior colliculus of the alert cat. J Neurophysiol 35:265-277, 1972.

Bregman AS. Auditory scene analysis: the perceptual organization of sound. Cambridge, MA: MIT Press; 1990.

Britt R and Starr A. Synaptic events and discharge patterns of cochlear nucleus cells. II. Frequency-modulated tones. J Neurophysiol 39:179-194, 1976.

Brosch M and Schreiner CE. Time course of forward masking tuning curves in cat primary auditory cortex. J Neurophysiol 77:923-943, 1997.

Brugge JF, Dubrovsky NA, Aitkin LM, and Anderson DJ. Sensitivity of single neurons in auditory cortex of cat to binaural tonal stimulation; effects of varying interaural time and intensity. J Neurophysiol 32:1005-1024, 1969.

Calford MB, Semple MN. Monaural inhibition in cat auditory cortex. J Neurophysiol 73:1876-1891, 1995.

Clopton BM and Winfield JA. Unit responses in the inferior colliculus of rat to temporal auditory patterns of tone sweeps and noise bursts. Exp Neurol 42:532-540, 1974.

Creutzfeldt O, Hellweg FC, and Schreiner C. Thalamocortical transformation of responses to complex auditory stimuli. Exp Brain Res 39:87-104, 1980.

David SV, Vinje WE, Gallant JL. Natural stimulus statistics alter the receptive field structure of V1 neurons. J Neurosci 24:6991-7006, 2004.

Davis KA and Young ED. Pharmacological evidence of inhibitory and disinhibitory neuronal circuits in dorsal cochlear nucleus. J Neurophysiol 83:926-940, 2000.

De Ribaupierre F, Goldstein MH Jr, and Yeni-Komshian G. Intracellular study of the cat's primary auditory cortex. Brain Res 48: 185-204, 1972.

deCharms RC, Blake DT, and Merzenich MM. Optimizing sound features for cortical neurons. Science 280:1439-1443, 1998.

Diehl RL, Lotto AJ, Holt LL. Speech perception. Annu Rev Psychol 55:149-179, 2004.

Ding J and Voigt HF. Intracellular response properties of units in the dorsal cochlear nucleus of unanesthetized decerebrate gerbil. J Neurophysiol 77:2549-2572, 1997.

Ding J, Benson TE, and Voigt HF. Acoustic and current-pulse responses of identified neurons in the dorsal cochlear nucleus of unanesthetized, decerebrate gerbils. J Neurophysiol 82:3434-3457, 1999.

Ehret G and Moffat AJM. Inferior colliculus of the house mouse. II. Single unit responses to tones, noise and tone-noise combinations as a function of sound intensity. J Comp Physiol A 156:619-635, 1985.

Elhilali M, Fritz JB, Klein DJ, Simon JZ, Shamma SA. Dynamics of precise spike timing in primary auditory cortex. J Neurosci 24:1159-1172, 2004.

Escabi MA and Schreiner CE. Nonlinear spectrotemporal sound analysis by neurons in the auditory midbrain. J Neurosci 22:4114-4131, 2002.

Foeller E, Vater M, and Kossl M. Laminar analysis of inhibition in the gerbil primary auditory cortex. J Assoc Res Otolaryngol 2:279-296, 2001.

Fritz J, Shamma S, Elhilali M, and Klein D. Rapid task-related plasticity of spectrotemporal receptive fields in primary auditory cortex. Nat Neurosci 6:1216-1223, 2003.

Fuzessery ZM. Response selectivity for multiple dimensions of frequency sweeps in the pallid bat inferior colliculus. J Neurophysiol 72:1061-1079, 1994.

Fuzessery ZM and Hall JC. Role of GABA in shaping frequency tuning and creating FM sweep selectivity in the inferior colliculus. J Neurophysiol 76:1059-1073, 1996.

Gaese BH, Ostwald J. Temporal coding of amplitude and frequency modulation in the rat auditory cortex. Eur J Neurosci 7:438-450, 1995.

Godfrey DA, Kiang NY, and Norris BE. Single unit activity in the posteroventral cochlear nucleus of the cat. J Comp Neurol 162:247-268, 1975a.

Godfrey DA, Kiang NY, and Norris BE. Single unit activity in the dorsal cochlear nucleus of the cat. J Comp Neurol 162:269-284, 1975b.

Heil P, Rajan R, and Irvine DR. Sensitivity of neurons in cat primary auditory cortex to tones and frequency-modulated stimuli. I: Effects of variation of stimulus parameters. Hear Res 63:108-134, 1992a.

Heil P, Rajan R, and Irvine DR. Sensitivity of neurons in cat primary auditory cortex to tones and frequency-modulated stimuli. II: Organization of response properties along the 'isofrequency' dimension. Hear Res 63:135-156, 1992b.

Heil P. Auditory cortical onset responses revisited. I. First-spike timing. J Neurophysiol 77:2616-2641, 1997a.

Heil P. Auditory cortical onset responses revisited. II. Response strength. J Neurophysiol 77:2642-2660, 1997b.

Hendry SH, Jones EG. GABA neuronal subpopulations in cat primary auditory cortex: co-localization with calcium binding proteins. Brain Res 543:45-55, 1991.

Hind JE, Goldberg JM, Greenwood DD, and Rose JE. Some discharge characteristics of single neurons in the inferior colliculus of the cat. II. Timing of the discharges and observations on binaural stimulation. J Neurophysiol 26:321-341, 1963.

Imig TJ and Morel A. Tonotopic organization in ventral nucleus of medial geniculate body in the cat. J Neurophysiol 53:309-340, 1985.

Kara P and Reid RC. Efficacy of retinal spikes in driving cortical responses. J Neurosci 23:8547-8557, 2003.

Kiang NYS, Watanabe T, Thomas EC, and Clark LF. Discharge patterns of single fibers in the cat's auditory nerve. Cambridge, MA: MIT Press; 1965.

Kowalski N, Depireux DA, and Shamma SA. Analysis of dynamic spectra in ferret primary auditory cortex. I. Characteristics of single-unit responses to moving ripple spectra. J Neurophysiol 76:3503-3523, 1996a.

Kowalski N, Depireux DA, and Shamma SA. Analysis of dynamic spectra in ferret primary auditory cortex. II. Prediction of unit responses to arbitrary dynamic spectra. J Neurophysiol 76:3524-3534, 1996b.

Kuhl PK. Early language acquisition: cracking the speech code. Nat Rev Neurosci 5:831-843, 2004.

Lee BB, Cleland BG, and Creutzfeldt OD. The retinal input to cells in area 17 of the cat's cortex. Exp Brain Res 30:527-538, 1977.

Linden JF, Liu RC, Sahani M, Schreiner CE, Merzenich MM. Spectrotemporal structure of receptive fields in areas AI and AAF of mouse auditory cortex. J Neurophysiol 90:2660-2675, 2003.

Machens CK, Wehr MS, and Zador AM. Linearity of cortical receptive fields measured with natural sounds. J Neurosci 24:1089-1100, 2004.

Marmeralis P and Marmeralis V. Analysis of physiological systems: the white noise approach. New York: Plenum; 1978.

Matsubara JA and Phillips DP. Intracortical connections and their physiological correlates in the primary auditory cortex (AI) of the cat. J Comp Neurol 268:38-48, 1988.

Mendelson JR, Schreiner CE, Sutter ML, and Grasse KL. Functional topography of cat primary auditory cortex: responses to frequency-modulated sweeps. Exp Brain Res 94:65-87, 1993.

Merzenich MM, Knight PL, Roth GL. Representation of cochlea within primary auditory cortex in the cat. J Neurophysiol 38:231-249, 1975.

Miller LM, Escabi MA, Read HL, Schreiner CE. Functional convergence of response properties in the auditory thalamocortical system. Neuron 32:151-160, 2001.

Mitani A and Shimokouchi M. Neuronal connections in the primary auditory cortex: an electrophysiological study in the cat. J Comp Neurol 235:417-429, 1985.

Mitani A, Shimokouchi M, Itoh K, Nomura S, Kudo M, and Mizuno N. Morphology and laminar organization of electrophysiologically identified neurons in the primary auditory cortex in the cat. J Comp Neurol 235:430-447, 1985.

Morest DK. Synaptic relationships of Golgi type II cells in the medial geniculate body of the cat. J Comp Neurol 162:157-193, 1975.

Nelken I and Versnel H. Responses to linear and logarithmic frequency-modulated sweeps in ferret primary auditory cortex. Eur J Neurosci 12:549-562.

Ojima H, Honda CN, and Jones EG. Patterns of axon collateralization of identified supragranular pyramidal neurons in the cat auditory cortex. Cereb Cortex 1:80-94, 1991.

Palombi PS and Caspary DM. Physiology of the young adult Fischer 344 rat inferior colliculus: responses to contralateral monaural stimuli. Hear Res 100:41-58, 1996a.

Palombi PS, Caspary DM. Physiology of the aged Fischer 344 rat inferior colliculus: responses to contralateral monaural stimuli. J Neurophysiol 76:3114-3125, 1996b.

Phillips DP and Kelly JB. Coding of tone-pulse amplitude by single neurons in auditory cortex of albino rats (Rattus norvegicus). Hear Res 37:269-279, 1989.

Phillips DP, Orman SS, Musicant AD, and Wilson GF. Neurons in the cat's primary auditory cortex distinguished by their responses to tones and wide-spectrum noise. Hear Res 18:73-86. 1985.

Pollak GK, Marsh DS, Bodenhamer R, and Souther A. A single-unit analysis of inferior colliculus in unanesthetized bats: response patterns and spike-count functions generated by constant-frequency and frequency-modulated sounds. J Neurophysiol 41:677-691, 1978.

Poon PW, Yu PP. Spectro-temporal receptive fields of midbrain auditory neurons in the rat obtained with frequency modulated stimulation. Neurosci Lett 289:9-12, 2000.

Rees A and Møller AR. Responses of neurons in the inferior colliculus of the rat to AM and FM tones. Hear Res 10: 301–330, 1983.

Prieto JJ, Peterson BA, and Winer JA. Morphology and spatial distribution of GABAergic neurons in cat primary auditory cortex (AI). J Comp Neurol 344:349-382, 1994a.

Prieto JJ, Peterson BA, and Winer JA. Laminar distribution and neuronal targets of GABAergic axon terminals in cat primary auditory cortex (AI). J Comp Neurol 344:383-402, 1994b.

Rees A and Møller AR. Stimulus properties influencing the responses of inferior colliculus neurons to amplitude-modulated sounds. Hear Res 27: 129–143, 1987.

Rees A and Palmer AR. Neuronal responses to amplitude-modulated and pure-tone stimuli in the guinea pig inferior colliculus, and their modification by broadband noise. J Acoust Soc Am 85: 1978–1994, 1989.

Rhode WS. Observations of the vibration of the basilar membrane in squirrel monkeys using the Mössbauer technique. J Acoust Soc Am 49: 1218-1231, 1971.

Rhode WS and Smith PH. Physiological studies on neurons in the dorsal cochlear nucleus of cat. J Neurophysiol 56:287-307, 1986.

Robles L, Rhode WS, and Geisler CD. Transient response of the basilar membrane measured in squirrel monkey using the Mössbauer effect. J Acoust Soc Am 59: 926-939, 1976

Rose JE, Galambos R, and Hughes JR. Microelectrode studies of the cochlear nuclei of the cat. Bull Johns Hopkins Hosp 104:211-251, 1959.

Rose JE, Greenwood DO, Goldberg JM, and Hind JE. Some discharge characteristics of single neurons in the inferior colliculus of the cat. I. Tonotopic-organization, relation of spike-counts to tone intensity and firing patterns of single elements. J. Neurophysiol 26:294-320, 1963.

Rouiller EM, de Ribaupierre Y, and de Ribaupierre F. Phase-locked responses to low frequency tones in the medial geniculate body. Hear Res 1:213-226, 1979.

Ryan A and Miller J. Single unit responses in the inferior colliculus of the awake and performing rhesus monkey. Exp Brain Res 32:389-407, 1978.

Sally SL, Kelly JB. Organization of auditory cortex in the albino rat: sound frequency. J Neurophysiol 59:1627-1638, 1988.

Schreiner CE and Mendelson JR. Functional topography of cat primary auditory cortex: distribution of integrated excitation. J Neurophysiol 64:1442-1459, 1990.

Schreiner CE and Urbas JV. Representation of amplitude modulation in the auditory cortex of the cat. I. The anterior auditory field (AAF). Hear Res 21: 227–241, 1986.

Schreiner CE and Urbas JV. Representation of amplitude modulation in the auditory cortex of the cat. II. Comparison between cortical fields. Hear Res 32: 49–64, 1988.

Shamma SA, Fleshman JW, Wiser PR, and Versnel H. Organization of response areas in ferret primary auditory cortex. J Neurophysiol 69:367-383, 1993.

Sharpee T, Rust NC, and Bialek W. Analyzing neural responses to natural signals: maximally informative dimensions. Neural Comput 16:223-250, 2004.

Sivaramakrishnan S, Sterbing-D'Angelo SJ, Filipovic B, D'Angelo WR, Oliver DL, and Kuwada S. GABA(A) synapses shape neuronal responses to sound intensity in the inferior colliculus. J Neurosci 24:5031-5043, 2004.

Suga N. Functional properties of auditory neurones in the cortex of echo-locating bats. J Physiol 181:671-700, 1965.

Tan AY, Atencio CA, Polley DB, Merzenich MM, and Schreiner CE. Effects of sound intensity on synaptic excitation and inhibition in the auditory cortex. Program No. 615.13. 2005 Abstract Viewer/Itinerary Planner. Washington, DC: Society for Neuroscience, 2005. Online.

Tan AY, Zhang LI, Merzenich MM, and Schreiner CE. Tone-evoked excitatory and inhibitory synaptic conductances of primary auditory cortex neurons. J Neurophysiol 92:630-643, 2004

Theunissen FE, Sen K, Doupe AJ. Spectral-temporal receptive fields of nonlinear auditory neurons obtained using natural sounds. J Neurosci 20:2315-2331, 2000.

Volkov IO and Galazjuk AV. Formation of spike response to sound tones in cat auditory cortex neurons: interaction of excitatory and inhibitory effects. Neuroscience 43: 307-321, 1991.

Volkov IO and Galazyuk AV. Peculiarities of inhibition in cat auditory cortex neurons evoked by tonal stimuli of various durations. Exp Brain Res 91: 115-120, 1992.

Von Békésy G. Experiments in Hearing. New York, NY: McGraw-Hill, 1960.

Wang J, McFadden SL, Caspary D, and Salvi R. Gamma-aminobutyric acid circuits shape response properties of auditory cortex neurons. Brain Res 944:219-231, 2002.

Wallace MN, Kitzes LM, and Jones EG. Intrinsic inter- and intralaminar connections and their relationship to the tonotopic map in cat primary auditory cortex. Exp Brain Res 86:527-544, 1991.

Wehr M, Zador AM. Synaptic mechanisms of forward suppression in rat auditory cortex. Neuron 47:437-445, 2005.

Winer JA. Identification and structure of neurons in the medial geniculate body projecting to primary auditory cortex (AI) in the cat. Neuroscience 13:395-413, 1984.

Winer JA. The functional architecture of the medial geniculate body and the primary auditory cortex. In: The Mammalian Auditory Pathway, edited by Webster DB, Popper AN, and Fay RR. New York: Springer-Verlag, 1992.

Winer JA and Larue DT. Anatomy of glutamic acid decarboxylase immunoreactive neurons and axons in the rat medial geniculate body. J Comp Neurol 278:47-68, 1988.

Zhang LI, Tan AY, Schreiner CE, and Merzenich MM. Topography and synaptic shaping of direction selectivity in primary auditory cortex. Nature 424:201-205, 2003.

Chapter 2

Topography and synaptic shaping of direction selectivity in primary auditory cortex

The direction of frequency-modulated (FM) sweeps is an important temporal cue in animal and human communication. FM direction selective neurons are found in the primary auditory cortex (AI)[1,2], but their topography and the mechanisms underlying their selectivity remain largely unknown. We report that in the rat AI, direction selectivity was topographically ordered in parallel with characteristic frequency (CF): low CF neurons preferred upward sweeps, and high CF neurons preferred downward sweeps. The asymmetry of 'inhibitory sidebands' flanking the tonal receptive field (TRF) of the spike response also covaried with CF. *In vivo* whole-cell recordings showed that the direction selectivity already present in the synaptic inputs was enhanced by cortical synaptic inhibition, which suppressed the synaptic excitation of the non-preferred direction more than that of the preferred. The excitatory and inhibitory synaptic TRFs had identical spectral tuning, but with inhibition delayed relative to excitation. The spectral asymmetry of the synaptic TRFs covaried with CF, as had direction selectivity and sideband asymmetry, and thus suggested a synaptic mechanism for the shaping of FM direction selectivity and its topographic ordering.

Extracellular multiunit spike responses to sweeps of various speeds and intensities were recorded in the mid layers of the adult rat AI. Responses from a representative low CF site are shown in Fig. 1. Sweeps of different speeds evoked distinct responses (Fig. 1a). The onset and duration of each response mostly reflected the timing of the sweep's intersection with the TRF of the spike response (Fig. 1b). A direction selectivity index (DSI) was calculated for responses to pairs of up- and down-sweeps of the same speed; a positive DSI indicates up-sweep selectivity (see Methods). The strongest direction selectivity was obtained for 70 oct/s sweeps, regardless of sweep intensity (Fig.1c)[3]. Accordingly, we chose sweeps of speed 70 oct/s and intensity 60 dB to further characterize direction selectivity in AI.

The primary auditory cortex was mapped. The CFs of neurons increased smoothly along the posterior-anterior axis, with low CFs at the posterior end (Fig. 2a)[4,5]. Strikingly, FM direction selectivity was topographically ordered in parallel with CF. DSI changed continuously and monotonically along the CF axis (Fig. 2b, c). Low CF sites (< 8 kHz) responded more strongly to up-sweeps, while high CF sites (> 14 kHz) responded more strongly to down-sweeps.

Any mechanism that generates FM direction selectivity must possess both spectral and temporal asymmetries. In bats and ferrets, it has been shown that spectrally asymmetric inhibition covaries with direction selectivity[6-8]. We examined if this was also the case in the rat AI by determining how the frequency and intensity of one tone affected its ability to suppress responses to a subsequent second tone[6-10]. Fig. 3a shows the inhibitory areas (outlined by blue) obtained for a low CF site and a high CF site. For the low CF site, the inhibitory region covered the whole TRF (in red) and extended beyond

the high frequency boundary of the TRF; for the high CF site, the inhibitory region had a greater extension on the low frequency side of the TRF. The suppressive regions flanking the TRF are known as 'inhibitory sidebands'. Since low CF neurons prefer up-sweeps and high CF neurons down-sweeps, these two particular neurons are consonant with the notion that inhibitory sideband asymmetry is correlated with direction selectivity. To assess the CF-dependence of inhibitory sideband asymmetry, we measured the bandwidths of the lower and upper inhibitory sidebands at an intensity of 60 dB. Fig. 3b shows the data for 84 sites grouped in one octave bins. The width of the lower inhibitory sideband increased with CF, while the width of the upper inhibitory sideband decreased with CF. Inhibitory sideband asymmetry therefore covaries with CF-dependent direction selectivity (Fig. 2d). This strongly suggests that the spectral asymmetry of inhibition is a source of the spectral asymmetry required for direction selectivity.

Inhibitory sidebands arise from inhibition accumulated along the central pathways leading up to and including AI, and could be due to inhibition from both synaptic inputs and intrinsic conductances[9,10]. To explore the contribution of cortical synapses to CF-dependent direction selectivity, *in vivo* whole-cell voltage-clamp recordings were carried out in AI. Fig. 4a shows the synaptic currents evoked by 70 oct/s sweeps for a low CF neuron. Excitatory inputs were examined by clamping the neuron at -70 mV (upper panels), while inhibitory inputs were revealed as outward-going currents at -30 mV (lower panels). Both excitatory and inhibitory inputs were direction selective, and had the same direction preference. The DSI of the excitatory current for the neuron of Fig 4a

was greatest for sweep speeds of 70 oct/s (Fig. 4b). Across 9 neurons the DSIs of the excitatory current for 70 oct/s sweeps decreased as a function of CF (Fig 4c).

The direction selectivity of the synaptic excitation presumably reflects direction selectivity that is already present at subcortical stations[11-13]. However, the extent to which synaptic excitation is thalamic or cortical in origin cannot be inferred from our data. Synaptic inhibition is, on the other hand, purely cortical in origin. As cortical synaptic inhibition may, together with synaptic excitation, influence the spike response, we examined the interaction of synaptic excitation with cortical synaptic inhibition.

Excitatory and inhibitory conductances were derived from the traces of Fig. 4a (see Methods). The linear I-V curve of Fig. 4d demonstrates that the neuron was reasonably well clamped. A 70 oct/s sweep in the preferred direction produced a fast, large and transient increase in the excitatory conductance, which was followed by a large inhibitory conductance (Fig. 4e, left panels). The non-preferred direction evoked less excitation and inhibition (right panels). For the preferred direction, the inhibitory peak occurred well after the excitatory peak. For the non-preferred direction, there was, interestingly, a greater overlap of the excitation by inhibition, with the inhibitory peak closer in time to the excitatory peak; in this particular neuron, the two peaks were in fact practically coincident. A similar difference between the two directions was exhibited by the 7 neurons of Fig. 4c that had strong direction selectivity (Fig. 4f; paired *t*-test: $p<0.01$). Therefore, by suppressing the synaptic excitation of the non-preferred direction more than that of the preferred, cortical synaptic inhibition can enhance direction selectivity.

To further characterize how the interaction of excitation and inhibition enhances direction selectivity, we examined the synaptic TRFs, as we expect them to be major determinants of the sweep responses[14-16]. Fig. 5a and b show the synaptic currents evoked by pure tones of various frequencies and intensities for a low and high CF neuron respectively. An inhibitory current was always preceded by an excitatory current, with strong inhibition following strong excitation. The strengths of the excitatory and inhibitory currents were strongly correlated (Fig 5c). In all 8 AI neurons for which complete synaptic TRFs were obtained, the TRFs of both excitatory and inhibitory currents had nearly identical spectral tuning, consistent with previous results[17-19].

In addition, the TRFs of excitatory and inhibitory currents exhibited the same spectral asymmetry. For the low CF neuron strong currents clustered at low frequencies, with a long tail of weaker responses at higher frequencies (Fig. 5a). The asymmetry was reversed for the high CF neuron, with strong currents clustered at high frequencies (Fig. 5b). We characterized asymmetries in the synaptic TRFs by the skewness of the iso-intensity profile at 60 dB (see Methods). A positive skewness indicates a long tail of small responses extending into high frequencies. For 18 neurons the skewness of the synaptic TRF changed monotonically with CF, changing sign at approximately 12 kHz (Fig. 5d). Synaptic TRF asymmetry therefore covaries with CF-dependent direction selectivity (Fig. 2d). This strongly suggests that the spectral asymmetry of synaptic TRFs is responsible for some of the spectral asymmetry required for direction selectivity.

In fact, the spectral asymmetry of the synaptic TRFs, combined with the temporal asymmetry provided by the delay of inhibition relative to excitation, suggests a mechanism for direction selectivity. Consider a model low CF neuron with synaptic TRF

asymmetry: let it have strong inputs on the low frequency side, and a long tail of weak inputs on the high frequency side. An up-sweep first evokes strong excitation that could trigger spiking before the onset of the following strong inhibition. But a down-sweep will first evoke only weak excitation; the following weak inhibition will extend into the onset of the strong excitation, reducing its ability to cause spiking. Thus, this model generates direction selectivity that is consistent with the observed covariation of direction selectivity and synaptic TRF asymmetry (Fig 5d). It does so with inhibition suppressing the excitation of the non-preferred direction more than that of the preferred, consistent with how direction selectivity is enhanced by AI neurons (Fig 4e, f).

The model also generates sideband asymmetry that is consistent with the observed covariation of direction selectivity and sideband asymmetry (Fig 3b). Sidebands can appear even if synaptic inhibition is not spectrally broader than synaptic excitation, because synaptic inhibition contributes to inhibitory areas outside the spike TRF if the excitation preceding the inhibition is subthreshold. By suggesting mechanisms for both direction selectivity and sideband asymmetry, synaptic TRF asymmetry unifies our previous observations and arguments.

The model, however, does not predict some features of the sweep responses, such as the direction selectivity of the synaptic conductances, or the duration of the excitatory conductance evoked by the preferred direction. This is presumably because it disregards both direction selectivity that is already present at subcortical stations[11-13], as well as nonlinearities of the cortical circuitry arising, for example, from recurrent connections. The excitatory synaptic input could be provided by an asymmetric convergence of frequency-tuned monosynaptic excitatory thalamic input onto the cortical neuron. The

temporally-delayed inhibition would be provided by the same thalamic input, disynaptically relayed by local inhibitory neurons.

The asymmetric receptive fields, reminiscent of those observed in hippocampal place cells and visual tectal neurons following directional stimulation, might have emerged from spike-timing-dependent plasticity (STDP) and directionally biased input[20,21]. Note that asymmetric receptive fields can be generated in a recurrent circuit by STDP without any input bias[22]. The circuit amplifies small asymmetries in the initial conditions, which might be provided by boundary effects arising from the finite frequency range of the auditory system.

Whereas a topographic order of CF, retinal position, ocular dominance or orientation represents spectral or spatial information, that of direction selectivity represents inherently temporal information. The data presented therefore sheds light on the synaptic mechanisms underlying both the coding of temporal information by single neurons, as well as its conversion into large-scale spatial organization.

Methods

Extracellular recording. All experimental procedures used in this study were approved under UCSF Animal Care Facility protocols. Experiments were carried out in a sound-attenuating chamber. Female Sprague-Dawley rats about 3 months-old and weighing 280-300g were anesthetized with pentobarbital, and their right auditory cortex exposed. Multiunit spike responses were recorded with parylene-coated tungsten microelectrodes at 500-600 μm below the pial surface[23]. Pure tones (0.5-64 kHz at 0.1 octave intervals, 25-ms duration) at eight 10-dB spaced sound intensities were delivered through a

calibrated free field speaker facing the left ear. The frequencies used covered the hearing range of the rat.

FM sweep and two-tone stimuli. Logarithmic FM stimuli sweeping between 0.5 kHz~64 kHz with speeds of 2 – 700 oct/s were generated and calibrated according to their output envelope. Sweeps were presented in a pseudorandom order. Except for the experiments in Fig. 1, sweep intensity was set at 60 dB. For two-tone stimuli, the first tone was varied as for determining the TRF. The second tone was a CF tone with intensity 5-10 dB above threshold, could consistently trigger spiking responses, and was played 20 ms after the onset of the first. The method of measuring sideband widths was similar to those previously described[8,9]. All sidebands lay entirely within the probed frequency range.

Whole-cell recording. AI was first located by roughly mapping with a tungsten electrode. Whole-cell recordings[24-27] were obtained from neurons located 400~700 μm beneath the cortical surface. 4% agarose prevented cortical pulsation. For voltage-clamp recording, the pipette (~7 MΩ) contained (in mM) Cs-gluconate 125, TeaCl 5 MgATP 4, GTP 0.3, phosphocreatine 10, Hepes 10, EGTA 0.5, QX-314 3.5, CsCl 2 with PH 7.2. Recordings were made with an Axopatch 200B. The whole-cell capacitance was compensated and the initial series resistance (35-60 MΩ) was compensated to achieve effective series resistances of 15-30 MΩ. Signals were filtered at 5 kHz and sampled at 10 kHz. The CFs of the synaptic TRFs matched their positions in the rough CF map.

Data analysis. The DSI is defined as $(r_1-r_2)/(r_1+r_2)$, where r_1 is the response triggered by the up-sweep, r_2 the response to the down-sweep.

The excitatory and inhibitory conductances were derived[28-30] using $I(t) = G_r(V-E_r) + G_e(V-E_e) + G_i(V-E_i)$. $I(t)$ is the amplitude of the synaptic current at time t, G_r *and* E_r are the resting conductance and membrane potential, $G_e(t)$ and $G_i(t)$ are the excitatory and inhibitory conductances, V is the holding voltage, and E_e (0 mV) and E_i (-65 mV) are the reversal potentials for excitatory and inhibitory currents. Changing E_e and E_i by ±10 mV did not change the time course of any conductance significantly.

Skewness, a measure of the asymmetry based on the third central moment of a distribution, is defined as $m_3/m_2^{3/2}$, where $m_1=\sum(r_f.f)$, $m_2=\sum(r_f.(f-m_1)^2)$, $m_3=\sum(r_f.(f-m_1)^3)$, $r_f=R_f/\sum(R_f)$. R_f is the synaptic current at -70 mV, averaged between 15 and 35 ms after the onset of a tone of frequency f, with f in units of octaves above 0.5 kHz. The sums are over all frequencies in the synaptic TRF at 60 dB. Skewness was calculated only for neurons whose synaptic TRFs lay entirely within the probed frequency range.

Acknowledgments

This work was supported by the Howard Hughes Medical Institute, the John C. and Edward Coleman Fund, the MacDonnell Foundation, the National Institutes of Health and the Sandler Fund.

1. Mendelson, J.R. & Cynader, M.S. Sensitivity of cat primary auditory cortex (AI) neurons to the direction and rate of frequency modulation. *Brain Res.* **327**:331-335 (1985).

2. Schreiner, C.E., Read, H.L. & Sutter, M.L. Modular organization of frequency integration in primary auditory cortex. *Annu. Rev. Neurosci.* **23**:501-529 (2000).

3. Ricketts, C., Mendelson, J.R., Anand, B. & English, R. Responses to time-varying stimuli in rat auditory cortex. *Hear Res.* **123**:27-30 (1998).

4. Merzenich, M.M., Knight, P.L. & Roth, G.L. Representation of cochlea within primary auditory cortex in the cat. *J. Neurophysiol.* **38**:231-249 (1975).

5. Sally, S.L. & Kelly, J.B. Organization of auditory cortex in the albino rat: sound frequency. *J. Neurophysiol.* **59**:1627-1638 (1988).

6. Suga, N. Functional properties of auditory neurones in the cortex of echo-locating bats. *J. Physiol.* **181**:671-700 (1965).

7. Shamma, S.A., Fleshman, J.W., Wiser, P.R. & Versnel H. Organization of response areas in ferret primary auditory cortex. *J. Neurophysiol.* **69**: 367-383 (1993).

8. Nelken, I. & Versnel, H. Responses to linear and logarithmic frequency-modulated sweeps in ferret primary auditory cortex. *Eur. J. Neurosci.* **12**: 549-562 (2000).

9. Calford, M.B. & Semple, M.N. Monaural inhibition in cat auditory cortex. *J. Neurophysiol.* **73**:1876-1891 (1995).

10. Brosch, M. & Schreiner, C.E. Time course of forward masking tuning curves in cat primary auditory cortex. *J Neurophysiol.* **77**:923-943 (1997).

11. Clopton, B.M., Winfield, J.A. Unit responses in the inferior colliculus of rat to temporal auditory patterns of tone sweeps and noise bursts. *Exp. Neurol.* **42**:532-540 (1974).

12. Britt, R. & Starr, A. Synaptic events and discharge patterns of cochlear nucleus cells. II. Frequency-modulated tones. *J. Neurophysiol.* **39**:179-194 (1976).

13. Poon, P.W. & Yu, P.P. Spectro-temporal receptive fields of midbrain auditory neurons in the rat obtained with frequency modulated stimulation. *Neurosci. Lett.* **289**:9-12 (2000).

14. Kowalski, N., Depireux, D.A. & Shamma, S.A. Analysis of dynamic spectra in ferret primary auditory cortex. II. Prediction of unit responses to arbitrary dynamic spectra. *J. Neurophysiol.* **76**:3524-3534 (1996).

15. deCharms, R.C., Blake, D.T., Merzenich, M.M. Optimizing sound features for cortical neurons. *Science* **280**:1439-1443 (1998).

16. Schnupp, J.W., Mrsic-Flogel, T.D., King, A.J. Linear processing of spatial cues in primary auditory cortex. *Nature* **414**:200-204 (2001).

17. De Ribaupierre, F., Goldstein, M.H. Jr. & Yeni-Komshian, G. Intracellular study of the cat's primary auditory cortex. *Brain Res.* **48**:185-204 (1972).

18. Volkov, I.O. & Galazjuk, A.V. Formation of spike response to sound tones in cat auditory cortex neurons: interaction of excitatory and inhibitory effects. *Neuroscience* **43**:307-321 (1991).

19. Ojima, H. & Murakami, K. Intracellular characterization of suppressive responses in supragranular pyramidal neurons of cat primary auditory cortex in vivo. *Cereb. Cortex* **12**:1079-1091 (2002).

20. Mehta, M.R., Quirk, M.C. & Wilson, M.A. Experience-dependent asymmetric shape of hippocampal receptive fields. *Neuron* **25**:707-715 (2000).

21. Engert, F., Tao, H.W., Zhang, L.I. & Poo M. Moving visual stimuli rapidly induce direction sensitivity of developing tectal neurons. *Nature* **419**:470-475 (2002).

22. Rao, R.P.N. & Sejnowski, T.J. *Predictive learning of temporal sequences in recurrent neocortical circuits.* In *Advances in Neural Information Processing Systems* **12** (eds Solla, S. A., Leen, T.K. & Muller, K.R.) 164-170 (MIT Press, Cambridge, Massachusetts, 2000).

23. Zhang, L.I., Bao, S. & Merzenich, M.M. Persistent and specific influences of early acoustic environments on primary auditory cortex. *Nat. Neurosci.* **4**:1123-1130 (2001).

24. Zhang, L.I., Tao, H.W., Holt, C.E., Harris, W.A. & Poo, M. A critical window for cooperation and competition among developing retinotectal synapses. *Nature* **395**:37-44 (1998).

25. Moore, C.I. & Nelson, S.B. Spatio-temporal subthreshold receptive fields in the vibrissa representation of rat primary somatosensory cortex. *J. Neurophysiol.* **80**:2882-2892 (1998).

26. Zhu, J.J. & Connors, B.W. Intrinsic firing patterns and whisker-evoked synaptic responses of neurons in the rat barrel cortex. *J. Neurophysiol.* **81**:1171-1183 (1999).

27. Margrie, T.W., Brecht, M. & Sakmann, B. In vivo, low-resistance, whole-cell recordings from neurons in the anaesthetized and awake mammalian brain. *Pflugers Arch.* **444**:491-498 (2002).

28. Borg-Graham, L.J., Monier, C. & Fregnac, Y. Visual input evokes transient and strong shunting inhibition in visual cortical neurons. *Nature* **393**:369-373 (1998).

29. Hirsch, J.A., Alonso, J.M., Reid, R.C. & Martinez, L.M. Synaptic integration in striate cortical simple cells. *J. Neurosci.* **18**:9517-9528 (1998).

30. Anderson, J.S., Carandini, M. & Ferster, D. Orientation tuning of input conductance, excitation, and inhibition in cat primary visual cortex. *J. Neurophysiol.* **84**:909-926 (2000).

Figure 1 Direction selectivity of multiunit sites. **a.** Rasters of responses from one site to 7-oct FM sweeps. The sweep speed of each panel is on the left. Positive speeds indicate up-sweeps. Within each panel are 3 repetitions of 15 intensities evenly spaced from 30 (top) to 75 dB (bottom). Schematic frequency versus time representations of four sweeps are on the right. **b.** TRF for the same site. Bar lengths indicate the number of spikes evoked by each tone. The vertical line indicates the CF. **c.** DSI versus sweep speed for the same site at different sweep intensities.

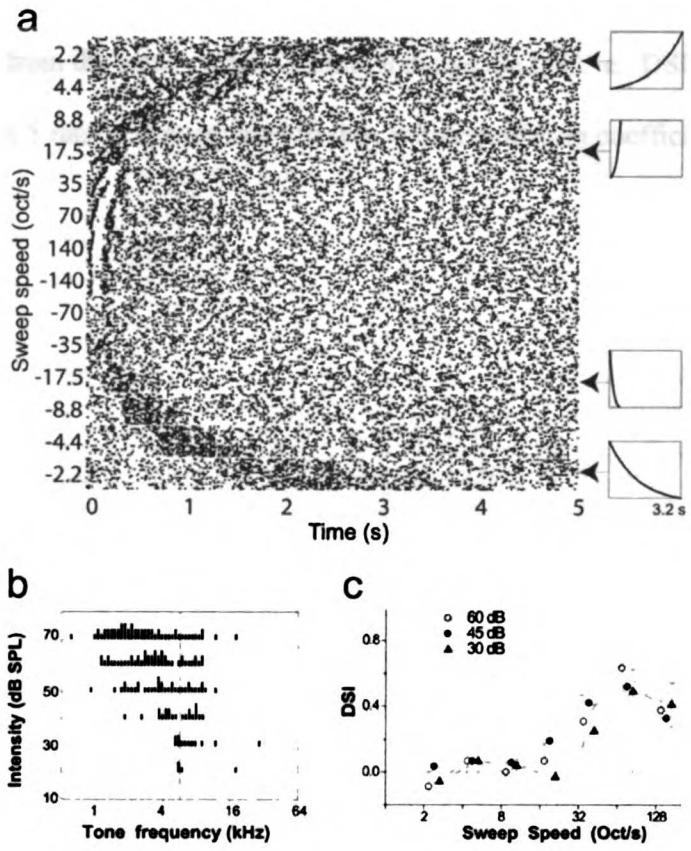

Figure 1

Figure 2 CF-dependence of direction selectivity in AI. **a.** CF map. Colors indicate the CFs of cortical locations. Sites without responses to tones or clear tuning are represented by 'o' and 'x' respectively. Scale bar: 0.5 mm. A, anterior; D, dorsal. **b.** Direction selectivity map from the same cortex. Colors indicate the DSI. **c.** DSI-CF dependence of 123 sites from 5 rats. Least-squares fit line, with correlation coefficient r, is shown in red.

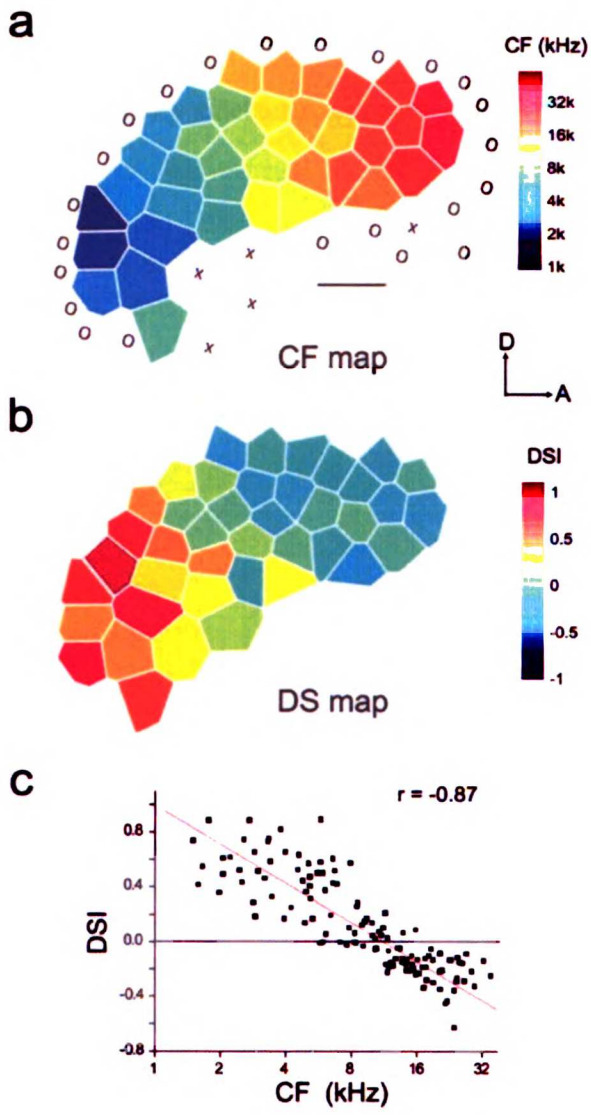

Figure 2

Figure 3 CF-dependence of inhibitory sideband asymmetry. **a.** Left panel shows a low CF neuron. Inhibitory areas are outlined by blue. Blue bars indicate responses to the second tone as a function of the frequency and intensity of the first. Red bars show the TRF. **b.** Mean width of inhibitory sidebands as a function of CF.

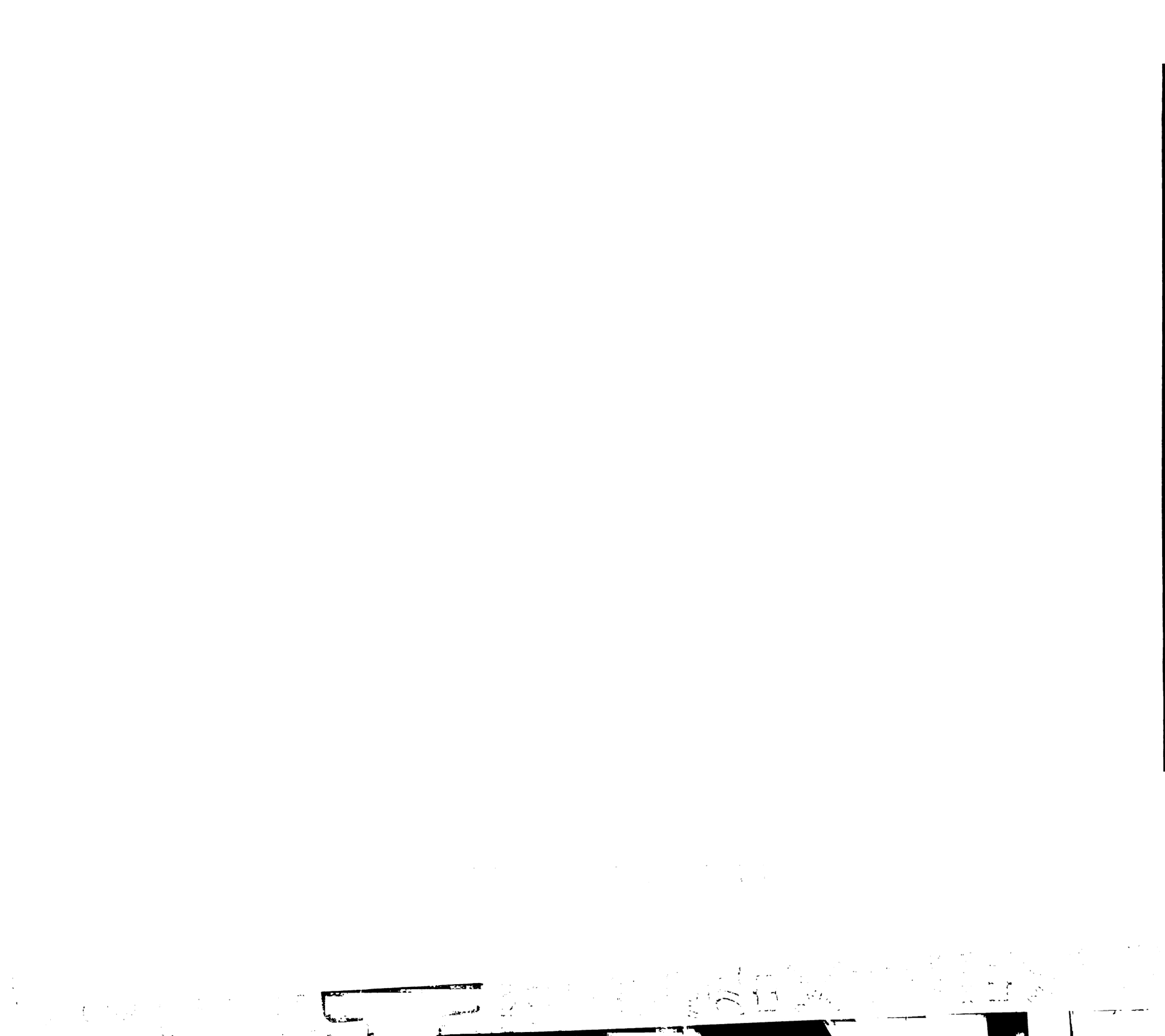

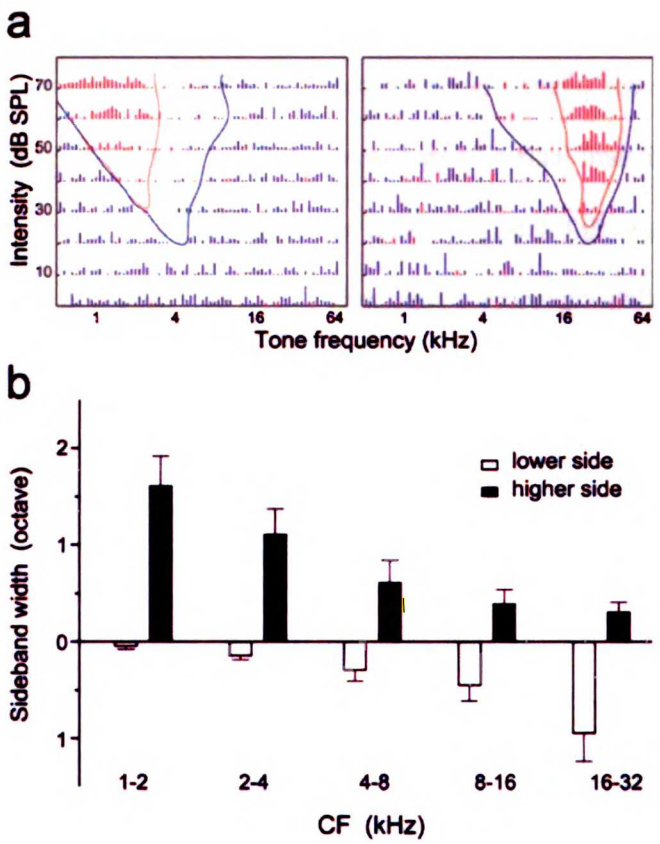

Figure 3

Figure 4 Synaptic responses to FM sweeps. **a**. Synaptic currents at -70 mV (upper panels) and -30 mV (lower panels) evoked by up- and down-sweeps (left and right panels respectively) in a 2 kHz neuron. Five stimulus repetitions are superimposed. **b**. DSI of excitatory current versus sweep speed. **c**. DSI of excitatory current versus CF. **d**. I-V curve at 20 ms after up-sweep onset. **e**. Excitatory (upper panels) and inhibitory (lower panels) conductances evoked by up- and down-sweeps. Vertical lines indicate peaks of excitatory conductances. **f**. Time by which the inhibitory peak follows the excitatory for the preferred (left) and non-preferred (right) directions for strongly (filled circles) or mid-CF, weakly (open circles) direction selective neurons. Points for the same neuron are connected.

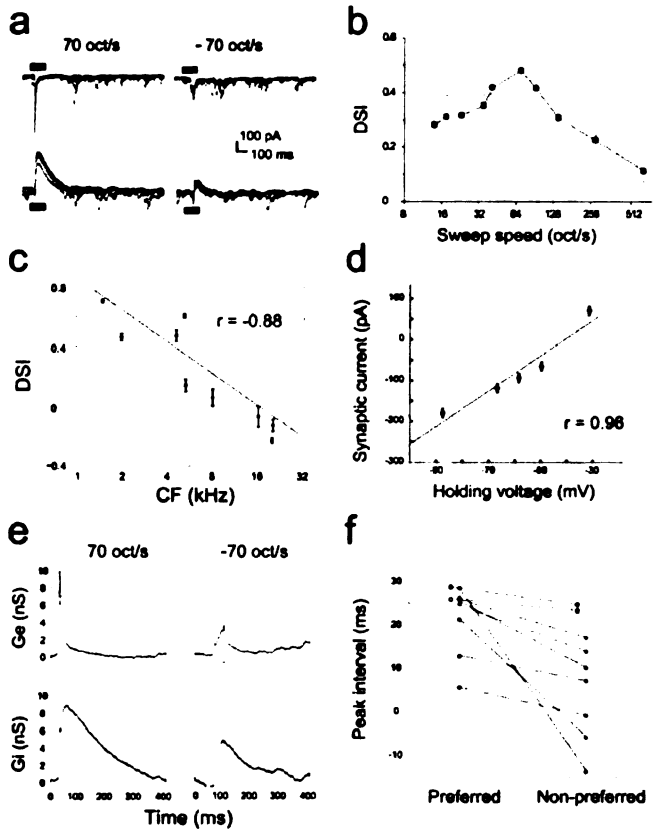
a
70 oct/s
-70 oct/s
100 pA
100 ms
b
DSI
Sweep speed (oct/s)
c
DSI
r = -0.88
CF (kHz)
d
Synaptic current (pA)
r = 0.96
Holding voltage (mV)
e
70 oct/s
-70 oct/s
Ge (nS)
Gi (nS)
Time (ms)
f
Peak interval (ms)
Preferred
Non-preferred

Figure 4

Figure 5 Asymmetric synaptic TRFs. **a.** Currents evoked in a low CF neuron at -70 mV (left panel) and -30 mV (right panel) to pure tones of various frequencies and intensities. Vertical, horizontal scale bars: 200 pA, 80 ms (left); 100 pA, 400 ms (right) **b.** Same as in a, but for a high CF neuron. Scale bars: 50 pA, 110 ms (left); 40 pA, 400 ms (right). **c.** Correlation of EPSC and IPSC amplitudes. Filled circles were from recordings shown in a, open circles from b. **d.** Skewness versus CF.

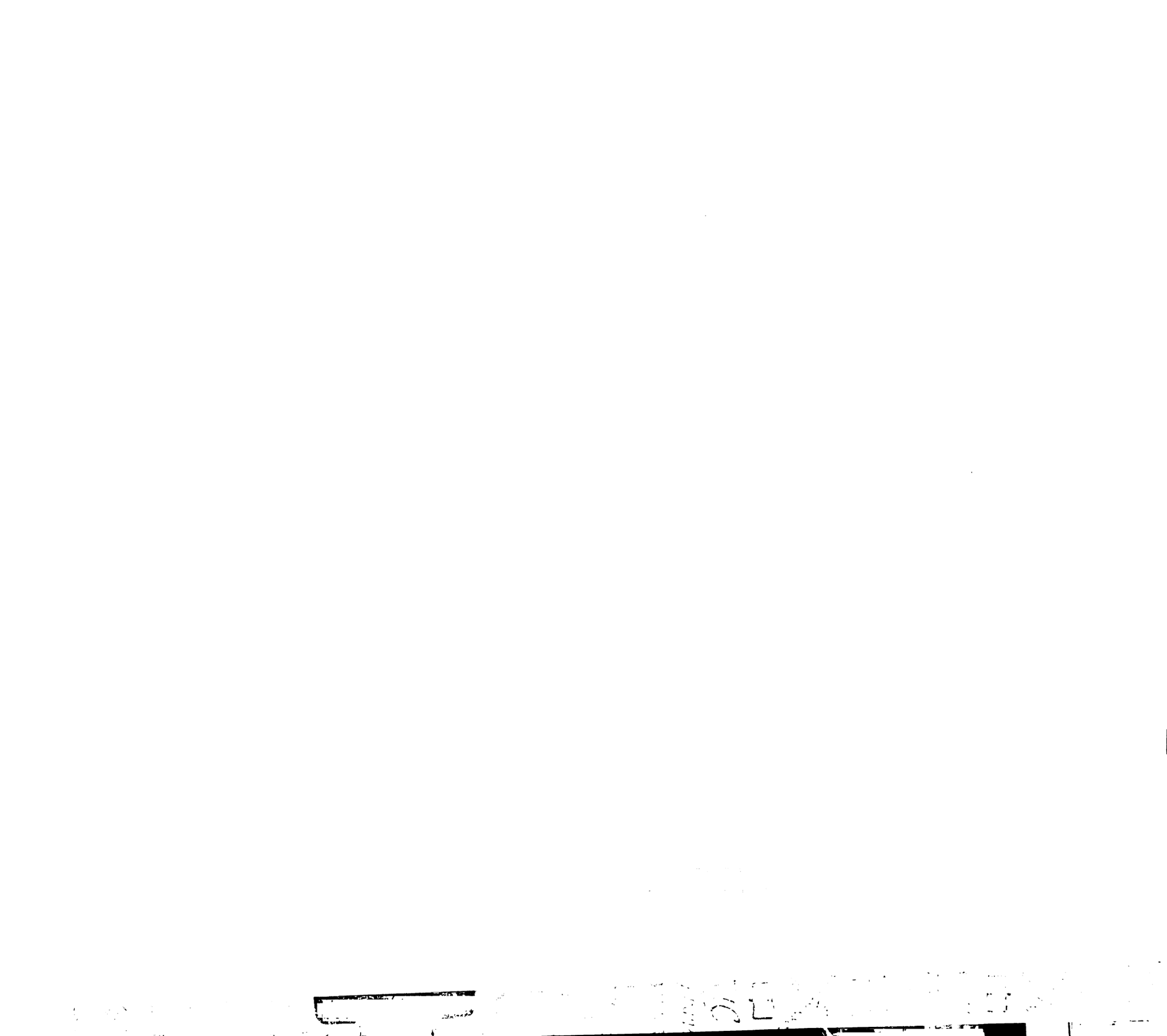

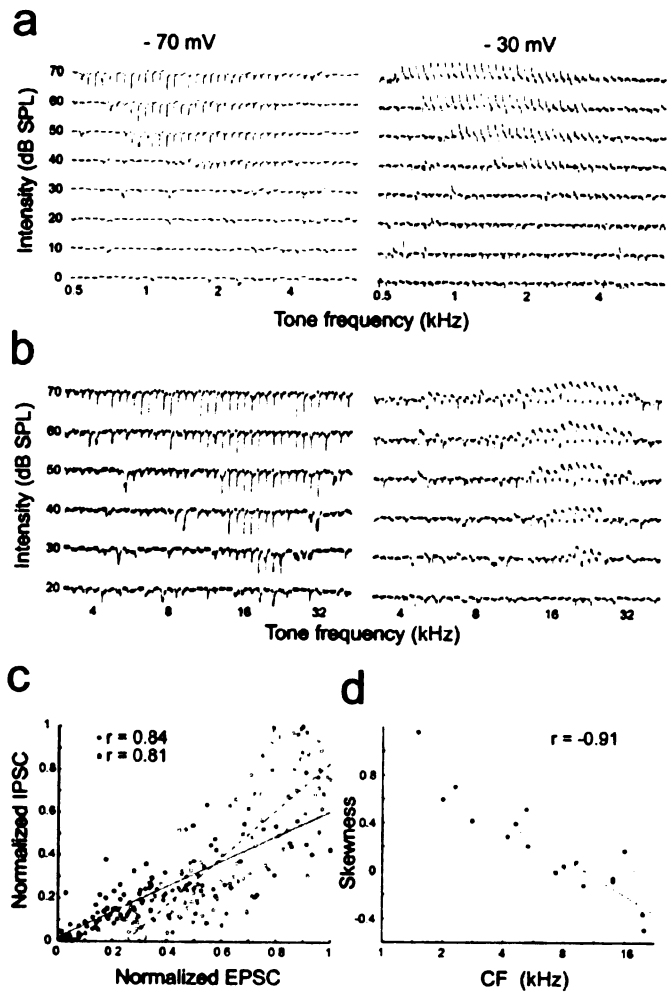
a
- 70 mV
- 30 mV
Intensity (dB SPL)
Tone frequency (kHz)
b
Intensity (dB SPL)
Tone frequency (kHz)
c
r = 0.84
r = 0.81
Normalized IPSC
Normalized EPSC
d
r = -0.91
Skewness
CF (kHz)

Figure 5

Chapter 3

Tone-evoked excitatory and inhibitory synaptic conductances of primary auditory cortex neurons

Abstract

In primary auditory cortex (AI) neurons, tones typically evoke a brief depolarization, which can lead to spiking, followed by a long-lasting hyperpolarization. The extent to which the hyperpolarization is due to synaptic inhibition has remained unclear. Here we report in vivo whole-cell voltage-clamp measurements of tone-evoked excitatory and inhibitory synaptic conductances of AI neurons of the pentobarbital-anesthetized rat. Tones evoke an increase of excitatory synaptic conductance, followed by an increase of inhibitory synaptic conductance. The synaptic conductances can account for the gross time course of the typical membrane potential response. Synaptic excitation and inhibition have the same frequency tuning. As tone intensity increases, the amplitudes of synaptic excitation and inhibition increase, and the latency of synaptic excitation decreases. Our data indicate that the interaction of synaptic excitation and inhibition shapes the time course and frequency tuning of the spike responses of AI neurons.

Introduction

The vast majority of electrophysiological studies of the primary auditory cortex (AI) have used tones as stimuli. AI's spike responses to tones have therefore been well described for some time, and much current research is directed towards its spike responses to more complex sounds. Because of the nonlinearity of AI and the infinite number of sounds, supplementing such research with investigations into the mechanisms underlying the spike responses will help the formulation of a model capable of predicting AI's spike responses to arbitrary sounds.

Insight into the network aspects of the mechanisms may be gained by decomposing the synaptic inputs of AI neurons into excitatory and inhibitory components. This is because any particular neuron provides either excitatory or inhibitory synaptic input to all of its postsynaptic neurons, but not both. Furthermore, inhibitory synaptic inputs to AI neurons are primarily cortical in origin, as AI neurons receive few inhibitory synaptic inputs from subcortical stations (Douglas and Martin 1998; Winer 1992).

While there have been many studies about the tone-evoked spike responses of AI neurons, far fewer have examined the synaptic inputs underlying those responses. Previous intracellular work has shown that tones typically evoke a brief depolarization, which can lead to spiking, followed by a long-lasting hyperpolarization (De Ribaupierre et al. 1972; Ojima and Murakami 2002; Volkov and Galazjuk 1991, 1992). This is consistent with synaptic excitation being followed by long-lasting synaptic inhibition. When the tone frequency and intensity are such that the depolarization is small, it is unlikely that intrinsic conductances are opened, and the hyperpolarization must be due

mainly to synaptic inhibition. But when the tone frequency and intensity are such that the depolarization is large and causes a spike, the extent to which the hyperpolarization is due to synaptic inhibition is unclear, because much of the hyperpolarization might be due to intrinsic potassium conductances opening as a result of the large depolarization. We have therefore carried out in vivo whole-cell voltage-clamp measurements of the tone-evoked excitatory and inhibitory synaptic conductances of AI neurons of the pentobarbital-anesthetized rat.

We have previously examined the relationship between tone-evoked synaptic inputs and frequency-modulated sweep-evoked spike responses (Zhang et al. 2003). Here we examine the relationship between tone-evoked synaptic inputs and tone-evoked membrane potential responses.

Methods

Surgery

All experimental procedures used in this study were approved under UCSF Animal Care Facility protocols. Experiments were carried out in a sound-attenuating chamber. Female Sprague-Dawley rats about 3 months-old and weighing 280-300g were used. Each rat was anesthetized by intraperitoneal injection of sodium pentobarbital (50-80 mg/kg), with the dose adjusted to make the rat areflexic. The rat was maintained in an areflexic state for the rest of the experiment by further intraperitoneal injections of sodium pentobarbital (20-60 mg/kg) when necessary. The rat was placed on a heating pad, and its temperature maintained at approximately 37 °C. Prior to any skin incision,

bupivacaine was injected subcutaneously at the incision site. A tracheotomy was performed to secure the airway, and to reduce spurious respiratory noise. (The animal was not artificially respirated.) The head was held fixed by a custom-made device that clamped it at both orbits and the palate, leaving the ears unobstructed. A cisternal drain was performed. The right auditory cortex was exposed by retracting the skin and muscle overlying it, followed by a craniotomy and a durotomy. The cortical surface was kept moist with normal saline. The location of AI was determined by coarse mapping of multiunit spike responses at 500-600 μm below the pial surface with a parlyene-coated tungsten electrode.

Cell-attached and whole-cell recordings

A silver wire, one end of which was coated with silver chloride, served as the reference electrode against which potentials were measured; its chlorided end was inserted between the skull and the dura. The reference electrode was assigned a potential of 0 mV. The potential of the cerebrospinal fluid was assumed to be uniform and equal to that of the reference electrode.

Patch pipettes with resistances of 7 MΩ were made. Pipettes contained a potassium based solution that consisted of (in mM) 135 K-gluconate, 5 NaCl, 5 MgATP, 0.3 GTP, 10 HEPES, 10 Phosphocreatine (2Na), pH 7.3. For whole-cell voltage-clamp recordings, pipettes contained a cesium based solution that consisted of (in mM) 125 Cs-gluconate, 5 TEA-Cl, 4 MgATP. 0.3 GTP, 10 phosphocreatine, 10 HEPES, 0.5 EGTA, 3.5 QX-314, 2 CsCl, pH 7.2. The pia was broken by slowly lowering and raising the jagged tip of a broken pipette in and out of the cortex. An unbroken pipette was then

lowered into the cortex, with the pressure in the pipette greater than atmospheric. Dimpling of the cortical surface was not visually detectable. The cortical depth of the pipette tip was estimated according to the distance it had travelled. The cortex was covered with 4% agarose in normal saline. Under voltage-clamp, an oscillating potential was set up at the pipette tip; the oscillating potential had a time average of -50 mV; its period was much faster than the breathing rate. The resulting current oscillation was measured. When the amplitude of the current oscillation decreased, and an even slower oscillation whose period was the breathing rate of the animal became superimposed on the current oscillation, this indicated that the pipette tip might be touching the cell membrane of a neuron. At this point, the pipette was slowly advanced to further reduce the amplitude of the current oscillation. The pressure in the pipette was suddenly reduced to less than atmospheric, and then returned to atmospheric. Often a giga-ohm seal would spontaneously form within a minute; if not, additional gentle suction sometimes helped. With a giga-ohm seal, or even a mega-ohm seal, the recording is in cell-attached mode. A giga-ohm seal is required to bring the recording into whole-cell mode. A pulse of reduced pressure in the pipette would often break the cell membrane, and bring the recording into whole-cell mode. Cell-attached and whole-cell current-clamp recordings used an Axoclamp 2B amplifier in current-clamp mode. Whole-cell voltage-clamp recordings used an Axopatch 200B amplifier in voltage-clamp mode; the whole-cell capacitance was compensated and the initial series resistance (25-60 MΩ) was compensated to achieve an effective series resistance of 15-30 MΩ. Signals were filtered at 5 kHz and sampled at 10 kHz. (Margrie et al. 2002; Metherate and Ashe 1993; Moore and Nelson 1998; Zhu and Connors 1999)

Stimuli

In cell-attached and whole-cell current clamp recordings, stimuli were delivered into the left ear canal by a tube sealed to a calibrated speaker. Stimuli consisted of 675 pure tone pips, each with one of 45 frequencies spanning 1.1 kHz to 31.1 kHz uniformly on a logarithmic frequency scale, and 15 intensities spanning 5 dB SPL to 75 dB SPL uniformly, each with a 50 ms duration and 3 ms cosine rising and falling phases. Single tone pips or noise bursts with the same duration, rising and falling phases were also used. The inter-stimulus interval was 500 ms.

In whole-cell voltage-clamp recordings, stimuli were delivered by a calibrated free field speaker directed towards the left ear. Stimuli consisted of 568 pure tone pips, each with one of 71 frequencies spanning 0.5 kHz to 64 kHz uniformly on a logarithmic frequency scale, and 8 intensities spanning 0 dB SPL to 70 dB SPL uniformly, each with a 25 ms duration and 5 ms cosine rising and falling phases. Single tone pips or noise bursts with the same duration, rising and falling phases were also used. The inter-stimulus interval was 500 ms.

It should be noted that the spike response of an AI neuron to a 50 ms tone with 3 ms rising and falling phases, and the spike response to a 25 ms tone with 5 ms rising and falling phases, are virtually identical (Heil 1997a, 1997b).

Synaptic conductances

The excitatory synaptic conductance $G_e(t)$ and inhibitory synaptic conductance $G_i(t)$ at time t were derived using

$$I(t,V) = G_e(t)(V-E_e) + G_i(t)(V-E_i), \quad (1)$$

where V is the clamping voltage, E_e and E_i are the reversal potentials of the excitatory and inhibitory synaptic conductances respectively; $I(V,t)$ is the amplitude of the synaptic current, relative to the resting current at V. The values of E_e and E_i were set by the ionic composition of the pipette solution and the cerebrospinal fluid (Johnston and Wu 1995; Davson and Segal 1996); the value of E_i was based on the permeability of GABA-A conductances to Cl^-, but it should be noted that they also pass HCO_3^- (Bormann et al 1987). $G_e(t)$ and $G_i(t)$ were the 2 unknowns in *Eq. 1* at any particular t. Measurement of $I(V,t)$ at two different values of V yielded a system of 2 equations which could then be solved for $G_e(t)$ and $G_i(t)$ at any particular t. (Borg-Graham et al. 1998; Anderson et al. 2000; Hirsch et al. 1998)

Currents into the neuron were assigned a negative value. E_e and E_i were 0 mV and -70 mV respectively; in some cases, values of -60 mV and -80 mV were also used for E_i.

The resting or leak conductance G_r was derived using

$$I_r(V)=G_r(V-E_r), \quad (2)$$

where E_r is the membrane potential, and $I_r(V)$ is the resting current. G_r and E_r were the 2 unknowns in Eq. 2. Measurement of $I_r(V)$ at two different values of V yielded a system of 2 equations which could then be solved for G_r and E_r.

Rather than using V in the equations above, a corrected clamping voltage V_c, given by

$$V_c=V-R_sI_r, \tag{3}$$

was actually used, where R_s is the effective series resistance.

We did not correct for any junction potentials.

Estimated membrane potential response

The estimated membrane potential response V_{est} for the voltage clamp recordings was derived using

$$V_{est}(t)=(G_rV_r+G_e(t)E_e+G_i(t)E_i)/(G_r(t)+G_e(t)+G_i(t)), \tag{4}$$

where V_r is the resting membrane potential. V_r was assumed to be -60 mV; and G_r, $G_e(t)$, and $G_i(t)$ were derived as described above. If only the excitatory synaptic conductance was taken into account, $G_i(t)$ was set to zero.

Results

We define two terms before proceeding: the tonal receptive field (TRF) of a neuron consists of its responses to tones of various frequencies and intensities; the characteristic frequency (CF) of a neuron is the tone frequency at which the intensity needed to evoke a response is lowest.

Sounds were played through a speaker directed to the left ear of a pentobarbital-anesthetized rat. Recordings were carried out in its right AI, or the surrounding auditory cortex. Cell-attached or whole-cell recordings of tone or noise-evoked responses were obtained from 71 neurons. Full TRFs were obtained for 32 neurons, all of which were in AI. AI, which is defined by a rostro-caudal CF gradient, was located by coarse mapping of multiunit spike responses (Sally and Kelly, 1988). The CFs of the spike responses, membrane potential responses, and synaptic conductances of the 32 neurons matched the CFs of multiunit spike responses at nearby locations.

The main aim of our measurements of tone-evoked synaptic conductances was to examine their contribution to the long-lasting hyperpolarization that follows tone-evoked depolarization. But because the measurements have permitted us to also examine the relationship between the synaptic inputs and several other aspects of tone-evoked spike and membrane potential responses, we first recapitulate the main characteristics of tone-evoked spike and membrane potential responses, before reporting the synaptic conductances underlying them.

Spike responses

Cell-attached recordings of tone-evoked spike responses were obtained from 3 neurons. Full TRFs were obtained for 2 neurons. In cell-attached recordings, the pipette is attached to the outside of the cell membrane of the fully intact neuron. Cell-attached recordings are equivalent to extracellular single-unit recordings.

The spike responses from one neuron are shown in Fig. 1. Fig. 1a shows 3 responses, each evoked by a 9 kHz, 75 dB tone. Each response consists of just one or

two spikes about 15 ms after tone onset. Fig. 1b shows the neuron's TRF; each trace shows the response to one tone; the responses are arranged in a grid according to the frequencies and intensities of the tones; tone frequency increases from left to right; tone intensity increases from bottom to top. The neuron's CF is 9 kHz. When tone intensity is low, only tones with frequencies very close to the CF can evoke spiking. As tone intensity increases, the tone frequency range capable of producing spikes also increases, giving the TRF a V-shape. Fig. 1c shows that the spike response strength increases then levels off as the intensity of a CF tone increases. Fig. 1d shows that the first-spike latency decreases as the intensity of a CF tone decreases.

The neuron of Fig. 1 is representative of the 3 neurons from which cell-attached recordings were obtained, except that one neuron often responded with bursts of 2 or 3 spikes. The onset-only responses, V-shaped TRFs, and monotonic rate-intensity and latency-intensity functions, are characteristic of AI neurons in anesthetized animals (Brugge et al. 1969; DeWeese et al. 2003; Erulkar et al. 1956; Heil 1997a, 1997b; Hind 1960; Katsuki et al. 1959; Merzenich et al. 1975; Oonishi and Katsuki 1965; Phillips et al. 1981, 1989; Sally and Kelly 1988).

Membrane potential responses

Whole-cell current-clamp recordings of tone or noise-evoked membrane potential responses were obtained from 29 neurons. Resting potentials ranged from -54 to -72 mV, with average and standard deviation -63 ± 5 mV. Full TRFs were obtained for 12 neurons. Cortical depths ranged from 400 to 700 μm, which corresponds to layers III to V (Games and Winer 1988).

The membrane potential responses from a neuron which had spike response characteristics like the neuron of Fig. 1, are shown in Fig. 2. The neuron was 400 μm deep. Its resting potential was -68 mV. Fig. 2a shows 3 responses, each evoked by a 20 kHz, 75 dB tone. About 15 ms after tone onset, depolarization begins, and leads to a spike about 5 ms later. A return to the resting potential occurs about 30 ms after the start of the depolarization. The brevity of the depolarization is such that the membrane potential is above the -40 mV threshold for spiking for only 10 ms. Thus the brief depolarization is the basis of the onset-only spike response. There is no hyperpolarization after the depolarization. Fig. 2b shows the neuron's TRF. Spikes have been truncated to display subthreshold responses more clearly. The neuron's CF is 20 kHz. Both the membrane potential and spike TRFs are V-shaped, but the membrane potential TRF is broader in its frequency extent, and has a tip lower in intensity (and frequency, in this case). Fig. 2c shows that the spike response strength increases then levels off as the intensity of a CF tone increases. Fig. 2d shows that the first-spike latency decreases as the intensity of a CF tone decreases.

The neuron of Fig. 2 is representative of the 29 neurons from which current-clamp recordings were obtained, except that a few neurons responded with bursts of spikes, and one neuron had nonmonotonic rate-intensity and latency-intensity functions. Across the 29 neurons, the time courses of tone-evoked and noise-evoked membrane potential responses were similar; the depolarization evoked by CF tones or noise at 60 dB began 15 ± 3 ms after tone onset, and lasted 53 ± 23 ms. The brief depolarizations, V-shaped membrane potential TRFs, and broader subthreshold TRFs, are characteristic of AI neurons in anesthetized animals (De Ribaupierre et al. 1972; Ojima and Murakami 2002;

Volkov and Galazjuk 1991, 1992). (Note that membrane potential responses are similar to local field potentials in some respects (Norena and Eggermont 2002)).

We only occasionally observed a long-lasting hyperpolarization following a tone-evoked depolarization, at least in individual membrane potential responses. Our observations, however, are not inconsistent with those of previous studies; if the conductances that were visible as hyperpolarizations in those studies had reversal potentials close to the resting potential, slightly lower resting potentials in our study could have rendered them invisible as hyperpolarizations. Furthermore, those conductances had an observable effect on the membrane potential of some neurons by affecting their spontaneous activity. In the period before tone onset, spontaneous activity usually consisted of spontaneous depolarizations from the resting potential; if tone onset was followed by the opening of a long-lasting conductance with a reversal potential close to the resting potential, this would cause a long-lasting suppression of the spontaneous depolarizations. The suppression would be visible as a long-lasting hyperpolarization of the average membrane potential in neurons with sufficient spontaneous activity, and for which there were recordings of the membrane potential responses to a sufficient number of repetitions of the tone (Destexhe et al 2003; Monier et al. 2003). In 17 neurons, the hyperpolarization of average membrane potential responses evoked by CF tones or noise at 60 dB lasted until 184 ± 52 ms after tone onset. These timings are comparable to those of the long-lasting hyperpolarizations of individual membrane potential responses previously observed (De Ribaupierre et al. 1972; Ojima and Murakami 2002; Volkov and Galazjuk 1991, 1992).

Voltage-clamp recordings

To measure the synaptic conductances underlying the above-described tone-evoked spike and membrane potential responses, whole-cell voltage-clamp recordings of tone or noise-evoked synaptic current responses were obtained from a separate population of 39 neurons. Full excitatory synaptic conductance TRFs were obtained for 18 neurons; full inhibitory synaptic conductance TRFs were also obtained for 8 of the 18 neurons. Cortical depths ranged from 400 and 700 μm, which corresponds to layers III to V (Games and Winer 1988).

Voltage-clamping suppresses the activation of intrinsic voltage-sensitive conductances, and helps ensure that the recorded current is synaptic. With the 18 neurons, the patch pipette contained a cesium based solution with TEA and QX-314, which further prevented the activation of intrinsic conductances. Cesium and TEA block intrinsic potassium conductances; QX-314 blocks intrinsic sodium conductances. Cesium also blocks GABA-B, an inhibitory synaptic conductance. The remaining unblocked excitatory synaptic conductances were AMPA and NMDA; the remaining unblocked inhibitory synaptic conductance was GABA-A. (Douglas and Martin 1998; Hille 2001)

The ionic composition of the patch pipette solution was such that the reversal potentials of AMPA receptors and NMDA receptors were both 0 mV, and that of GABA-A receptors was -70 mV. Thus, when a neuron was clamped at -70 mV, the synaptic current would be mainly excitatory (or more precisely, the synaptic current would be mainly from the excitatory synaptic conductances), and the excitatory current inward; when a neuron was clamped at -30 mV, the synaptic current would be a mixture of

excitatory and inhibitory currents, with the excitatory current inward, and the inhibitory current outward. From the synaptic currents at -70 mV and -30 mV, the corresponding excitatory and inhibitory synaptic conductances were derived with the assumption that each of the currents is linearly proportional to the membrane potential. This assumption is only approximately met by the excitatory current, because the NMDA current is voltage-sensitive. The voltage-sensitivity of NMDA receptors is such that more than half of them can be opened only at membrane potentials greater than -30 mV (Hestrin et al. 1990; Jahr and Stevens 1990a, 1990b). We clamped neurons only at membrane potentials less than -30 mV to suppress the NMDA current, and accordingly avoid, if only partially, the excitatory current nonlinearity.

We present in detail the time courses of tone-evoked synaptic currents and conductances of 5 of the 8 neurons for which full excitatory and inhibitory synaptic conductance TRFs were obtained. We chose the 5 out of the 8 as they had traces that were the cleanest, or most representative of the 39 neurons. Parts A through E of the remaining figures will each show data corresponding to a particular one of the 5 neurons: the neuron of Fig. 3C will, for example, be the same as the neuron of Fig. 4C.

Tone-evoked synaptic conductances

The first 3 panels of Fig. 3A show the synaptic currents evoked by an approximately 1 kHz, 70 dB tone in the first of these neurons. The neuron was 680 μm deep. The first panel shows the synaptic current evoked by 3 repetitions of the tone with the neuron clamped at -70 mV; the net inward current is indicative of the time course of synaptic excitation. The second panel shows the synaptic current evoked by 3 repetitions

of the tone with the neuron clamped at -30 mV; the initial net inward current is followed by a net outward current, indicating that synaptic excitation is followed by synaptic inhibition. The third panel shows the average -70 mV and -30 mV currents in black and grey respectively. The resting currents have been subtracted. The last panel shows the corresponding excitatory and inhibitory conductances in black and grey respectively. The excitatory conductance begins approximately 16 ms after the tone onset, rises quickly, and peaks 10 ms after that, and takes a further 20 ms to fall to half its peak. The inhibitory conductance begins later, peaks later and last longer. It begins 21 ms after the tone onset, peaks 15 ms after that, and takes another 70 ms to fall to half its peak. The conductances have had their negative portions set to zero. This only removed a presumably artifactual negative peak from the inhibitory conductance that was coincident with the start of the excitatory conductance. The negative peak was probably due to voltage-clamp errors that resulted in the initial rise of the inward current being faster at -30 mV than at -70 mV, as can be seen by comparing the first and second panels. Voltage-clamp errors would have been most common near the start of the excitatory conductance, because the initial rise of the inward current was faster than all other phases of the recorded currents. The negative peak causes an uncertainty in the start times of the excitatory and inhibitory conductances of 1 ms, the half-width at half-height of the negative peak.

Fig. 3B through E similarly show the synaptic currents, excitatory and inhibitory conductances evoked by a tone in the other 4 neurons. The 4 tone frequencies and intensities were 1 kHz and 60 dB, 1.4 kHz and 70 dB; 1.2 kHz and 60 dB; and 22 kHz and 40 dB respectively. The 4 neurons were 670 μm, 474 μm, 570 μm and 630 μm deep

respectively. The 5 cases all show current and conductance time courses which are qualitatively similar, except that in some cases, the start of the inhibitory conductance rather than coming a few milliseconds after the start of the excitatory conductance, appears to be almost coincident with it. The neuron of Fig. 3C was the only other neuron that had a negative peak like that of the neuron of Fig. 3A; its negative peak causes an uncertainty in the start times of its excitatory and inhibitory conductances of 3 ms. There are probably voltage-clamp errors of similar magnitude in all neurons. We therefore estimate the uncertainty in the start times of the excitatory and inhibitory conductances of the neurons of Fig. 3B, D and E to be between 1 and 3 ms.

Table 1 gives the resting and peak amplitudes of each conductance, and the times in its rising and falling phases when it was at 47.5% and 95% of its peak amplitude. As the respective excitatory and inhibitory reversal potentials of 0 mV and -70 mV used to derive the conductances of Fig. 3 are approximate, the amplitudes and times obtained with inhibitory reversal potentials of -60 mV or -80 mV are also shown in Table 1. Assuming different reversal potentials affects the amplitudes of each excitatory and inhibitory conductance and the (peak normalized) falling phase of each excitatory conductance; it hardly affects either the rising phase of each excitatory conductance, or the full time course of each inhibitory conductance. The considerable uncertainty in the falling phase of each excitatory conductance may be because the NMDA current, whose nonlinearity we have only approximately taken into account, contributes more significantly to the falling phase of the excitatory current. There is no similar uncertainty in each inhibitory conductance, although each inhibitory conductance overlaps the falling

phase of an excitatory conductance; this is probably because the inhibitory conductance is much larger than the excitatory conductance during its falling phase.

Indeed, the most salient feature of the conductances of Fig. 3 is that the inhibitory conductances last much longer than the excitatory. This was generally true. Across 39 neurons, the time courses of tone-evoked and noise-evoked synaptic conductances were similar; the excitatory conductance evoked by CF tones or noise at 60 dB began 12 ± 3 ms after tone onset, and lasted 48 ± 35 ms. In 14 neurons, the inhibitory conductance evoked by CF tones or noise at 60 dB lasted until 215 ± 52 ms after tone onset. The inhibitory conductance can therefore account for the long-lasting hyperpolarization or suppression of spontaneous activity lasting until 184 ms after tone onset on average.

A second feature of the conductances of Fig. 3 is that the inhibitory conductances have substantial temporal overlap with the excitatory conductances. This shows that inhibitory conductance also shapes the depolarization. To examine this shaping, we have estimated the membrane potential responses that the conductances would produce

Fig. 4, shows the membrane potential responses estimated with excitatory and inhibitory conductances taken into account in black; while those estimated with the excitatory conductances taken into account, but not the inhibitory, are grey. They were estimated by assuming that the membrane capacitance could be neglected, and that the membrane potential responds so quickly to any synaptic conductance change that it is always instantaneously in equilibrium. The resting conductances in Table 1 were used; the resting potential was assumed to be -60 mV; the reversal potentials of the excitatory and inhibitory conductances were assumed to be 0 mV and -70 mV respectively. Comparison of the black and grey traces shows that the temporal overlap of the inhibitory

conductance with the excitatory conductance often reduces the amplitude of the depolarization (Fig. 4A, B, D, E), and is essential for the brevity of the depolarization, as it always reduces the depolarization's duration closer to the observed average of 53 ms (Fig. 4A-E).

The long-lasting hyperpolarization visible in some of the estimated membrane potentials (Fig. 4B, C, E) illustrates the ability of the falling phases of the inhibitory conductances to account for the long-lasting hyperpolarizations and suppressions of spontaneous activity. Overall, the estimated membrane potential responses show that the synaptic conductances can account for the gross time course of those typically measured.

TRFs of excitatory and inhibitory synaptic conductances

The TRFs of the currents are shown in Fig. 5; the TRFs of the conductances are shown in Fig. 6. As expected, the TRFs of the excitatory conductances (Fig. 6, column 1) are V-shaped, as spike and membrane potential TRFs typically are. The TRFs of the inhibitory conductances (Fig. 6, column 2) are also V-shaped, with the same frequency tuning as the excitatory conductances. Furthermore, tones of all frequencies and intensities capable of evoking responses cause an increase of excitatory synaptic conductance, followed by an increase of inhibitory synaptic conductance, as was shown in Fig. 3 for selected tones. In fact, the time courses of the conductances are similar for all tones; only their amplitudes change, with the peak amplitude of the excitatory conductance covarying with the peak amplitude of the inhibitory conductance (Fig. 6). In other words, to first approximation, the TRFs are frequency-time and intensity-time separable.

However, deviations from frequency-time and intensity-time separability are revealed upon examination of the TRFs of the peak amplitudes, the time in the rising phase of the excitatory conductance at which it was at 95% of its peak amplitude ('excitatory conductance latency'), and the time in the falling phase of the inhibitory conductance at which it was at 47.5% of its peak amplitude ('inhibitory conductance duration'). These parameters are little affected by the errors discussed above. Although also little affected by these errors, the TRFs of the times at which the inhibitory conductance was at 95% of its peak were not plotted, because the inhibitory peak is broad and near 95% of its peak for a long time. Again, it may be seen that the peak amplitudes of the excitatory and inhibitory conductances covary (Fig. 7, columns 1 and 2). The peak amplitudes (Fig. 7, columns 1 and 2) increase as the intensity of a CF tone increases, as the spike response strength is known to do (e.g. Fig. 1C, 2C). The excitatory conductance latency (Fig. 7, column 3) decreases as the intensity of a CF tone increases, as the first-spike latency is known to do (e.g. Fig. 1D, 2D). There are also systematic changes in the excitatory conductance latency and inhibitory conductance duration with tone frequency (Fig. 7, columns 3 and 4). These non-uniformities in the TRFs of the excitatory conductance latency and inhibitory conductance duration are deviations from frequency-time and intensity-time separability (Fig. 7, columns 3 and 4). In some neurons, the inhibitory conductance duration appears to covary with the peak amplitudes, with longer durations corresponding to larger amplitudes (Fig 7B and D, columns 2 and 4).

Discussion

We have shown that tones evoke an increase of excitatory synaptic conductance, followed by an increase of inhibitory synaptic conductance, in AI of the pentobarbital-anesthetized rat. The synaptic conductances can account for the gross time course of the typical membrane potential responses. Intrinsic conductances will further shape membrane potential responses by determining, for example, whether the gross time course results in a single spike or a burst of spikes, and will contribute additional long-lasting inhibition (McCormick et al. 1985; Schwindt et al. 1989, 1992).

In this work, we have assumed that neurons are isopotential, and that a pipette at the cell body would be able to hold the cell body and the dendrites at the same potential. If neurons have extensive, non-isopotential dendrites that are passive, and if the excitatory and inhibitory inputs due to different tones are evenly distributed over the dendrites, then violation of the isopotentiality assumption might result in underestimation of the synaptic conductances (relative to the apparent resting conductance) and the ratio of synaptic inhibition to excitation; a distortion of the fastest portions of the synaptic conductances will also occur; the frequency and intensity tuning of the excitatory and inhibitory inputs will probably be preserved, as well as their gross time courses. However, anatomical data suggests that excitatory and inhibitory input is not uniformly distributed over the dendrites, with most inhibitory inputs to neocortical pyramidal neurons lying close to the cell body; in this case, the ratio of synaptic inhibition to excitation might be overestimated. More complex distributions of synaptic input in the dendrites will lead to other errors. Problems also arise because dendrites are not passive; active dendrites with voltage-sensitive conductances can magnify small fluctuations in

the clamping voltage. An estimation of the contribution of such conductances requires knowledge of their location, as well that of the synaptic input, in the dendrites. If dendritic processing is important, a neuron cannot be modelled as isopotential. In this work, we have made the assumption of isopotentiality twice: once in obtaining the conductances, and once in obtaining the estimated membrane potentials. Since the estimated membrane potentials are reasonable, it appears that the two assumptions of isopotentiality are consistent with each other, and reasonable. Nonetheless the deviation of real neurons from isopotentiality must be kept in mind (Häusser et al, 2000; Segev and London 2000; Meunier and Segev 2002).

Similar results have been obtained recently by Wehr and Zador (2003). They showed that tones evoke synaptic excitation. Synaptic inhibition follows shortly after the onset of the synaptic excitation, and temporally overlaps it to ensure a brief depolarization. Synaptic inhibition also had the same frequency tuning as synaptic excitation. However, the durations of the synaptic inhibition they observed were shorter than what we observed. This is probably because they anesthetized rats with ketamine, whereas we used pentobarbital, which increases the duration of synaptic inhibition (Nicoll et al. 1975). A second explanation might be that they used young rats whose ages ranged from P17 to P24, whereas we used 3 month-old adult rats; it is intriguing, and plausible that the duration of synaptic inhibition is different between rats of those two age groups, as it is known that they differ in tonotopy and plasticity (Chang and Merzenich, 2003; Zhang et al. 2001, 2002). Since Wehr and Zador (2003) recorded in the auditory cortex, but not necessarily AI, another explanation might be that most of their recordings were made in a different part of the auditory cortex. For these reasons, it is unclear

whether the long-lasting hyperpolarizations or suppressions of spontaneous activity that have been observed in awake and ketamine-anesthetized animals (De Ribaupierre et al. 1972; Volkov and Galazjuk 1991, 1992) are due to the same synaptic inputs as those in pentobarbital-anesthetized animals (Ojima and Murakami 2002).

Temporal shaping of spike responses by cortical inhibition

Our data indicate that tone-evoked synaptic inhibition contributes to two forms of adaptation, which is a decrease in the ability of a neuron to respond to sound due to previous sound exposure. First, tone-evoked synaptic inhibition, being essential for the brevity of the depolarization, helps ensure that the neuron spikes only in response to the tone onset, but not the remainder of the tone duration (Fig. 4). Second, the long falling phase of the inhibitory conductance, which can account for the hyperpolarization that typically follows the depolarization, reduces the ability of the neuron to spike in response to a second tone (Fig. 4B, C, E).

Cortical synaptic inhibition thus helps generate the increasing amount and duration of adaptation present in successive auditory neural stages from the auditory nerve to AI, and which may be ultimately manifested in forward masking. Forward masking is a perceptual phenomenon in which a tone causes a reduction in the listener's ability to hear subsequent tones. Forward masking is so robust a perceptual phenomenon that it can be used by the MPEG digital file format to store sounds compactly (Painter and Spanias 2000). The increasing adaptation of the successive stages is important for explaining forward masking, as the adaptation of the auditory nerve is insufficient to explain it (Eggermont 2001; Frisina 2001; Langner 1992; Phillips et al. 2002; Relkin and

Turner 1988). Interestingly, the synaptic inhibition we observed had durations of 100 – 200 ms, similar to the durations of the adaptation observed in the spike responses of AI neurons, and of forward masking (Brosch and Schreiner 1997; Calford and Semple 1995; Moore 2003). Adaptation generally permits a system to ignore the constant, less immediately relevant aspects of its surroundings, and frees it to better deal with the changing, more immediately relevant aspects (Phillips and Hall 1992; Ulanovsky et al. 2003). Constancy and change, however, are relative concepts, and have meaning only with respect to a given time scale. The build-up of adaptation in successive neural stages may be to provide multiple time scales of adaptation which correspond to the multiple time scales on which aural features occur (Atzori et al. 2001; Fairhall et al. 2001; Risset 1991; Kronland-Martinet and Grossmann 1991). Adaptation can also explain a stream segregation phenomenon in which two tones of different frequencies are perceptually grouped into a single stream when alternated at a low rate, but are perceptually divided into two streams when alternated at a high rate (Fishman et al. 2001).

Frequency shaping of spike responses by cortical inhibition

Our data also indicate that tone-evoked synaptic inhibition sharpens the frequency tuning of the spike responses of AI neurons. The temporal overlap of tone-evoked synaptic inhibition with tone-evoked synaptic excitation often reduces the amplitude of the depolarization that would be produced by synaptic excitation alone (Fig. 4A, B, D, E). If this is the case for all tone frequencies, tone-evoked synaptic inhibition will result in the range of frequencies capable of causing suprathreshold depolarization being narrower than that resulting from tone-evoked synaptic excitation alone. Previous

pharmacological work has shown that cortical synaptic inhibition sharpens the frequency tuning of the spike responses of AI neurons; as all cortical synaptic inhibition was pharmacologically blocked in those studies, whether the sharpening is due to continually present spontaneous synaptic inhibition, or to tone-evoked synaptic inhibition has not been determined (Wang et al. 2000, 2002).

Implications for cortical circuitry

Our recordings were made within layers III to V. Layers III and IV are the major thalamo-recepient layers of AI. The tone-evoked synaptic excitation which we measured might therefore be provided by frequency-tuned, monosynaptic excitatory thalamic input onto the cortical neuron. The temporally-delayed synaptic inhibition might be provided by the same thalamic input, disynaptically relayed by inhibitory cortical interneurons (Cruikshank et al. 2002). Other possibilities involving recurrent cortical circuitry also exist. As discussed above, the long duration of the synaptic inhibition may be due to the pentobarbital anesthesia we used. It would also be consistent with the long time that GABA-B receptors take to close (Connors et al. 1988); however, cesium in our pipette probably blocked most of the GABA-B receptors. Another possibility is that the synaptic inhibition is due to inhibitory cortical interneurons which fire at a considerable delay after the end of the stimulus.

Although onset-only responses are the most common type of response in AI of the anesthetized animal, other types of responses have been observed. For example, neurons that fire throughout the duration of the stimulus have been observed in layers V and VI (Volkov and Galazjuk 1991). Such neurons presumably lack synaptic inhibition at the

tone frequencies and intensities which evoke spiking. Interestingly, there is evidence to suggest that neurons in layer II also lack long-lasting synaptic inhibition at the tone frequencies and intensities which evoke spiking (Ojima and Murakami 2002). These and other studies (Atzori et al 2001; Hefti and Smith 2000, 2003; Martinez et al 2002; Monier et al 2003) indicate that patterns of tone-evoked synaptic excitation and inhibition other than what we have reported are probably found in AI, particularly outside its major thalamo-recepient layers.

Acknowledgements

This work was supported by the Hearing Research Institute (M. M. Merzenich and C. E. Schreiner), a Howard Hughes Medical Institute Predoctoral Fellowship (to A. Y. Y. Tan), the John C. and Edward Coleman Fund to C. E. Schreiner and M. M. Merzenich, National Institutes of Health Grants DC-02260 to C. E. Schreiner and NS-10414 to M. M. Merzenich, a National Organization for Hearing Research Foundation research award to L. I. Zhang, and the Sooy Fund to M. M. Merzenich. We thank C. Atencio, M. Caywood, K. Imaizumi, T. Lauritzen, and K. Miller for discussions.

References

Anderson JS, Carandini M, and Ferster D. Orientation tuning of input conductance, excitation, and inhibition in cat primary visual cortex. J Neurophysiol 84: 909-26, 2000.

Atzori M, Lei S, Evans DI, Kanold PO, Phillips-Tansey E, McIntyre O, and McBain CJ. Differential synaptic processing separates stationary from transient inputs to the auditory cortex. Nat Neurosci 4: 1230-7, 2001.

Borg-Graham LJ, Monier C, and Fregnac Y. Visual input evokes transient and strong shunting inhibition in visual cortical neurons. Nature 393: 369-73, 1998.

Bormann J, Hamill OP, Sakmann B. Mechanism of anion permeation through channels gated by glycine and gamma-aminobutyric acid in mouse cultured spinal neurones. J Physiol 385:243-86, 1987.

Brosch M and Schreiner CE. Time course of forward masking tuning curves in cat primary auditory cortex. J Neurophysiol 77: 923-943, 1997.

Brugge JF, Dubrovsky NA, Aitkin LM, Anderson DJ. Sensitivity of single neurons in auditory cortex of cat to binaural tonal stimulation: effects of varying interaural time and intensity. J Neurophysiol 32: 1005-1024, 1969.

Calford MB and Semple MN. Monaural inhibition in cat auditory cortex. J Neurophysiol 73: 1876-1891, 1995.

Chang EF and Merzenich MM. Environmental noise retards auditory cortical development.
Science 300:498-502, 2003.

Connors BW, Malenka RC, and Silva LR. Two inhibitory postsynaptic potentials, and GABAA and GABAB receptor-mediated responses in neocortex of rat and cat. J Physiol 406:443-468, 1988.

Cruikshank SJ, Rose HJ, and Metherate R. Auditory thalamocortical synaptic transmission in vitro. J Neurophysiol 87: 361-384, 2002.

Davson H and Segal MB. Physiology of the CSF and Blood-Brain Barriers. Boca Raton: CRC Press, 1996.

De Ribaupierre F, Goldstein MH Jr, and Yeni-Komshian G. Intracellular study of the cat's primary auditory cortex. Brain Res 48: 185-204, 1972.

Destexhe A, Rudolph M, and Pare D. The high-conductance state of neocortical neurons in vivo. Nat Rev Neurosci 4:739-51, 2003.

DeWeese MR, Wehr M, and Zador AM. Binary Spiking in Auditory Cortex. J Neurosci 23: 7940-7949, 2003.

Douglas R and Martin K. Neocortex. In: The synaptic organization of the brain, edited by Shepherd GM. New York: Oxford University Press, 1998.

Eggermont JJ. Between sound and perception: reviewing the search for a neural code. Hear Res 157: 1-42, 2001.

Erulkar SD, Rose JE, and Davies PW. Single unit activity in the auditory cortex of the cat. Bull Johns Hopkins Hosp 99: 55-86, 1956.

Fairhall AL, Lewen GD, Bialek W, and de Ruyter Van Steveninck RR. Efficiency and ambiguity in an adaptive neural code. Nature 412: 787-792, 2001.

Fishman YI, Reser DH, Arezzo JC, and Steinschneider M. Neural correlates of auditory stream segregation in primary auditory cortex of the awake monkey. Hear Res 151:167-187, 2001.

Frisina RD. Subcortical neural coding mechanisms for auditory temporal processing. Hear Res 158: 1-27, 2001.

Games KD and Winer JA. Layer V in rat auditory cortex: projections to the inferior colliculus and contralateral cortex. Hear Res 34: 1-25, 1988.

Häusser M, Spruston N, and Stuart GJ. Diversity and dynamics of dendritic signaling. Science 290:739-44, 2000.

Hefti BJ and Smith PH. Anatomy, physiology, and synaptic responses of rat layer V auditory cortical cells and effects of intracellular GABA(A) blockade. J Neurophysiol 83: 2626-2638, 2000.

Hefti BJ and Smith PH. Distribution and kinetic properties of GABAergic inputs to layer v pyramidal cells in rat auditory cortex. J Assoc Res Otolaryngol 4: 106-21, 2003

Heil P. Auditory cortical onset responses revisited. I. First-spike timing. J Neurophysiol 77: 2616-2641, 1997a.

Heil P. Auditory cortical onset responses revisited. II. Response strength. J Neurophysiol 77, 2642-2660, 1997b.

Hestrin S, Nicoll RA, Perkel DJ, and Sah P. Analysis of excitatory synaptic action in pyramidal cells using whole-cell recording from rat hippocampal slices. J Physiol 422: 203-25, 1990.

Hille B. Ion channels of excitable membranes, 3rd edition. Sunderland, MA: Sinauer, 2001.

Hind JE. Unit activity in the auditory cortex. In: Neural Mechanisms of the Auditory and Vestibular Systems, edited by G.T. Rasmussen and W.F. Windle. Springfield, IL: C. C. Thomas, 1960.

Hirsch JA, Alonso JM, Reid RC, and Martinez LM. Synaptic integration in striate cortical simple cells. J Neurosci 18: 9517-28, 1998.

Jahr CE and Stevens CF. A quantitative description of NMDA receptor-channel kinetic behavior. J Neurosci 10: 1830-7, 1990a.

Jahr CE and Stevens CF. Voltage dependence of NMDA-activated macroscopic conductances predicted by single-channel kinetics. J Neurosci 10: 3178-82, 1990b.

Johnston D and Wu SM. Foundations of cellular neurophysiology. Cambridge, MA: MIT Press, 1995.

Katsuki Y, Watanabe T, and Maruyama N. Activity of auditory neurons in upper levels of brain of cat. J Neurophysiol 22: 603-623, 1959.

Kronland-Martinet R and Grossmann A. Application of time-frequency and time-scale methods (wavelet transforms) to the analysis, synthesis, and transformation of natural sounds. In: Representations of Musical Signals, edited by De Poli G, Piccialli A, and Roads C. Cambridge, MA: MIT Press, 1991.

Langner G. Periodicity coding in the auditory system. Hear Res 60: 115-142, 1992.

Margrie TW, Brecht M, and Sakmann B. In vivo, low-resistance, whole-cell recordings from neurons in the anaesthetized and awake mammalian brain. Pflugers Arch 444: 491-8, 2002.

Martinez LM, Alonso JM, Reid RC, and Hirsch JA. Laminar processing of stimulus orientation in cat visual cortex. J Physiol 540:321-33, 2002.

McCormick DA, Connors BW, Lighthall JW, and Prince DA. Comparative electrophysiology of pyramidal and sparsely spiny stellate neurons of the neocortex. J Neurophysiol 54:782-806, 1985.

Meunier C and Segev I. Playing the devil's advocate: is the Hodgkin-Huxley model useful? Trends Neurosci 25:558-63, 2002.

Merzenich MM, Knight PL, and Roth GL. Representation of cochlea within primary auditory cortex in the cat. J Neurophysiol 38: 231-249, 1975.

Metherate R and Ashe JH. Ionic flux contributions to neocortical slow waves and nucleus basalis-mediated activation: whole-cell recordings in vivo. J Neurosci 13: 5312-23, 1993.

Miller LM, Escabi MA, Read HL, and Schreiner CE. Functional convergence of response properties in the auditory thalamocortical system. Neuron 32: 151-60, 2001.

Monier C, Chavane F, Baudot P, Graham LJ, and Fregnac Y. Orientation and direction selectivity of synaptic inputs in visual cortical neurons: a diversity of combinations produces spike tuning. Neuron 37:663-80 (2003).

Moore BCJ. An Introduction to the Psychology of Hearing, 5th ed. Boston, MA: Academic Press, 2003, p. 107-111.

Moore CI and Nelson SB. Spatio-temporal subthreshold receptive fields in the vibrissa representation of rat primary somatosensory cortex. J Neurophysiol 80: 2882-92, 1998.

Nicoll RA, Eccles JC, Oshima T, and Rubia F. Prolongation of hippocampal inhibitory postsynaptic potentials by barbiturates. Nature 258:625-627.

Norena A and Eggermont JJ. Comparison between local field potentials and unit cluster activity in primary auditory cortex and anterior auditory field in the cat. Hear Res 166:202-13, 2002.

Ojima H and Murakami K. Intracellular characterization of suppressive responses in supragranular pyramidal neurons of cat primary auditory cortex in vivo. Cereb Cortex 12, 1079-1091, 2002.

Oonishi S and Katsuki Y. Functional organization and integrative mechanism on the auditory cortex of the cat. Jpn J Physiol 15: 342-365, 1965.

Painter T and Spanias A. Perceptual coding of digital audio. P IEEE 88: 451-513, 2000.

Phillips DP and Hall SE. Multiplicity of inputs in the afferent path to cat auditory cortex neurons revealed by tone-on-tone masking. Cereb Cortex 2: 425-433, 1992.

Phillips DP, Hall SE, and Boehnke SE. Central auditory onset responses, and temporal asymmetries in auditory perception. Hear Res 167: 192-205, 2002.

Phillips DP and Irvine DR. Responses of single neurons in physiologically defined primary auditory cortex (AI) of the cat: frequency tuning and responses to intensity. J Neurophysiol 45: 48-58, 1981.

Phillips DP and Kelly JB. Coding of tone-pulse amplitude by single neurons in auditory cortex of albino rats (Rattus norvegicus). Hear Res 37: 269-279, 1989.

Relkin EM and Turner CW. A reexamination of forward masking in the auditory nerve. J Acoust Soc Am 84: 584-91, 1988.

Risset JC. Timbre analysis by synthesis: representations, imitations, and variants for musical composition. In: Representations of Musical Signals, edited by De Poli G, Piccialli A, and Roads C. Cambridge, MA: MIT Press, 1991.

Sally SL and Kelly JB. Organization of auditory cortex in the albino rat: sound frequency. J Neurophysiol 59: 1627-1638, 1988.

Schwindt PC, Spain WJ, and Crill WE. Long-lasting reduction of excitability by a sodium-dependent potassium current in cat neocortical neurons. J Neurophysiol 61:233-44, 1989.

Schwindt PC, Spain WJ, and Crill WE. Calcium-dependent potassium currents in neurons from cat sensorimotor cortex. J Neurophysiol 67:216-26, 1992.

Segev I and London M. Untangling dendrites with quantitative models. Science 290:744-50, 2000.

Ulanovsky N, Las L, and Nelken I. Processing of low-probability sounds by cortical neurons. Nat Neurosci 6: 391-398, 2003.

Volkov IO and Galazjuk AV. Formation of spike response to sound tones in cat auditory cortex neurons: interaction of excitatory and inhibitory effects. Neuroscience 43: 307-321, 1991.

Volkov IO and Galazyuk AV. Peculiarities of inhibition in cat auditory cortex neurons evoked by tonal stimuli of various durations. Exp Brain Res 91: 115-120, 1992.

Wang J, Caspary D, and Salvi RJ. GABA-A antagonist causes dramatic expansion of tuning in primary auditory cortex. Neuroreport 11: 1137-1140, 2000.

Wang J, McFadden SL, Caspary D, and Salvi R. Gamma-aminobutyric acid circuits shape response properties of auditory cortex neurons. Brain Res 944: 219-231, 2002.

Wehr M and Zador AM. Balanced inhibition underlies tuning and sharpens spike timing in auditory cortex. Nature 426:442-446, 2003.

Winer JA. The functional architecture of the medial geniculate body and the primary auditory cortex. In: The Mammalian Auditory Pathway, edited by Webster DB, Popper AN, and Fay RR. New York: Springer-Verlag, 1992.

Zhang LI, Bao S, Merzenich MM. Persistent and specific influences of early acoustic environments on primary auditory cortex. Nat Neurosci 4:1123-30, 2001.

Zhang LI, Bao S, and Merzenich MM. Disruption of primary auditory cortex by synchronous auditory inputs during a critical period. Proc Natl Acad Sci USA 99:2309-2314, 2002.

Zhang LI, Tan AYY, Schreiner CE, and Merzenich MM. Topography and synaptic shaping of direction selectivity in primary auditory cortex. Nature 424: 201-205, 2003.

Zhu JJ and Connors BW. Intrinsic firing patterns and whisker-evoked synaptic responses of neurons in the rat barrel cortex. J Neurophysiol 81: 1171-83, 1999.

FIG. 1. Spike responses. A: 3 responses, each evoked by a 9 kHz, 75 dB tone. The horizontal bar under each response represents the timing of the tone relative to the response. Horizontal scale: 25 ms; vertical scale: 50 pA. B: TRF. Horizontal scale: 50 ms; vertical scale: 200 pA. C: Number of spikes in 3 repetitions of a CF tone, as a function of tone intensity. D: Average first-spike latency for 3 repetitions of a CF tone, versus tone-intensity.

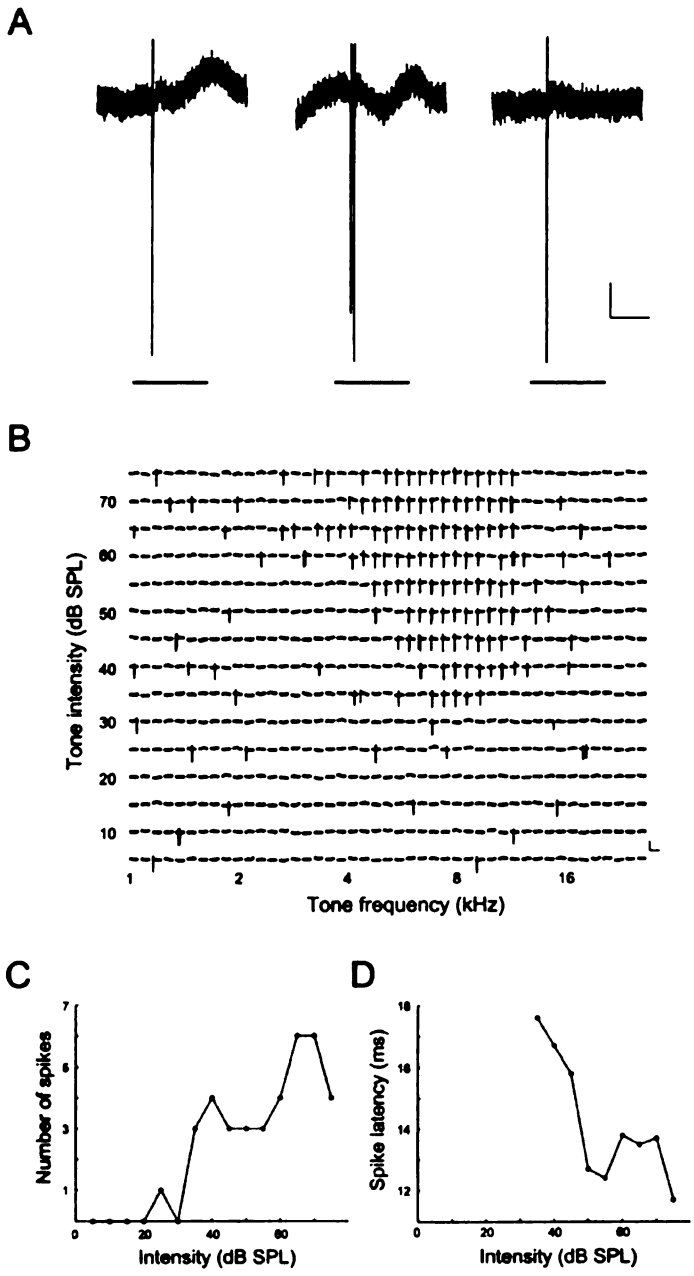
A
B
Tone intensity (dB SPL)
70
60
50
40
30
20
10
1
2
4
8
16
Tone frequency (kHz)
C
Number of spikes
7
6
3
1
0
20
40
60
Intensity (dB SPL)
D
Spike latency (ms)
18
16
14
12
0
20
40
60
Intensity (dB SPL)

Figure 1

FIG. 2. Membrane potential responses. A: 3 responses, each evoked by a 20 kHz, 75 dB tone. The horizontal bar under each response represents the timing of the tone relative to the response. B: TRF. Spikes have been truncated to display subthreshold responses more clearly. Horizontal scale: 40 ms; vertical scale: 40 mV. C: Number of spikes in 6 repetitions of a CF tone, as a function of tone intensity. D: Average first spike-latency for 6 repetitions of a CF tone, versus tone-intensity.

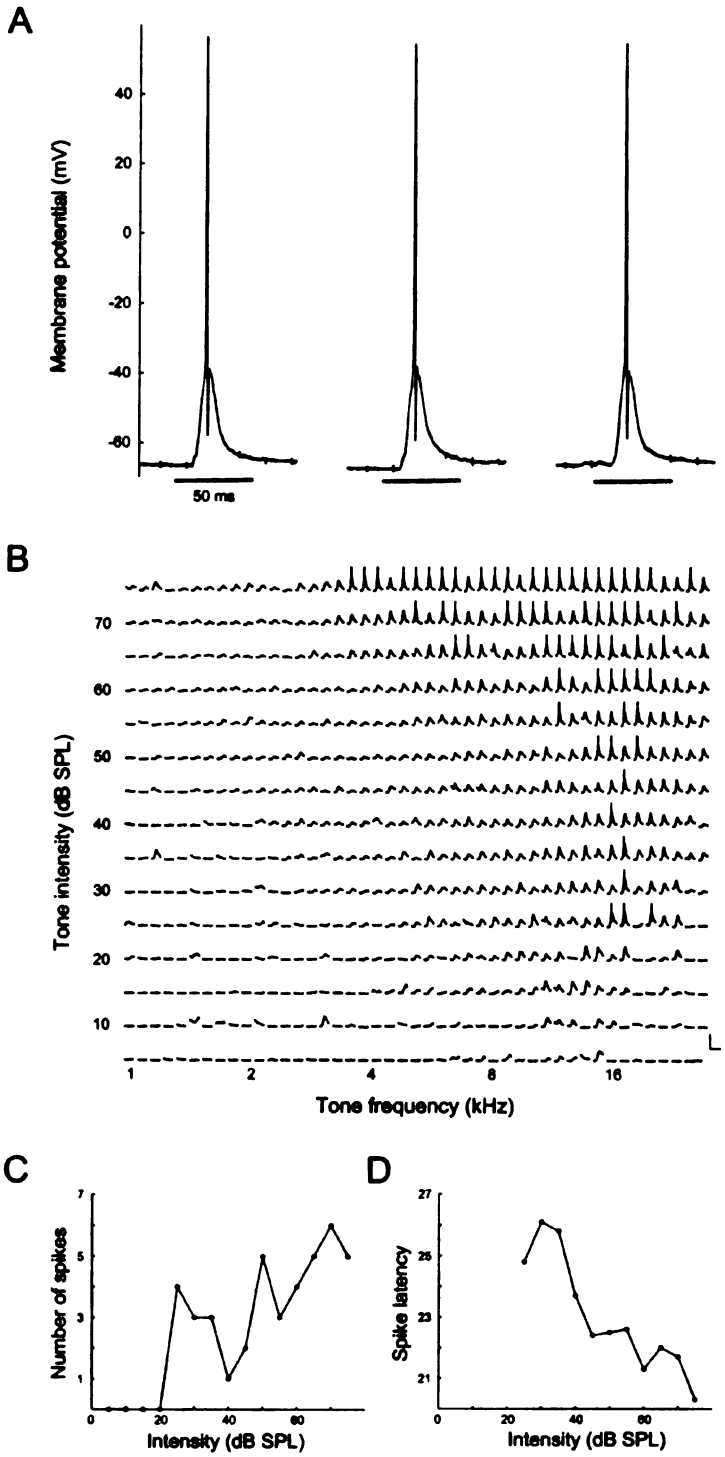
A
Membrane potential (mV)
40
20
0
-20
-40
-60
50 ms
B
Tone intensity (dB SPL)
70
60
50
40
30
20
10
1
2
4
8
16
Tone frequency (kHz)
C
Number of spikes
7
5
3
1
0
20
40
60
Intensity (dB SPL)
D
Spike latency
27
25
23
21
0
20
40
60
Intensity (dB SPL)

Figure 2

FIG. 3. Synaptic currents and conductances. A - E are each from a different neuron. Column 1: 3 superimposed tone-evoked synaptic currents at -70 mV. Column 2: 3 superimposed tone-evoked synaptic currents at -30 mV. Column 3. Superimposed averages of the currents in the column 1(black) and 2 (grey). Column 4. Excitatory (black) and inhibitory (grey) conductances from the currents in column 3.

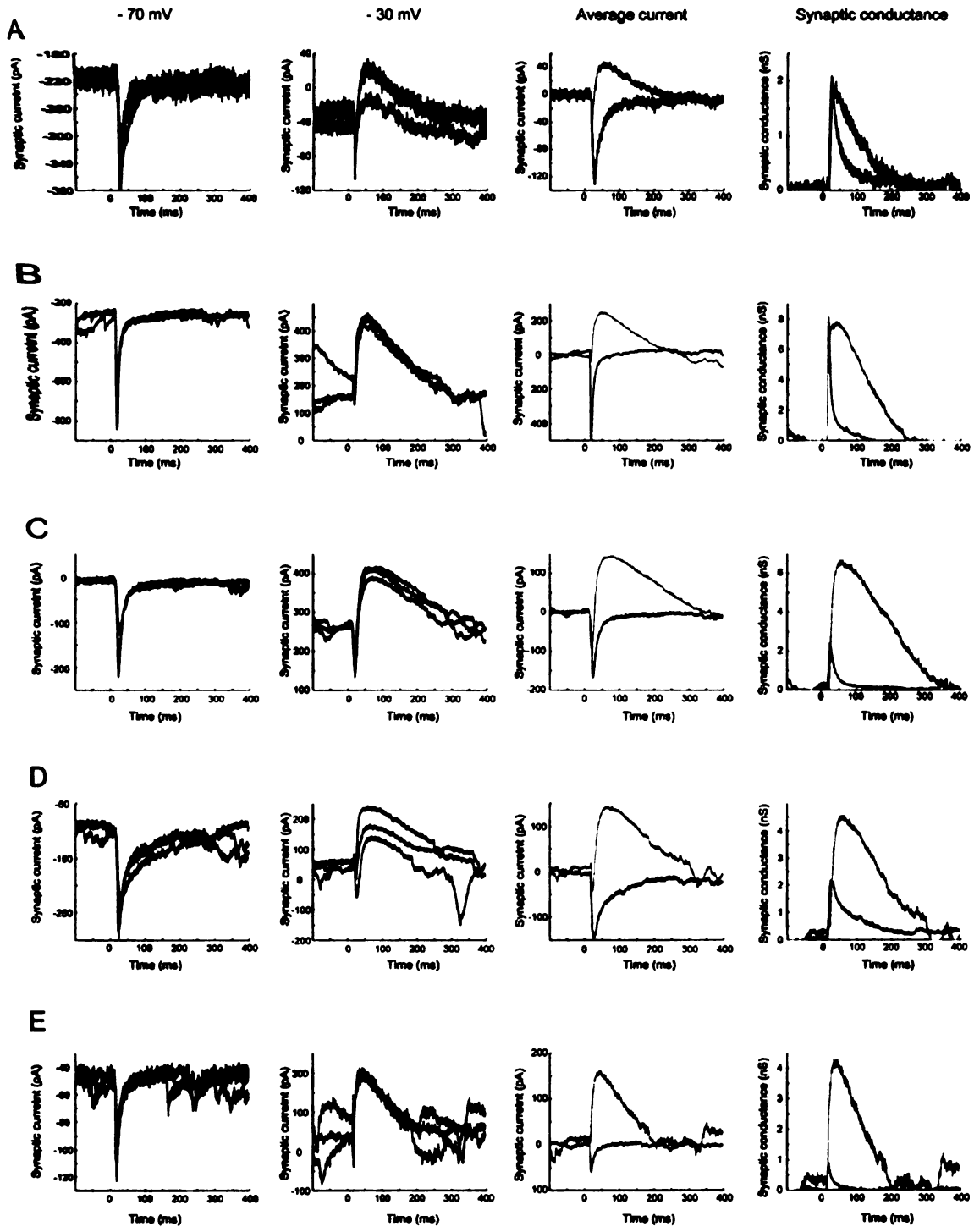
A
B
C
D
E
- 70 mV
- 30 mV
Average current
Synaptic conductance
Synaptic current (pA)
Synaptic conductance (nS)
Time (ms)

Figure 3

FIG. 4. Estimated membrane potentials. The neurons of Fig. 4A - E correspond to those of Fig. 3A – E respectively. Estimated membrane potentials with excitatory and inhibitory conductances taken into account (black), and with only excitatory conductances taken into account (grey).

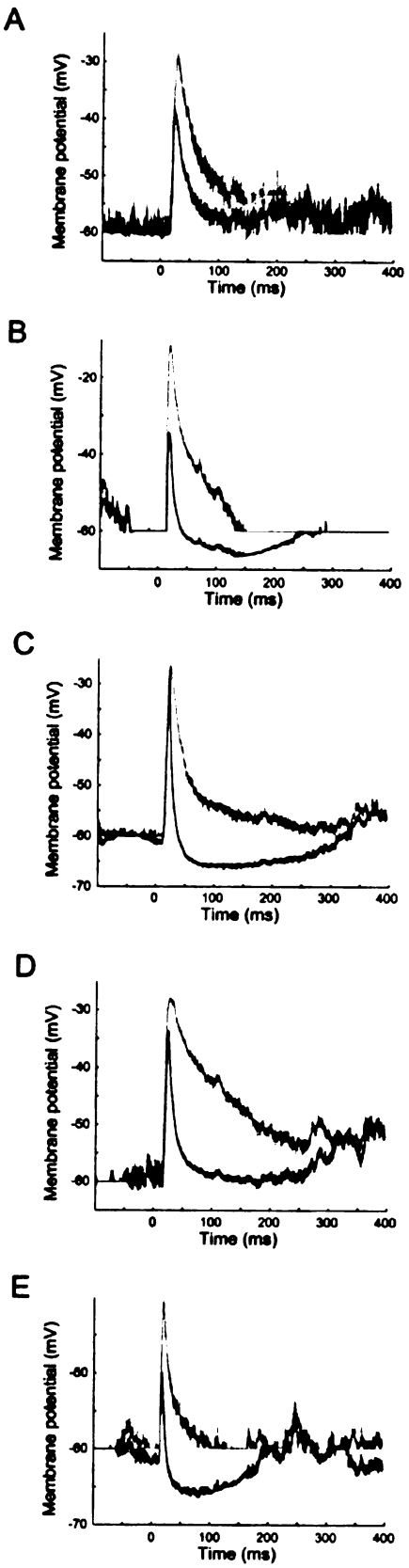
A
Membrane potential (mV)
-30
-40
-50
-60
0
100
200
300
400
Time (ms)
B
Membrane potential (mV)
-20
-40
-60
0
100
200
300
400
Time (ms)
C
Membrane potential (mV)
-30
-40
-50
-60
-70
0
100
200
300
400
Time (ms)
D
Membrane potential (mV)
-30
-40
-50
-60
0
100
200
300
400
Time (ms)
E
Membrane potential (mV)
-50
-60
-70
0
100
200
300
400
Time (ms)

Figure 4

FIG. 5. TRFs of synaptic currents. The neurons of Fig. 5A - E correspond to those of Fig. 3A – E respectively. Left panels: TRFs of synaptic currents at -70 mV. Right panels: TRFs of synaptic currents at -30 mV. Vertical scale bar: 105 pA (A, left panel); 85 pA (A, right panel); 468 pA (B, left); 300 pA (B, right); 145 pA (C, left); 238 pA (C, right); 169 pA (D, left); 184 pA (D, right); 60 pA (E, left); 210 pA (E, right). Horizontal scale bar: 100 ms (left panels); 400 ms (right panels).

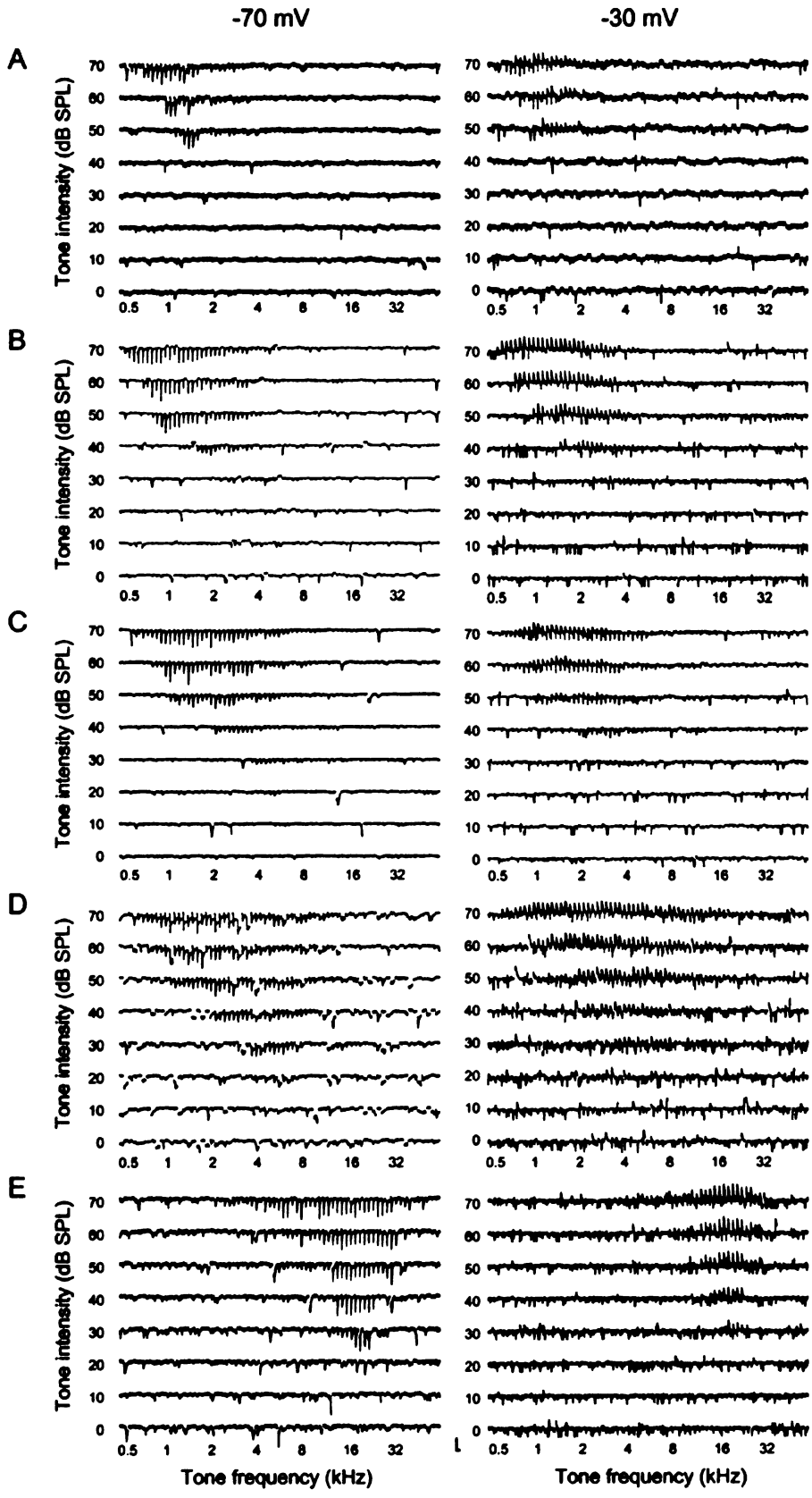
-70 mV
-30 mV
A
B
C
D
E
Tone intensity (dB SPL)
70
60
50
40
30
20
10
0
0.5
1
2
4
8
16
32
Tone frequency (kHz)

Figure 5

FIG. 6. TRFs of synaptic conductances. The neurons of Fig. 6A - E correspond to those of Fig. 3A – E respectively. Left panel: excitatory conductances. Right panel: inhibitory conductances. Vertical scale bar: 1.1 nS (A, left panel); 1.4 nS (A, right panel); 4.8 nS (B, left); 5 nS (B, right); 1.6 nS (C, left panel); 2.6 nS (C, right); 1.9 nS (D, left); 3.5 nS (D, right); 0.8 nS (E, left); 3.9 nS (E, right). Horizontal scale bar: 100 ms (left panels); 400 ms (right panels).

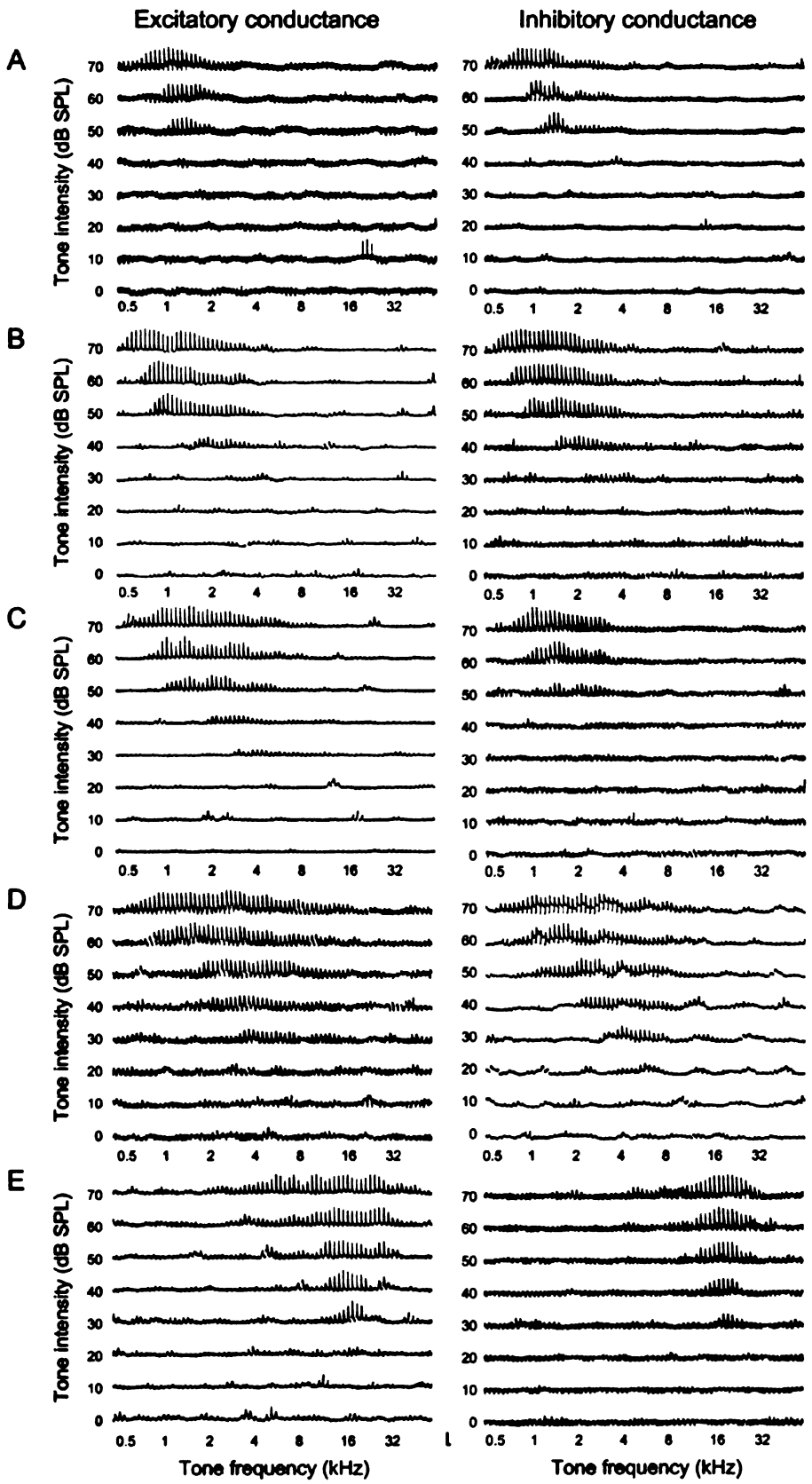
Excitatory conductance
Inhibitory conductance
A
B
C
D
E
Tone intensity (dB SPL)
70
60
50
40
30
20
10
0
0.5
1
2
4
8
16
32
Tone frequency (kHz)

Figure 6

FIG. 7. TRFs of parameters. The neurons of Fig. 7A - E correspond to those of Fig. 3A - E respectively. Column 1: TRF of excitatory conductance peak amplitude. Column 2: TRF of inhibitory conductance peak amplitude. Column 3: TRF of time in rising phase of the excitatory conductance at which it was at 95% of its peak amplitude ('excitatory conductance latency'). Column 4: TRF of time in falling phase of inhibitory conductance at which it was at 47.5% of its peak amplitude ('inhibitory conductance duration').

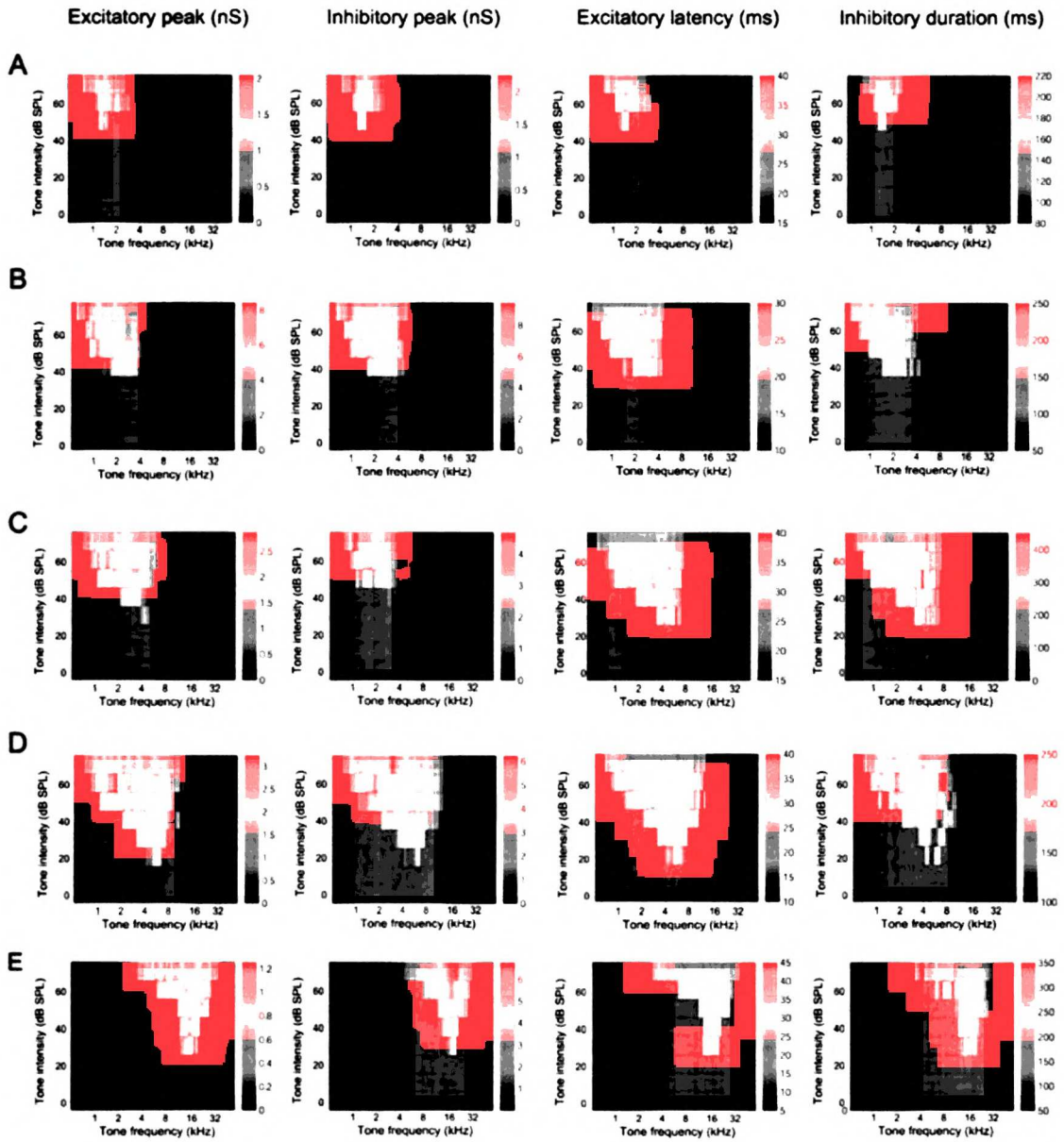
Excitatory peak (nS)
Inhibitory peak (nS)
Excitatory latency (ms)
Inhibitory duration (ms)
A
B
C
D
E
Tone intensity (dB SPL)
Tone frequency (kHz)

Figure 7

TABLE 1. Parameters of the excitatory and inhibitory conductances of Fig. 3. The neurons of rows A – E correspond to those of Fig. 3A - E respectively. All times are given with respect to the tone onset. In each cell, the unbracketed value is obtained with an inhibitory reversal potential of -70 mV; the first and second bracketed values are obtained with inhibitory reversal potentials of -60 mV and -80 mV respectively.

Table 1

	Resting conductance (nS)	Excitatory peak (nS)	Time for excitation to rise to 47.5% of peak (ms)	Time for excitation to rise to 95% of peak (ms)	Time for excitation to fall to 95% of peak (ms)	Time for excitation to fall to 47.5% of peak (ms)	Inhibitory peak (nS)	Time for inhibition to rise to 47.5% of peak (ms)	Time for inhibition to rise to 95% of peak (ms)	Time for inhibition to fall to 95% of peak (ms)	Time for inhibition to fall to 47.5 of peak (ms)
A	4.3	2.1 (1.8) (2.3)	21.8 (20.8) (21.9)	27.5 (25.8) (27.4)	28.8 (28.7) (28.9)	47.7 (41.0) (51.7)	2.0 (2.3) (1.8)	24.8 (24.8) (24.8)	36.6 (36.6) (36.6)	41.0 (41.0) (41.0)	122.0 (122.0) (122.0)
B	11.3	8.1 (7.0) (8.9)	16.1 (16.2) (16.1)	18.0 (18.0) (18.0)	19.9 (19.9) (19.9)	25.2 (23.8) (26.5)	7.9 (9.2) (6.9)	15.9 (15.9) (15.9)	25.7 (25.7) (25.7)	57.4 (57.4) (57.4)	138.4 (138.4) (138.4)
C	7.0	2.4 (2.3) (2.6)	19.8 (18.2) (20.5)	22.9 (22.0) (23.4)	25.6 (24.0) (26.9)	36.0 (29.5) (63.1)	6.7 (7.8) (5.9)	27.2 (27.2) (27.2)	44.3 (44.3) (44.3)	86.5 (86.5) (86.5)	214.3 (214.3) (214.3)
D	3.6	2.2 (2.0) (2.5)	20.2 (20.4) (20.2)	24.6 (24.1) (28.0)	33.5 (27.1) (34.9)	74.8 (40.2) (100.1)	4.6 (5.3) (4.0)	29.2 (29.2) (29.2)	45.8 (45.8) (45.8)	82.6 (82.6) (82.6)	184.8 (184.8) (184.8)
E	1.9	0.9 (0.6) (1.2)	16.5 (16.2) (16.6)	18.7 (18.0) (19.4)	20.3 (18.8) (20.9)	27.8 (21.6) (63.5)	4.3 (5.0) (3.8)	19.2 (19.2) (19.2)	31.5 (31.5) (31.5)	50.9 (50.9) (50.9)	122.8 (122.8 (122.8)

Chapter 4

Unbalanced synaptic inhibition can create intensity-tuned auditory cortex neurons

Abstract

Intensity-tuned auditory cortex neurons may be formed by intensity-tuned synaptic excitation. Synaptic inhibition has also been shown to enhance, and possibly even create intensity-tuned neurons. Here we show, using in vivo whole cell recordings in pentobarbital-anesthetized rats, that some intensity-tuned neurons are indeed created solely through disproportionally large inhibition at high intensities, without any intensity-tuned excitation. Since inhibition is essentially cortical in origin, these neurons provide examples of auditory feature-selectivity arising de novo at the cortex.

Introduction

The intensity of a sound is often behaviourally important. For example, it can convey the distance of a sound source, or prosodic information in speech and music. Most auditory cortex neurons have monotonic spike rate versus sound intensity functions; they encode sound intensity by increasing spike rate as sound intensity is increased. A different encoding strategy, however, is used by the intensity-tuned neurons whose spike rates are nonmonotonic functions of sound intensity: their spike rate initially increases

and peaks as sound intensity is increased, then decreases as sound intensity is further increased (Phillips et al 1985; Phillips and Kelly 1989). The number of intensity-tuned auditory cortex neurons increases in rats trained to perform a task requiring fine intensity discrimination, which suggests that intensity-tuned neurons are required for sound intensity to be precisely encoded (Polley et al 2004).

Central inhibition is required for the formation of intensity-tuned neurons, as there are no intensity-tuned neurons at the auditory periphery. However, there are intensity-tuned neurons at subcortical auditory stations (Rhode and Smith 1986; Ding and Voigt 1997; Ding et al 1999; Davis and Young 2000; Pollak et al 1978; Ryan and Miller 1978, Palombi and Caspary 1996a, 1996b; Sivaramakrishnan et al 2004). The formation of intensity-tuned auditory cortex neurons does not therefore necessarily require cortical inhibition.

However, Ojima and Murakami's (2002) intracellular study of the cat auditory cortex described 12 'unbalanced' intensity-tuned neurons which received disproportionally large synaptic inhibition at high intensities. As Ojima and Murakami (2002) did not measure synaptic excitation and inhibition separately, they could not determine whether inhibition enhanced intensity-tuning already present in the excitation, or whether the interaction of inhibition with excitation actually created intensity-tuning that was not present in the excitation. In Wehr and Zador's (2003) intracellular study of the rat auditory cortex synaptic excitation and inhibition were separately measured. Wehr and Zador (2003) described 7 'balanced' intensity-tuned neurons which received intensity-tuned synaptic excitation and identically tuned synaptic inhibition which neither created nor enhanced intensity-tuning. The small sample size of Wehr and Zador (2003)

would not be inconsistent with unbalanced intensity-tuned neurons being present in the auditory cortex of the rat, as they are in the cat's.

We therefore performed in vivo whole cell measurements of the synaptic excitation and inhibition received by intensity-tuned auditory cortex neurons of pentobarbital-anesthetized rats. To increase the chances of obtaining in vivo whole cell recordings from intensity-tuned neurons in these rats, we increased the number of such neurons in their auditory cortices using the above mentioned training (Polley et al 2004).

Methods

Behavioural training

All experimental procedures used in this study were approved under UCSF Animal Care Facility protocols. Adult female Sprague-Dawley rats were trained as described by Polley et al (2004). Behavioural training took place in a behavioral apparatus contained within a sound-attenuating chamber. Rats were allowed to move freely on a rectangular platform (58 x 38 cm) that rested on force transducers. The rat's position in two-dimensional space was triangulated in real time according to the distribution of weight across the force transducers. A speaker suspended 44 cm above the platform continuously delivered an amplitude-modulated stimulus for the duration of a single trial. The training stimulus was a band-limited noise (0.65-octave bandwidth) with an amplitude envelope modulated by 10% at 8 Hz. For each trial, the center frequency of the band-limited noise stimulus was randomly selected from a 2.2- to 28-kHz range. The intensity of the band-limited noise was proportional to the distance between the rat and a

'bull's-eye'. For each trial, the computer pseudorandomly selected a circumscribed area on the platform to serve as the bull's eye. The rat's task, on any given trial, was to use the sound intensity cues to locate the position of the bull's-eye within 3 min to receive a pellet reward. As training progressed, the bull's-eye diameter was decreased from 10 cm to 4 cm, and the amount of time the rat was required to continuously remain within the perimeter of the bull's-eye was increased from 0 s to 1.5 s to discourage random search strategies and promote identification of the bull's-eye position through the use of sound intensity cues. Over a period of 4-7 weeks, rats demonstrated learning by decreasing their path length to the bull's-eye.

Surgery

Experiments were carried out in a sound-attenuating chamber. Each rat was anesthetized by intraperitoneal injection of sodium pentobarbital (50-80 mg/kg), with the dose adjusted to make the rat areflexic. The rat was maintained in an areflexic state for the rest of the experiment by further intraperitoneal injections of sodium pentobarbital (20-60 mg/kg) when necessary. The rat was placed on a heating pad, and its temperature was maintained at ~37°C. Prior to any skin incision, bupivacaine was injected subcutaneously at the incision site. A tracheotomy was performed to secure the airway. The head was held fixed by a custom-made device that clamped it at both orbits and the palate, leaving the ears unobstructed. A cisternal drain was performed. The right auditory cortex was exposed by retracting the skin and muscle overlying it, followed by a craniotomy and a durotomy. The cortical surface was kept moist with normal saline. The auditory cortex was coarsely mapped at 500-600 μm below the pial surface with a

parlyene-coated tungsten electrode to determine the location of intensity-tuned multiunit sites.

Whole cell recordings

A silver wire, one end of which was coated with silver chloride, served as the reference electrode against which potentials were measured; its chlorided end was inserted between the skull and the dura. The reference electrode was assigned a potential of 0 mV. The potential of the cerebrospinal fluid was assumed to be uniform and equal to that of the reference electrode.

Patch pipettes with resistances of 7 MΩ were made. Patch pipettes contained a cesium based solution that consisted of (in mM) 130 Cs-gluconate, 5 TEA-Cl, 4 MgATP. 0.3 GTP, 10 phosphocreatine, 10 HEPES, 0.2 EGTA, 5 QX-314, pH 7.3. The pia was broken by slowly lowering and raising the jagged tip of a broken pipette in and out of the cortex. An unbroken pipette was lowered into the cortex, with the pressure in the pipette greater than atmospheric. Dimpling of the cortical surface was not visually detectable. The cortical depth of the pipette tip was estimated according to the distance it had travelled. The cortex was covered with 4% agarose in normal saline. Under voltage clamp, an oscillating potential was set up at the pipette tip; the oscillating potential had a time average of –50 mV; its period was much faster than the breathing rate. The resulting current oscillation was measured. When the amplitude of the current oscillation decreased and an even slower oscillation whose period was the breathing rate of the animal became superimposed on the current oscillation, the pipette tip might be touching the cell membrane of a neuron. At this point, the pipette was slowly advanced to further

reduce the amplitude of the current oscillation. The pressure in the pipette was suddenly reduced to less than atmospheric and then returned to atmospheric. Often a giga-ohm seal would spontaneously form within 1 min; if not, additional gentle suction sometimes helped. The pipette capacitance was compensated. A pulse of reduced pressure in the pipette would often break the cell membrane and bring the recording into whole cell mode. The whole cell capacitance was compensated and the initial series resistance (25-60 MΩ) was compensated to achieve an effective series resistance of 15-30 MΩ. The input resistance was 100-400 MΩ. Signals were filtered at 5 kHz and sampled at 10 kHz. A Multiclamp 700B amplifier was used.

Stimuli

Noise bursts were delivered by a calibrated free field speaker directed toward the left ear. The intensities of the noise bursts ranged from 0 dB SPL to 80 dB SPL, and were evenly spaced over that range. Noise bursts were white, 50 ms in duration with 5 ms linear rising and falling phases.

Predicted membrane potential

The predicted membrane potential V_p was calculated using

$$C_m dV_p(t)/dt = G_r(t)(V_p(t)-E_r)+G_e(t)(V_p(t)-E_e)+G_i(t)(V_p(t)-E_i), \quad (1)$$

where E_r is the resting membrane potential, C_m is the membrane capacitance, and G_r is the resting or leak conductance, $G_e(t)$ is the excitatory synaptic conductance, and $G_i(t)$ is

the inhibitory synaptic conductance, E_e and E_i are the reversal potentials of the excitatory and inhibitory synaptic conductances respectively. Eq. 1 is a good model of the membrane voltage of cortical neurons in the absence of spiking (McCormick et al 1985; Troyer and Miller 1997). C_m was derived from the whole cell capacitance compensation procedure. $G_e(t)$ and $G_i(t)$ were derived using

$$\Delta I(t,V) = G_e(t)(V-E_e) + G_i(t)(V-E_i), \quad (2)$$

where V is the clamping voltage, $\Delta I(t,V)$ is the amplitude of the synaptic current, relative to the resting current at V. The values of E_e and E_i were set by the ionic composition of the pipette solution and the cerebrospinal fluid (Johnston and Wu 1995; Davson and Segal 1996); the value of E_i was based on the permeability of GABA-A conductances to Cl^-, but it should be noted that they also pass HCO_3^- (Bormann et al 1987). $G_e(t)$ and $G_i(t)$ were the 2 unknowns in *Eq. 1* at any particular t. Measurement of $\Delta I(t,V)$ at two different values of V yielded a system of 2 equations which could then be solved for $G_e(t)$ and $G_i(t)$ at any particular t (Borg-Graham et al. 1998; Anderson et al. 2000; Hirsch et al. 1998). Currents into the neuron were assigned a negative value. E_e and E_i were 0 mV and -70 mV respectively. The resting or leak conductance G_r was derived using

$$I_r(V)=G_r(V-E_r), \quad (3)$$

where E_r is the membrane potential, and $I_r(V)$ is the resting current. G_r and E_r were the 2 unknowns in Eq. 2. Measurement of $I_r(V)$ at two different values of V yielded a system

of 2 equations which could then be solved for G_r and E_r. We did not correct the measured membrane potential for the series resistance or the junction potential.

Results

Intensity-tuned neurons are rare in the rat auditory cortex. To increase the chances of obtaining in vivo whole cell recordings from intensity-tuned neurons, rats underwent training that increases the proportion of intensity-tuned neurons. Rats were anesthetized with pentobarbital and their auditory cortices coarsely mapped to locate intensity-tuned multiunit sites, to which whole cell recording attempts were then directed. Noise bursts ranging from 0 dB to 80 dB in 5 dB steps, with at least 10 repetitions per intensity, were used to determine intensity-tuning. The patch pipette contained cesium, TEA, and QX-314, which blocked spiking and most intrinsic conductances, and prevented them from contaminating measurements of the synaptic conductances. Because spiking was blocked, the peak membrane potential was used as gauge of spike rate. Synaptic excitation was seen as inward currents when the neuron was voltage-clamped at -70 mV, near the inhibitory reversal potential; synaptic inhibition was seen as outward currents when the neuron was clamped nearer the excitatory reversal potential. Whole cell recordings were obtained from 17 neurons at intensity-tuned multiunit sites. Unbalanced synaptic excitation and inhibition were demonstrated in 5 neurons. These 5 neurons are described below.

Responses from an unbalanced neuron are shown in Fig. 1. Figure 1A shows the average synaptic currents obtained at 45 dB and 70 dB. The inward currents representing synaptic excitation (blue traces, downward deflections) were obtained when the neuron

was clamped at -70 mV, and the outward currents representing synaptic inhibition (red traces, upward deflections) when the neuron was clamped at 0 mV. The synaptic excitation at both intensities has the same amplitude, but no synaptic inhibition is observed at 45 dB, while there is substantial synaptic inhibition at 70 dB. This suggests that synaptic inhibition would cause less depolarization of the membrane potential at 70 dB than at 45 dB, and thus contribute to some intensity tuning in this neuron. Fig. 1B shows that synaptic excitation itself is nonmonotonic, showing a distinct peak around 40 dB to 50 dB. From 60 dB to 70 dB, inhibition increases faster than excitation, suggesting that inhibition enhances the intensity-tuning of this neuron. However, from 75 dB to 80 dB, inhibition decreases as excitation increases. Thus this neuron might show 2 peaks in its intensity-tuning profile. It is also possible that the timing of the inhibition at 75 dB and 80 dB is shifted, so as to decrease the membrane depolarization at those intensities. Distinguishing these possibilities requires a record of the membrane potential, which was not obtained for this neuron.

Responses from a second, unbalanced intensity-tuned neuron are shown in Fig. 2. Fig. 2A shows the average membrane potential responses at 15 dB, 25 dB and 75 dB. The noise-evoked depolarization at 25 dB is greater than at 15 dB, but that at 75 dB is less than at 25 dB. Fig. 2B graphs the peak average membrane potential versus sound intensity. The peak average membrane potential increases to a maximum at 25 dB, then decreases above that, showing that this neuron is intensity-tuned. (Figs. 2C and 2D show the same data as Figs. 2A and 2B respectively, but with the membrane potential immediately preceding sound onset subtracted from each trace before averaging.) Fig. 2E shows the average synaptic currents obtained at 25 dB and 80 dB. When the neuron is

clamped at -70 mV the inward currents (blue traces, downward deflections) representing synaptic excitation are equal for 25 dB and 80 dB. In contrast, at -30 mV the outward current (red traces, upward deflections) representing synaptic inhibition is much greater at 80 dB than at 25 dB. The synaptic current at -30 mV at 25 dB displays an initial inward portion that represents synaptic excitation. This inward current at -30 mV is as large as the inward current at -70 mV, indicating that the excitatory conductance has a nonlinear dependence (possibly the NMDA channel) on the membrane potential. This nonlinearity might cause synaptic inhibition to be underestimated. It will not, however, affect the conclusion that synaptic excitation and inhibition are unbalanced in this neuron. This is because the inward current at -70 mV is the same at both 25 dB and 80 dB, indicating that the excitatory conductance is the same at both intensities. Thus, the nonlinearity observed in the synaptic current at -30 mV should be present in equal amounts for both 25 dB and 80 dB. Unlike the synaptic current at -30 mV at 25 dB, there is almost no indication of the nonlinearity in the synaptic current at -30 mV at 80 dB because the synaptic current is disproportionally very much larger. Fig. 2F graphs the peak average inward and outward currents (blue and red lines respectively) versus intensity. The magnitude of the peak average inward current reaches a maximum at 25 dB, then decreases above that. The maximum of the peak average inward current occurs at the same intensity as that of the peak average membrane potential, showing that the intensity-tuning of the membrane potential is partially present in the excitation. Yet the peak average inward current increases above 65 dB, while the peak average membrane potential decreases, showing that excitation alone cannot account for the membrane potential for intensities above 65 dB. In that intensity range, the increase with intensity

of the peak average outward current is much sharper than that of the peak average inward current. This increasing ratio of inhibition to excitation can explain the continued decrease in membrane potential above 65 dB. To confirm these points, we used the excitatory and inhibitory currents to predict the membrane potential. Fig. 2G shows example predicted membrane potential traces at 15 dB, 25 dB and 75 dB; these resemble the actual membrane potential traces at those intensities in Fig. 2A. The graph of peak predicted membrane potential versus intensity shown in Fig. 2H matches the actual curve in Fig. 2B. This neuron thus provides an example of an unbalanced intensity-tuned neuron in which synaptic inhibition enhances, but does not create intensity-tuning.

Responses from a third, unbalanced intensity-tuned neuron are shown in Fig. 3. Fig. 3A shows the average membrane potential responses at 3 intensities. The noise-evoked depolarization at 25 dB is greater than at 55 dB, but that at 80 dB is less than at 55 dB. Fig. 3B graphs the peak average membrane potential versus sound intensity. The peak average membrane potential increases to a maximum at 55 dB, then decreases above that, showing that this neuron is intensity-tuned. Fig. 3E shows the average synaptic currents obtained at 55 dB and 80 dB. At -70 mV, the inward currents representing synaptic excitation are equal for 55 dB and 80 dB. In contrast, at -20 mV the outward current representing synaptic inhibition is much greater at 80 dB than at 25 dB. Like the neuron of Fig. 2, there is thus disproportionally large inhibition at the higher intensity which will either enhance or create intensity-tuning. Fig. 3F graphs the peak average inward and outward currents versus intensity. Unlike the neuron of Fig. 2, the peak average inward current is not intensity-tuned, but increases monotonically with intensity. Therefore the intensity-tuning must be created by synaptic inhibition. The sharper

increase with intensity of the peak average outward current over that of the peak average inward current for intensities above 55 dB, produces an increasing ratio of inhibition to excitation that can explain the continued decrease in membrane potential above 55 dB. Fig. 3G shows example predicted membrane potential traces at 25 dB, 55 dB and 80 dB; these resemble the actual membrane potential traces at those intensities in Fig. 3A. The graph of peak predicted membrane potential versus intensity shown in Fig. 3H matches the actual curve in Fig. 3B. This neuron thus provides an example of an unbalanced intensity-tuned neuron in which synaptic inhibition actually creates intensity-tuning.

The responses from a fourth, unbalanced intensity-tuned neuron are shown in Fig. 4. Again, Fig 4A and 4B demonstrate that the membrane potential is intensity-tuned. (Figs. 4C and 4D show the same data as Figs. 4A and 4B respectively, but with the membrane potential immediately preceding sound onset subtracted from each trace before averaging. In this case, examining the peak membrane potential suggests, but does not confirm intensity-tuning: the curves of Fig. 4B and 4D have maxima at different intensities, indicating that the intensity at which the maximum occurs is uncertain, and suggesting that the intensity at which the minimum occurs is also uncertain. However, Fig. 4A and 4C show that the membrane potential at 80 dB, compared with that at 60 dB, clearly exhibits only the shortest depolarization, but a sustained and much greater hyperpolarization, confirming that the membrane potential is intensity-tuned.) Fig. 4E shows examples of the excitatory and inhibitory synaptic currents, showing disproportionally large inhibition at the higher intensities. Figure 4F shows that the peak average excitatory currents are monotonic, and display no intensity-tuning. Therefore the intensity-tuning must be created by synaptic inhibition. The peak average inhibitory

current does indeed increase faster from 65 dB to 70 dB. However, it increases just as quickly as the excitation from 70 dB to 80 dB, even though the membrane potential continues to decrease in that range (Fig 4B). A linear least squares fit of the peak of inhibition versus the peak of excitation yields a correlation coefficient whose square is 0.63, within the range of a balanced neuron (Wehr and Zador 2003; Zhang et al 2003). This suggests that changes in the timing of the inhibition relative to the excitation are responsible for the further decrease of the membrane potential from 70 dB to 80 dB. To test this, we used the excitatory and inhibitory currents to predict the membrane potential. Fig. 4G shows example predicted membrane potential traces at 60 dB and 80 dB; these resemble the actual membrane potential traces at those intensities in Fig. 4A. The graph of peak predicted membrane potential versus intensity is shown in Fig 4H, and resembles the actual curve of Fig 4B. The final fall-off in the peak predicted membrane potential is too small to indicate intensity-tuning. As was the case with the peak membrane potential, examining the peak predicted membrane underestimates intensity-tuning. Fig. 4G shows that the predicted membrane potential at 80 dB, compared with that at 60 dB, clearly exhibits only the shortest depolarization, but a sustained and much greater hyperpolarization, confirming that the predicted membrane potential is intensity-tuned.

Fig. 5 shows another intensity-tuned neuron. Once again, Fig. 5A and 5B demonstrate that the membrane potential is intensity-tuned. Fig. 5E shows examples of the excitatory and inhibitory synaptic currents. Fig. 5F shows that synaptic excitation is monotonic. Thus inhibition must create the intensity tuning. However, a linear least squares fit of the peak of inhibition versus the peak of excitation yields a correlation coefficient whose square is 0.90, well within the range of a balanced neuron (Wehr and

Zador 2003; Zhang et al 2003). It thus appears that changes in the relative timing of excitation and inhibition account for the intensity-tuning of the membrane potential. This is confirmed by using the synaptic currents to predict the membrane potential. Fig 5G shows example predicted membrane potential traces at 3 intensities; these resemble the actual membrane potential traces at those intensities in Fig. 5A. The graph of peak predicted membrane potential versus intensity shown in Fig. 5H matches the actual curve in Fig. 5B.

Discussion

We have described 5 unbalanced intensity-tuned neurons in the auditory cortex. In some of these synaptic inhibition enhanced the intensity-tuning; in others it even created the intensity-tuning. Since synaptic inhibition is essentially cortical in origin, the latter have provided examples of auditory feature-selectivity arising de novo at the auditory cortex.

We used the peak membrane potential as a gauge of spike rate; the precise relationship between them requires further investigation. Entering the measured synaptic currents into a model Hodgkin-Huxley neuron might give a good estimate of the spike responses of these neurons. A simple approximation to the spike rate generated by a Hodgkin-Huxley neuron is the net synaptic current at the spike threshold; however, it is uncertain if this holds for transient synaptic inputs like those observed here (Koch et al 1995, Wilent and Contreras 2005). Experimentally, this may be addressed by recording the spikes in cell-attached mode before the whole-cell mode is established, or by

removing pharmacological blockers of spiking from the intracellular solution (Borg-Graham et al 1998, Wehr and Zador 2003).

Intensity-tuned neurons are generated by diverse patterns of synaptic inhibition, from the balanced intensity-tuned neurons observed by Wehr and Zador (2003), to the many patterns of unbalanced synaptic excitation and inhibition described here. Perhaps these different patterns occur in different layers or areas of the auditory cortex. In the cat primary auditory cortex, the distribution of inhibitory neurons and inhibitory axon terminals depends on layer and position in the isofrequency contour (Prieto et al 1994a, 1994b). Tones evoke greater synaptic inhibition in layer 3 neurons than in layer 2 neurons (Ojima and Murakami 2002). In the visual cortex, diverse patterns of synaptic excitation and inhibition generate orientation selectivity (Borg-Graham et al 1998, Monier et al 2003); some of these patterns are organized by layer (Martinez et al 2002).

A previous study addressed the role of synaptic inhibition in creating intensity-tuning by using a pharmacological blocker of synaptic inhibition. They found that only 2 of 31 intensity-tuned neurons became monotonic when synaptic inhibition was blocked. However, they also found that 12 of 38 monotonic neurons became intensity tuned when inhibition was blocked. It is not straightforward to fit their data and ours into a single picture. Disrupting inhibition pharmacologically affects the inhibition at all neurons in a network in which there may be complex feedback connections; for a straightforward comparison with our work, inhibition should be disrupted at only a single neuron. Disrupting inhibition pharmacologically also raises the spike rate of all cells, which may produce intensity-tuning via a combination of synaptic and voltage-gated intrinsic

conductances (Sivaramakrishnan et al 2004); in comparison we have examined only synaptic conductances.

As behavioural training can convert balanced, monotonic neurons into intensity-tuned neurons, the question is raised as to whether the new intensity-tuned neurons are balanced or unbalanced, and if they are unbalanced, whether inhibition enhances or creates their intensity-tuning. Extracellular recordings show that training doubles the number of intensity-tuned neurons (Polley et al 2004). If an overwhelming majority of intensity-tuned neurons in trained animals are unbalanced, that would suggest that balanced, monotonic neurons are being converted to unbalanced, intensity-tuned neurons. This would place a severe constraint on models of cortical circuitry, which would have to robustly ensure that monotonic neurons in an untrained animal are balanced, but not so robustly that training cannot undo it. Unfortunately, the small number of neurons in our sample and the heterogeneity of the patterns of synaptic excitation and inhibition observed make it impossible, at the moment, for us to determine the ratio of balanced to unbalanced intensity-tuned neurons in trained animals.

Acknowledgements

This work was supported by the National Institutes of Health.

References

Anderson JS, Carandini M, and Ferster D. Orientation tuning of input conductance, excitation, and inhibition in cat primary visual cortex. J Neurophysiol 84: 909-26, 2000.

Borg-Graham LJ, Monier C, and Fregnac Y. Visual input evokes transient and strong shunting inhibition in visual cortical neurons. Nature 393:369-373, 1998.

Bormann J, Hamill OP, Sakmann B. Mechanism of anion permeation through channels gated by glycine and gamma-aminobutyric acid in mouse cultured spinal neurones. J Physiol 385:243-86, 1987.

Davis KA and Young ED. Pharmacological evidence of inhibitory and disinhibitory neuronal circuits in dorsal cochlear nucleus. J Neurophysiol 83:926-940, 2000.

Davson H and Segal MB. Physiology of the CSF and Blood-Brain Barriers. Boca Raton: CRC Press, 1996.

Ding J and Voigt HF. Intracellular response properties of units in the dorsal cochlear nucleus of unanesthetized decerebrate gerbil. J Neurophysiol 77:2549-2572, 1997.

Ding J, Benson TE, and Voigt HF. Acoustic and current-pulse responses of identified neurons in the dorsal cochlear nucleus of unanesthetized, decerebrate gerbils. J Neurophysiol 82:3434-3457, 1999.

Hirsch JA, Alonso JM, Reid RC, and Martinez LM. Synaptic integration in striate cortical simple cells. J Neurosci 18: 9517-28, 1998.

Johnston D and Wu SM. Foundations of cellular neurophysiology. Cambridge, MA: MIT Press, 1995.

Koch C, Bernander O, and Douglas RJ. Do neurons have a voltage or a current threshold for action potential initiation? J Comput Neurosci 2:63-82, 1995.

Martinez LM, Alonso JM, Reid RC, and Hirsch JA. Laminar processing of stimulus orientation in cat visual cortex. J Physiol 540:321-333, 2002.

McCormick DA, Connors BW, Lighthall JW, and Prince DA. Comparative electrophysiology of pyramidal and sparsely spiny stellate neurons of the neocortex. J Neurophysiol 54:782-806, 1985.

Monier C, Chavane F, Baudot P, Graham LJ, and Fregnac Y. Orientation and direction selectivity of synaptic inputs in visual cortical neurons: a diversity of combinations produces spike tuning. Neuron 37:663-680, 2003.

Ojima H and Murakami K. Intracellular characterization of suppressive responses in supragranular pyramidal neurons of cat primary auditory cortex in vivo. Cereb Cortex 12, 1079-1091, 2002.

Palombi PS and Caspary DM. Physiology of the young adult Fischer 344 rat inferior colliculus: responses to contralateral monaural stimuli. Hear Res 100:41-58, 1996a.

Palombi PS, Caspary DM. Physiology of the aged Fischer 344 rat inferior colliculus: responses to contralateral monaural stimuli. J Neurophysiol 76:3114-3125, 1996b.

Phillips DP and Kelly JB. Coding of tone-pulse amplitude by single neurons in auditory cortex of albino rats (Rattus norvegicus). Hear Res 37:269-279, 1989.

Phillips DP, Orman SS, Musicant AD, and Wilson GF. Neurons in the cat's primary auditory cortex distinguished by their responses to tones and wide-spectrum noise. Hear Res 18:73-86. 1985.

Pollak GK, Marsh DS, Bodenhamer R, and Souther A. A single-unit analysis of inferior colliculus in unanesthetized bats: response patterns and spike-count functions generated by constant-frequency and frequency-modulated sounds. J Neurophysiol 41:677-691, 1978.

Polley DB, Heiser MA, Blake DT, Schreiner CE, and Merzenich MM. Associative learning shapes the neural code for stimulus magnitude in primary auditory cortex. Proc Natl Acad Sci USA 101:16351-6, 2004.

Prieto JJ, Peterson BA, and Winer JA. Morphology and spatial distribution of GABAergic neurons in cat primary auditory cortex (AI). J Comp Neurol 344:349-82, 1994a.

Prieto JJ, Peterson BA, and Winer JA. Laminar distribution and neuronal targets of GABAergic axon terminals in cat primary auditory cortex (AI). J Comp Neurol 344:383-402, 1994b.

Rhode WS and Smith PH. Physiological studies on neurons in the dorsal cochlear nucleus of cat. J Neurophysiol 56:287-307, 1986.

Ryan A and Miller J. Single unit responses in the inferior colliculus of the awake and performing rhesus monkey. Exp Brain Res 32:389-407, 1978.

Sivaramakrishnan S, Sterbing-D'Angelo SJ, Filipovic B, D'Angelo WR, Oliver DL, and Kuwada S. GABA(A) synapses shape neuronal responses to sound intensity in the inferior colliculus. J Neurosci 24:5031-5043, 2004.

Tan AY, Zhang LI, Merzenich MM, and Schreiner CE. Tone-evoked excitatory and inhibitory synaptic conductances of primary auditory cortex neurons. J Neurophysiol 92:630-43,2004.

Troyer TW and Miller KD. Physiological gain leads to high ISI variability in a simple model of a cortical regular spiking cell. Neural Comput 9:971-983, 1997.

Wehr M and Zador AM. Balanced inhibition underlies tuning and sharpens spike timing in auditory cortex. Nature 426:442-446, 2003.

Wilent WB and Contreras D. Dynamics of excitation and inhibition underlying stimulus selectivity in rat somatosensory cortex. Nat Neurosci 8:1364-1370, 2005.

FIG. 1. Unbalanced neuron. A: Average synaptic currents at 2 intensities, at -70 mV (blue) or 0 mV (red). B: Peak average inward (blue) and outward (red) currents versus sound intensity.

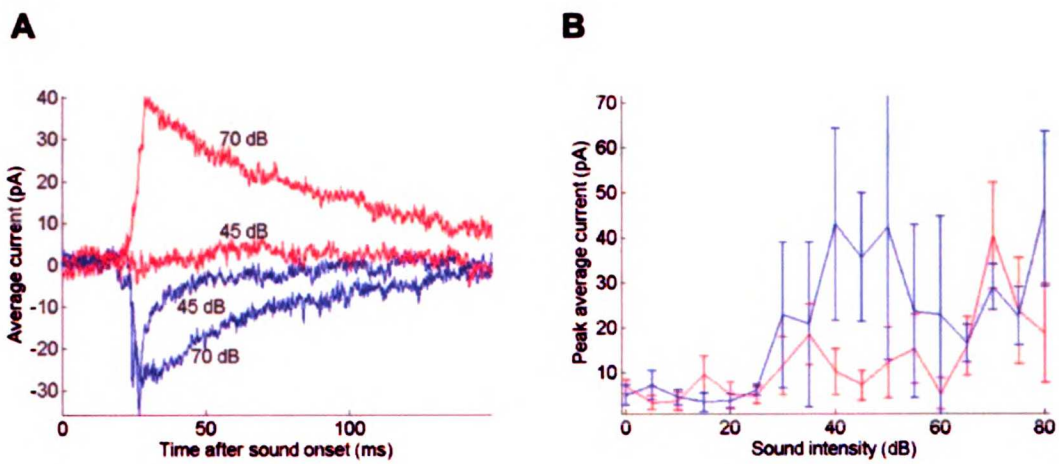
A
B
Average current (pA)
Time after sound onset (ms)
70 dB
45 dB
45 dB
70 dB
Peak average current (pA)
Sound intensity (dB)

Figure 1

FIG. 2. Unbalanced neuron in which inhibition enhances intensity-tuning. A: Average membrane potential responses at 3 intensities. B: Peak average membrane potential versus sound intensity. C: Same as A, but with the membrane potential immediately preceding sound onset subtracted from each trace before averaging. D: Same as B, but with the membrane potential immediately preceding sound onset subtracted from each trace before averaging. E: Average synaptic currents at 2 intensities, at -70 mV (blue) or -30 mV (red). F: Peak average inward (blue) and outward (red) currents versus sound intensity. G: Predicted membrane potential responses at 3 intensities. H: Peak predicted membrane potential versus sound intensity.

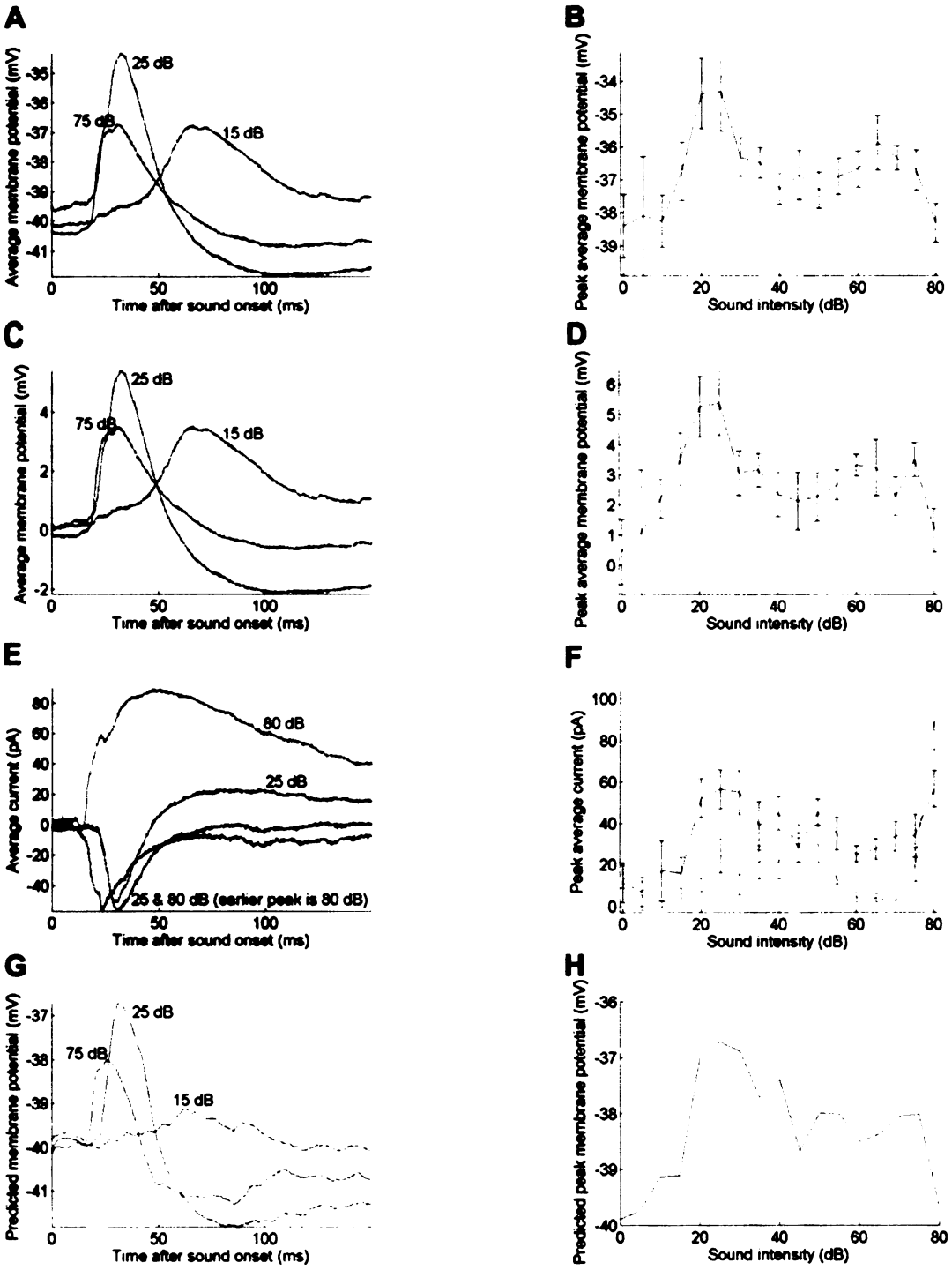
A
Average membrane potential (mV)
25 dB
75 dB
15 dB
Time after sound onset (ms)
B
Peak average membrane potential (mV)
Sound intensity (dB)
C
Average membrane potential (mV)
25 dB
75 dB
15 dB
Time after sound onset (ms)
D
Peak average membrane potential (mV)
Sound intensity (dB)
E
Average current (pA)
80 dB
25 dB
25 & 80 dB (earlier peak is 80 dB)
Time after sound onset (ms)
F
Peak average current (pA)
Sound intensity (dB)
G
Predicted membrane potential (mV)
25 dB
75 dB
15 dB
Time after sound onset (ms)
H
Predicted peak membrane potential (mV)
Sound intensity (dB)

Figure 2

FIG. 3. Unbalanced neuron in which inhibition creates intensity-tuning. A: Average membrane potential responses at 3 intensities. B: Peak average membrane potential versus sound intensity. C: Same as A, but with the membrane potential immediately preceding sound onset subtracted from each trace before averaging. D: Same as B, but with the membrane potential immediately preceding sound onset subtracted from each trace before averaging. E: Average synaptic currents at 2 intensities, at -70 mV (blue) or -20 mV (red). F: Peak average inward (blue) and outward (red) currents versus sound intensity. G: Predicted membrane potential responses at 3 intensities. H: Peak predicted membrane potential versus sound intensity.

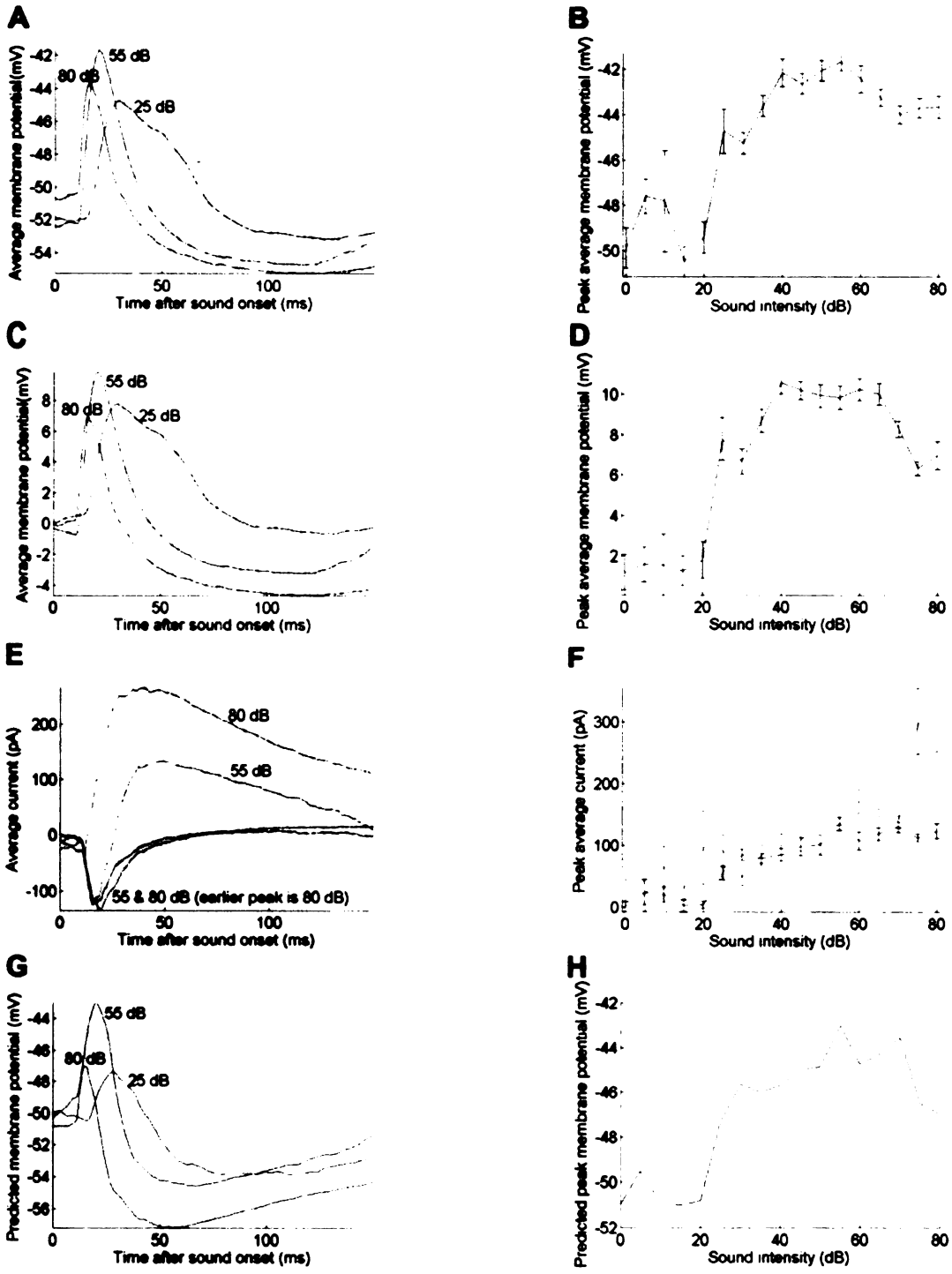
A
Average membrane potential(mV)
55 dB
80 dB
25 dB
Time after sound onset (ms)
B
Peak average membrane potential (mV)
Sound intensity (dB)
C
Average membrane potential(mV)
55 dB
80 dB
25 dB
Time after sound onset (ms)
D
Peak average membrane potential (mV)
Sound intensity (dB)
E
Average current (pA)
80 dB
55 dB
55 & 80 dB (earlier peak is 80 dB)
Time after sound onset (ms)
F
Peak average current (pA)
Sound intensity (dB)
G
Predicted membrane potential (mV)
55 dB
80 dB
25 dB
Time after sound onset (ms)
H
Predicted peak membrane potential (mV)
Sound intensity (dB)

Figure 3

FIG. 4. Unbalanced neuron in which inhibition creates intensity-tuning. A: Average membrane potential responses at 3 intensities. B: Peak average membrane potential versus sound intensity. C: Same as A, but with the membrane potential immediately preceding sound onset subtracted from each trace before averaging. D: Same as B, but with the membrane potential immediately preceding sound onset subtracted from each trace before averaging. E: Average synaptic currents at 2 intensities, at -70 mV (blue) or -30 mV (red). F: Peak average inward (blue) and outward (red) currents versus sound intensity. G: Predicted membrane potential responses at 2 intensities. H: Peak predicted membrane potential versus sound intensity.

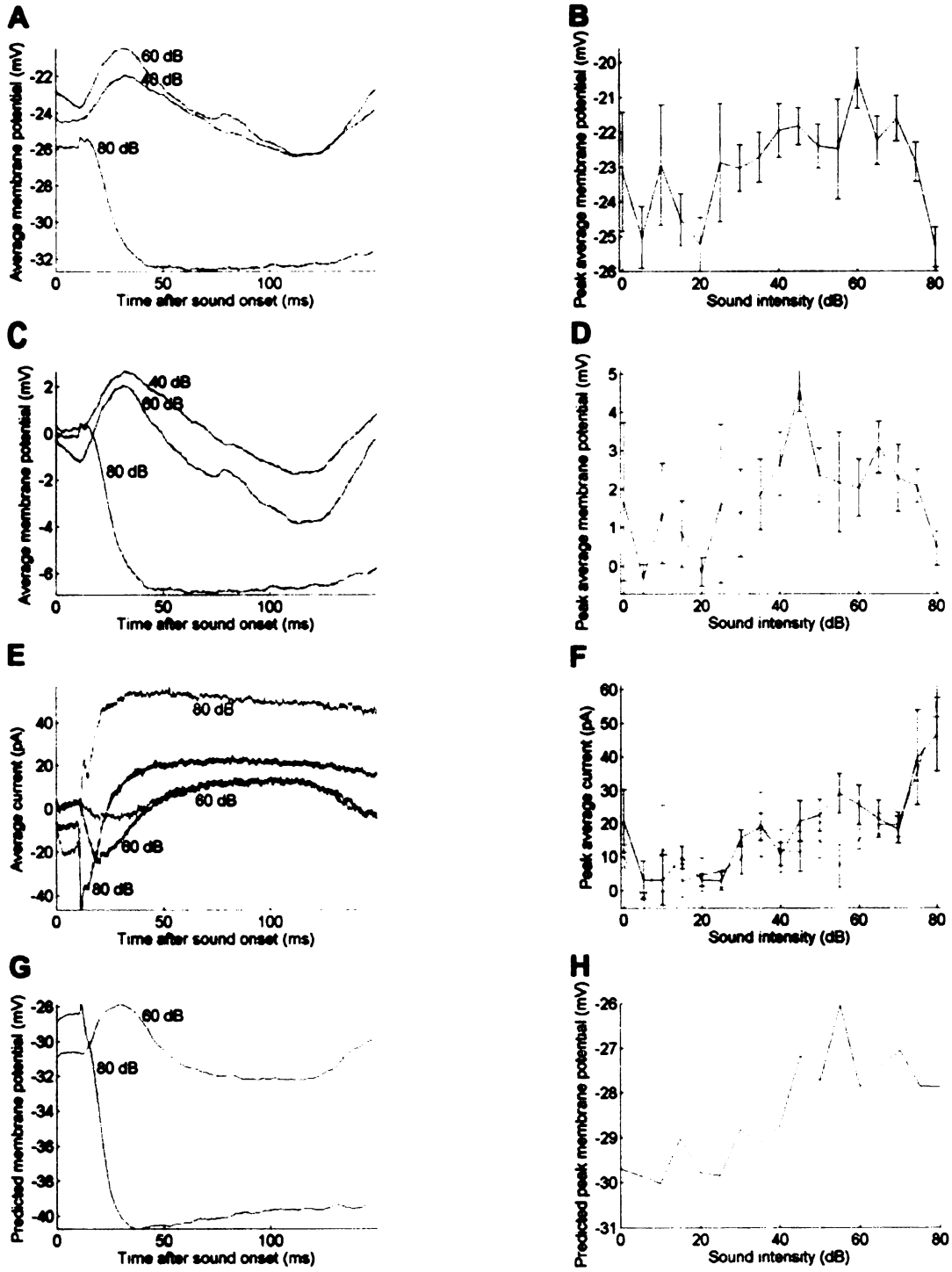
A
Average membrane potential (mV)
60 dB
40 dB
80 dB
Time after sound onset (ms)
B
Peak average membrane potential (mV)
Sound intensity (dB)
C
Average membrane potential (mV)
40 dB
60 dB
80 dB
Time after sound onset (ms)
D
Peak average membrane potential (mV)
Sound intensity (dB)
E
Average current (pA)
80 dB
60 dB
40 dB
80 dB
Time after sound onset (ms)
F
Peak average current (pA)
Sound intensity (dB)
G
Predicted membrane potential (mV)
60 dB
80 dB
Time after sound onset (ms)
H
Predicted peak membrane potential (mV)
Sound intensity (dB)

Figure 4

FIG. 5. Unbalanced neuron in which inhibition creates intensity-tuning. A: Average membrane potential responses at 3 intensities. B: Peak average membrane potential versus sound intensity. C: Same as A, but with the membrane potential immediately preceding sound onset subtracted from each trace before averaging. D: Same as B, but with the membrane potential immediately preceding sound onset subtracted from each trace before averaging. E: Average synaptic currents at 2 intensities, at -70 mV (blue) or 0 mV (red). F: Peak average inward (blue) and outward (red) currents versus sound intensity. G: Predicted membrane potential responses at 2 intensities. H: Peak predicted membrane potential versus sound intensity.

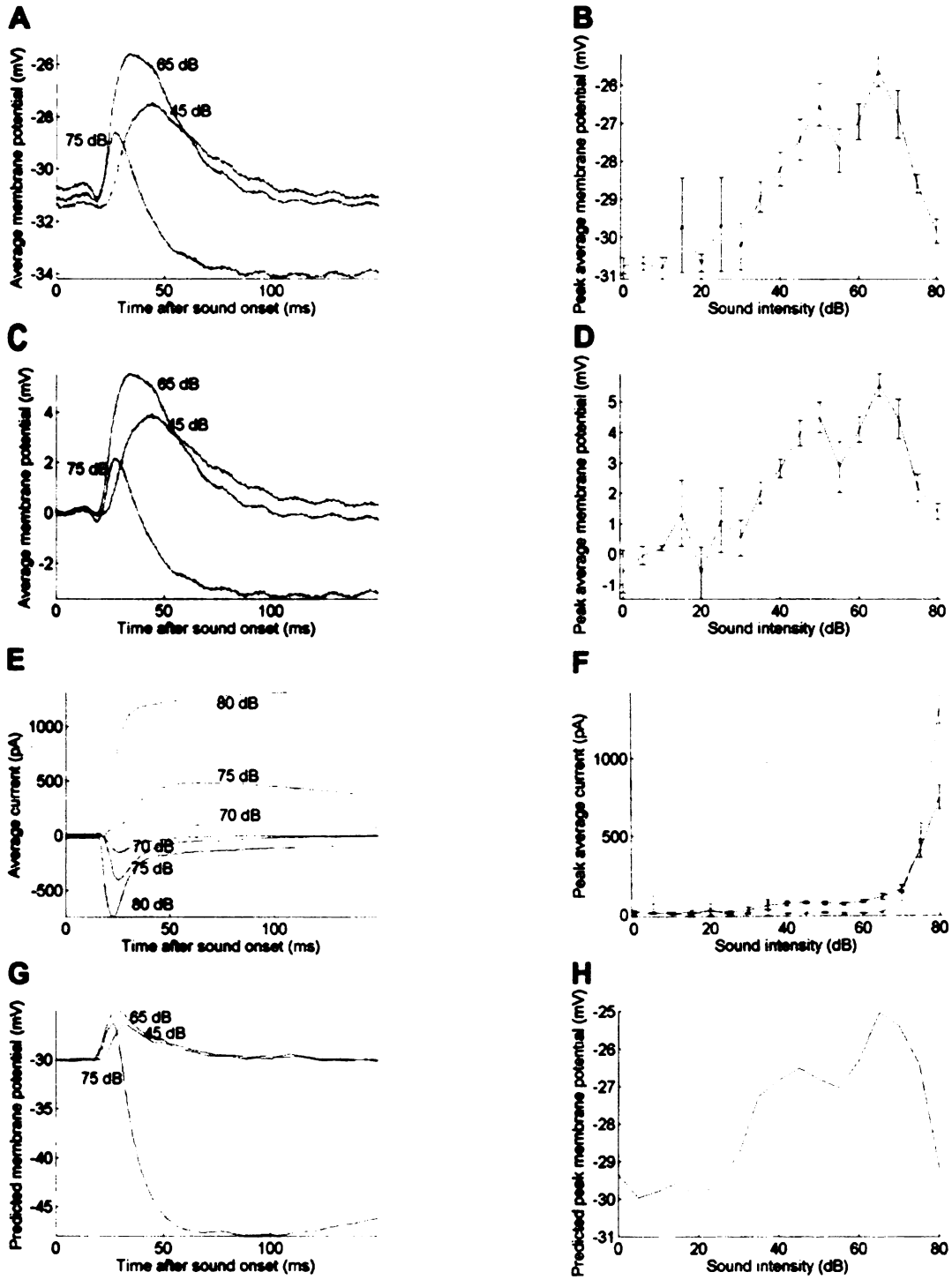
A
Average membrane potential (mV)
65 dB
45 dB
75 dB
Time after sound onset (ms)
B
Peak average membrane potential (mV)
Sound intensity (dB)
C
Average membrane potential (mV)
65 dB
45 dB
75 dB
Time after sound onset (ms)
D
Peak average membrane potential (mV)
Sound intensity (dB)
E
Average current (pA)
80 dB
75 dB
70 dB
70 dB
75 dB
80 dB
Time after sound onset (ms)
F
Peak average current (pA)
Sound intensity (dB)
G
Predicted membrane potential (mV)
65 dB
45 dB
75 dB
Time after sound onset (ms)
H
Predicted peak membrane potential (mV)
Sound intensity (dB)

Figure 5

Chapter 5

Conclusion

Summary

The synaptic excitation and inhibition evoked by tones, frequency sweeps and noise bursts has been described. Synaptic inhibition was shown to contribute to onset-only responses, frequency sweep direction selectivity and intensity-tuning. Because synaptic inhibition is cortical, the shaping and even creation of these selectivities represents cortical processing. At least 4 patterns of synaptic excitation and inhibition were described: balanced monotonic (Chapters 2,3); balanced nonmonotonic; unbalanced, with enhancement of intensity-tuning; and unbalanced, with creation of intensity-tuning (Chapter 4).

Use of a single-compartment model

The intracellular measurements have been interpreted with a single-compartment model. Interpreting the data using such a model would, if it is possible, be most useful for constraining a large-scale computational model of the cortex, as these usually use single-compartment neurons (eg. Ben-Yishai et al 1995; Somers et al 1995). Generally, the complex dendritic pattern of a neuron means that it cannot be described with a single-compartment. Furthermore, there are voltage-dependent channels in the dendrites that could contribute to the membrane potential response (Häusser et al, 2000; Segev and

London 2000; Meunier and Segev 2002). However, for the stimuli we have used, the synaptic currents seem to predict reasonably well the neuron's membrane potential response, justifying the use of single-compartment models.

Comparison with the visual cortex

There are also diverse patterns of excitation and inhibition in the primary visual cortex. In layer 4 of the cat primary visual cortex, sinusoidal gratings evoke synaptic excitation and inhibition share the same orientation tuning, but with opposite temporal phase (Ferster 1986; Hirsch et al 1998; Anderson et al 2000). Other patterns of excitation and inhibition have also been observed (Borg-Graham et al 1998; Monier et al 2003). The different patterns are at least partially organized by cortical layer. In contrast to layer 4, the preferred orientation of synaptic excitation from that of synaptic inhibition by 50° on average in layer 5 (Martinez et al 2002). The patterns also differ systematically in the width of their orientation tuning according to their proximity to a pinwheel in the orientation map (Marino et al 2005). It should be noted that there is no uncontroversial framework which reconciles all the different patterns of synaptic inputs observed in the primary visual cortex (Ferster and Miller 2000; Sompolinsky and Shapley 1997).

Primary visual cortex neurons are also tuned for direction of movement. This is analogous to selectivity for the direction of a frequency sweep along the tonotopic axis. Intracellular experiments have demonstrated that, like neurons of the primary auditory cortex, primary visual cortex neurons have synaptic excitation and inhibition with the same direction selectivity, but with inhibition enhancing the direction selectivity by

suppressing more greatly the excitation of the non-preferred direction (Monier et al 2003; Priebe and Ferster 2005).

Length-tuned neurons of the primary visual cortex provide another interesting comparison. In these neurons, spike rate is nonmonotonic, first increasing, then decreasing with increasing stimulus length. Like the intensity-tuned neurons of the auditory cortex, disproportionally large synaptic inhibition at long stimulus lengths enhances the length-tuning. However, synaptic excitation itself is already length-tuned, and synaptic inhibition does not create length-tuning (Anderson et al 2001).

Implications for circuitry

Balanced synaptic excitation and inhibition suggests a simple feedforward circuit in which the neuron receives monosynaptic thalamic input, and disynaptic inhibition from the same thalamic neurons. But as most of the neurons in this work were obtained at depths corresponding to layers 3 to 5, the data may also indicate that the local circuitry of layer 5 is similar to those of the thalamorecipient layers. That data on both tones and frequency sweeps were obtained from the same neurons, places a further constraint on models of auditory cortex circuitry. The simple feedforward circuit is consistent with the sweep responses could be predicted, at least in part, from the tone responses.

A circuit model should also be able to explain the failure of the tone responses to predict certain aspects of the sweep responses, such as excitation and inhibition each already being direction selective. If neurons of the inferior colliculus also receive balanced synaptic excitation and inhibition with the appropriate temporal and spectral asymmetry to render them direction selective, their direction selectivity would

feedforward and cause the thalamocortical excitation to be direction selective. The direction selectivity of the thalamocortical excitation would not be predicted by its tonal receptive field, because the direction selectivity arises from synaptic inhibition in the inferior colliculus (Tan et al 2004).

Future directions

Although the inhibitory component of auditory cortical processing has been described, the excitatory input measured may be thalamic as well as cortical. Kaur et al (2004) showed that the application of muscimol, an agonist of synaptic inhibition that silences the cortex, caused a narrowing of the frequency tuning of local field potentials in the primary auditory cortex, without changing their latency. Kaur et al (2004) interpreted this as indicating that thalamic excitation is responsible for a neuron's characteristic frequency, while cortical excitation is responsible for its bandwdith. However, local field potentials do not necessarily correspond to the synaptic input onto a single neuron. Testing the interpretation of Kaur et al (2004) would involve recording intracellularly, and comparing the sum of cortical and thalamic excitation that a neuron normally receives, with the thalamic excitation observed when the cortex is silenced. Experiments in the primary visual cortex which used either low temperatures or electrical shock to silence the cortex reversibly, have shown that the orientation tuning of the thalamic excitation onto simple cells is identical to that of its normal membrane potential response (Ferster et al 1996; Chung and Ferster 1998). These experiments demonstrated that the Hubel and Wiesel model of orientation tuning was at least partially right, in contrast to

models which had very broadly tuned thalamic excitation (Hubel and Wiesel 1962; Ben-Yishai et al 1995; Somers et al 1995).

Synaptic depression is an additional mechanism that should be considered in the formation of receptive fields of the primary auditory cortex. Intracellular measurement of the synaptic excitation and inhibition evoked by click trains showed that both synaptic excitation and inhibition decreased with successive clicks. The decrease in excitation was suggested to be the result of thalamocortical depression because thalamic neurons are known to phase-lock to much higher rates than cortical neurons. Synaptic depression may be measured by electrically stimulating the thalamus while recording intracellularly in the cortex (Swadlow and Gusev 2001; Castro-Alamancos 2002; Chung and Nelson 2002; Boudreau and Ferster 2005).

Characterizing synaptic inputs with more complex stimuli would further constrain models of the primary auditory cortex. A particularly interesting set of stimuli are the ripples. These stimuli are spectrotemporally more complex than tones, frequency sweeps and noise bursts, but remain well parameterized. A nonlinear model in which two filters are multiplied was able to describe the spike responses of primary auditory cortex neurons. It was also shown that the nonlinear model could be implemented by thalamic excitation and cortical synaptic inhibition, or by synaptic depression and facilitation, or by a mix of both mechanisms (Elhilali et al 2004). It would therefore be interesting to determine what combination of the two mechanisms is involved in the ripple response.

The ripple should also be useful for examining if different layers of the primary auditory cortex receive different patterns of synaptic input. As the ripple-evoked spike response differs systematically by cortical layer (Ahmed et al 2006), so should the ripple-

evoked synaptic excitation and inhibition. Simple stimuli should not be overlooked in examining laminar differences. Volkov and Galazyuk (1992) found that there are more neurons that fire a sustained tone-evoked response in the deep layers of the cortex. Ojima and Murakami (2002) found that neurons in layer 2 receive less tone-evoked synaptic inhibition than those in layer 3. Perhaps the different patterns of synaptic input underlying intensity-tuning are also organized by layer. This could be tested by filling neurons with biocytin during intracellular recording so that their laminar position can be later identified by staining for biocytin.

Biocytin staining also informs us as whether a neuron has a smooth or spiny morphology; smooth neurons are inhibitory, while spiny neurons are excitatory; the former are spiny while the latter are smooth (Douglas and Martin 1998). However, because inhibitory neurons are rare and have small cell bodies, it is difficult, but possible, to use blind in vivo intracellular recordings to determine their receptive fields (Azouz et al 1997; Hirsch et al 2003). Two-photon microscopy, coupled with ways of making fluorescent genetically-defined populations of neurons, has now made visually targeted patching possible (Margrie et al 2003, Dittgen et al 2004). This should enable the systematic study of the receptive fields of the various sorts of inhibitory interneurons.

In principle, a neuron's synaptic input can be dissected even more finely than just distinguishing thalamic excitation, and cortical excitation and inhibition. Miller et al (2001) have, by paired recordings in the thalamus and the cortex, shown that a thalamic neuron can have a very different receptive field from the cortical neuron it connects to. However, they did not record from all neurons presynaptic to particular neuron. Nor did they demonstrate monosynaptic connectivity unequivocally.

Peterlin et al (2000) have, in slice, recorded from multiple neurons postsynaptic to a particular neuron. They loaded neurons in a cortical slice with a fluorescent calcium indicator. They then patched onto a "trigger" neuron and made it spike by injecting current. By simultaneously imaging the calcium activity in hundreds of neurons in the vicinity of the trigger neuron, they identified tens of postsynaptic neurons that spiked in response to the trigger neuron. Kozloski et al (2001) selectively patched layer 5 corticotectal neurons, used them as trigger neurons, and found that postsynaptic neurons were restricted to a few anatomically and physiologically defined types.

It seems that the corresponding in vivo experiment can now be done. One would load the cortex in vivo with a fluorescent calcium indicator (Stosiek et al 2003), patch a trigger neuron and make it spike by injecting current. With two-photon microscopy to provide single neuron resolution in vivo, not only would the postsynaptic neurons be identified, but their receptive fields obtained (Ohki et al 2005). Limitations of calcium indicators include an ability to indicate neither subthreshold synaptic excitation nor synaptic inhibition, and a much lower temporal resolution than electrical recordings (Smetters et al 1999).

As for a method that might permit the identification of large numbers of presynaptic neurons, one possibility would be the use a fluorescent retrograde virus (DeFalco et al 2001). This would be introduced into a single neuron by a patch pipette while the neuron's receptive field is obtained. One returns two days later and with the help of two-photon microscopy finds all the presynaptic neurons now labelled. The cortex is then loaded with fluorescent calcium indicator and the receptive fields of the

presynaptic neurons obtained after Ohki et al (2005). This method, however, would not determine the strength, nor even the sign of the synaptic connection.

It is now possible to optically stimulate single neurons by expressing optically-activated ion channels in them (Zemelman et al 2002, 2003; Banghart et al 2004; Lima and Miesenbock 2005; Boyden et al 2005). These methods have so far been demonstrated only in oocytes, flies and cultured neurons, but they will probably be implementable in vivo. An ideal experiment would be to express an optically activated ion channel in all neurons of the cortex. The cortex would also be bulk loaded with calcium indicator. One would then patch onto a neuron, and then optically stimulate each of the neurons in the vicinity of the patched neuron. A monosynaptic connection between an optically-stimulated neuron and the patched neuron would be indicated by the detection of excitatory or inhibitory postsynaptic potentials in the patched neuron. The receptive field of each presynaptic neuron would be determined by calcium imaging. The receptive field of the patched, postsynaptic neuron could be determined either by whole-cell recording or by calcium imaging.

In the auditory system, as in the visual system, the cat cortex presents interesting topography that is not present in the rat. In the cat, the width of the frequency tuning of small clusters of neurons changes systematically along the isofrequency contour: there are three broadly-tuned regions and two narrowly-tuned ones; the ventral edge of an isofrequency contour is broad, and broad regions alternate with narrow (Schreiner and Mendelson 1990; Schreiner and Sutter 1992). The central narrowly tuned region was found by retrograde anatomical tracing to receive connections from the dorsal narrowly tuned region lying 1 mm away (Read et al 2001). The narrowly-tuned regions have been

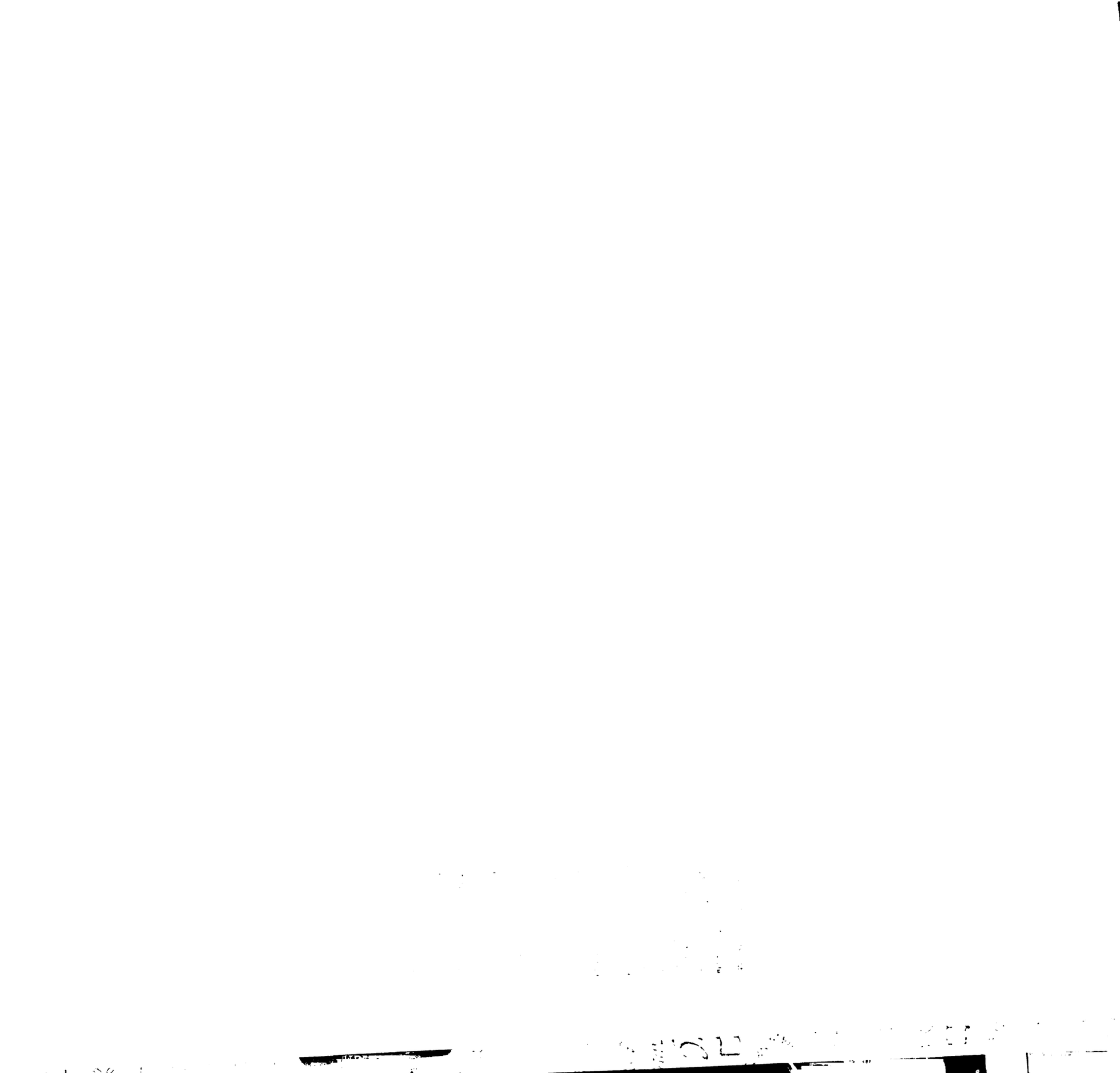

hypothesized to result from stronger lateral synaptic inhibition, which can be tested by intracellular measurements.

Another response pattern present in the cat, but not yet described in the rat, are the off responses in the dorsal zone of the cat auditory cortex. The off responses often exhibit duration selectivity (He et al 1997). Duration-tuned off responses are also found in the inferior colliculus of the bat (Casseday et al 1994). Such responses have been suggested to arise from three stimulus locked synaptic inputs: initial synaptic inhibitin that lasts as long as the sound; a transient synaptic excitation input that marks the sound onset, but with a long latency; and off synaptic excitation. The two excitatory inputs are subthreshold when they occur alone, but for a tone of the right duration, they sum to give a suprathreshold response (Covey et al 1996). This hypothesis can also be tested with intracellular recordings.

Responses in the unanesthetized animal also differ from those in the anesthetized. In the unanesthetized animal, a greater number of neurons give sustained responses to tones; there are also neurons which give onset-only responses, or sustained responses, depending on tone frequency (Brugge and Merzenich 1973; Merzenich and Brugge 1973; Wang et al 2005). Unanesthetized animals therefore present another opportunity for future intracellular work (Margrie et al 2002, Brecht et al 2004).

References

Ahmed B, Garcia-Lazaro JA, and Schnupp JW. Response Linearity in Primary Auditory Cortex of the Ferret. J Physiol Feb 23, 2006; DOI: 10.1113/jphysiol.2005.104380v1.

Anderson JS, Lampl I, Gillespie DC, and Ferster D. Membrane potential and conductance changes underlying length tuning of cells in cat primary visual cortex. J Neurosci 21:2104-2112, 2001.

Anderson JS, Carandini M, Ferster D. Orientation tuning of input conductance, excitation, and inhibition in cat primary visual cortex. J Neurophysiol 84:909-926, 2000.

Azouz R, Gray CM, Nowak LG, and McCormick DA. Physiological properties of inhibitory interneurons in cat striate cortex. Cereb. Cortex 7:534-545, 1997.

Banghart M, Borges K, Isacoff E, Trauner D, and Kramer RH. Light-activated ion channels for remote control of neuronal firing. Nat Neurosci 7:1381-1386, 2004.

Ben-Yishai R, Bar-Or RL, and Sompolinsky H. Theory of orientation tuning in visual cortex. Proc Natl Acad Sci USA 92:3844-3848, 1995.

Boudreau CE and Ferster D. Short-term depression in thalamocortical synapses of cat primary visual cortex. J Neurosci 25:7179-7190, 2005.

Borg-Graham LJ, Monier C, Fregnac Y. Visual input evokes transient and strong shunting inhibition in visual cortical neurons. Nature 393:369-373, 1998.

Boyden ES, Zhang F, Bamberg E, Nagel G, and Deisseroth K. Millisecond-timescale, genetically targeted optical control of neural activity. Nat Neurosci 8:1263-1268, 2005.

Brecht M, Schneider M, Sakmann B, and Margrie TW. Whisker movements evoked by stimulation of single pyramidal cells in rat motor cortex. Nature 427:704-710, 2004.

Brugge JF and Merzenich MM. Responses of neurons in auditory cortex of the macaque monkey to monaural and binaural stimulation. J Neurophysiol 36:1138-1158, 1973.

Casseday JH, Ehrlich D, and Covey E. Neural tuning for sound duration: role of inhibitory mechanisms in the inferior colliculus. Science 264:847-850, 1994.

Castro-Alamancos MA. Different temporal processing of sensory inputs in the rat thalamus during quiescent and information processing states in vivo. J Physiol 539:567-78, 2002.

Chung S and Ferster D. Strength and orientation tuning of the thalamic input to simple cells revealed by electrically evoked cortical suppression. Neuron 20:1177-1189, 1998.

Chung S, Li X and Nelson SB. Short-term depression at thalamocortical synapses contributes to rapid adaptation of cortical sensory responses in vivo. Neuron 34:437-446, 2002.

Covey E, Kauer JA, and Casseday JH. Whole-cell patch-clamp recording reveals subthreshold sound-evoked postsynaptic currents in the inferior colliculus of awake bats. J Neurosci 16:3009-3018, 1996.

DeFalco J, Tomishima M, Liu H, Zhao C, Cai X, Marth JD, Enquist L, and Friedman JM. Virus-assisted mapping of neural inputs to a feeding center in the hypothalamus. Science 291:2608-13, 2001.

Dittgen T, Nimmerjahn A, Komai S, Licznerski P, Waters J, Margrie TW, Helmchen F, Denk W, Brecht M, and Osten P. Lentivirus-based genetic manipulations of cortical neurons and their optical and electrophysiological monitoring in vivo. Proc Natl Acad Sci USA 101:18206-18211, 2004.

Douglas R and Martin K. Neocortex. In: The synaptic organization of the brain, edited by Shepherd GM. New York: Oxford University Press, 1998.

Elhilali M, Fritz JB, Klein DJ, Simon JZ, and Shamma SA. Dynamics of precise spike timing in primary auditory cortex. J Neurosci 24:1159-1172, 2004.

Ferster D. Orientation selectivity of synaptic potentials in neurons of cat primary visual cortex. J Neurosci 6:1284-1301, 1986.

Ferster D, Chung S, Wheat H. Orientation selectivity of thalamic input to simple cells of cat visual cortex. Nature 380:249-252, 1996.

Ferster D and Miller KD. Neural mechanisms of orientation selectivity in the visual cortex. Annu Rev Neurosci 23:441-471, 2000.

Häusser M, Spruston N, and Stuart GJ. Diversity and dynamics of dendritic signaling. Science 290:739-44, 2000.

He J, Hashikawa T, Ojima H, and Kinouchi Y. Temporal integration and duration tuning in the dorsal zone of cat auditory cortex. J Neurosci 17:2615-2625, 1997.

Hirsch JA, Alonso JM, Reid RC, and Martinez LM. Synaptic integration in striate cortical simple cells. J Neurosci 18:9517-9528, 1998.

Hirsch JA, Martinez LM, Pillai C, Alonso JM, Wang Q, and Sommer FT. Functionally distinct inhibitory neurons at the first stage of visual cortical processing. Nat Neurosci 6:1300-1308, 2003.

Hubel DH and Wiesel TN. Receptive fields, binocular interaction and functional architecture in the cat's visual cortex. J Physiol 160:106-54, 1962.

Kaur S, Lazar R, and Metherate R. Intracortical pathways determine breadth of subthreshold frequency receptive fields in primary auditory cortex. J Neurophysiol 91:2551-2567, 2004.

Lima SQ and Miesenbock G. Remote control of behavior through genetically targeted photostimulation of neurons. Cell 121:141-152, 2005.

Marino J, Schummers J, Lyon DC, Schwabe L, Beck O, Wiesing P, Obermayer K, Sur M. Invariant computations in local cortical networks with balanced excitation and inhibition. Nat Neurosci 8:194-201, 2005.

Margrie TW, Meyer AH, Caputi A, Monyer H, Hasan MT, Schaefer AT, Denk W, Brecht M. Targeted whole-cell recordings in the mammalian brain in vivo. Neuron 39:911-918, 2003.

Martinez LM, Alonso JM, Reid RC, Hirsch JA. Laminar processing of stimulus orientation in cat visual cortex. J Physiol 540:321-333, 2002.

Merzenich MM and Brugge JF. Representation of the cochlear partition of the superior temporal plane of the macaque monkey. Brain Res 50:275-296, 1973.

Schreiner CE and Mendelson JR. Functional topography of cat primary auditory cortex: distribution of integrated excitation. J Neurophysiol 64:1442-1459, 1990.

Margrie TW, Brecht M, and Sakmann B. In vivo, low-resistance, whole-cell recordings from neurons in the anaesthetized and awake mammalian brain. Pflugers Arch 444:491-498, 2002.

Meunier C and Segev I. Playing the devil's advocate: is the Hodgkin-Huxley model useful? Trends Neurosci 25:558-63, 2002.

Miller LM, Escabi MA, Read HL, and Schreiner CE. Functional convergence of response properties in the auditory thalamocortical system. Neuron 32:151-160, 2001.

Monier C, Chavane F, Baudot P, Graham LJ, and Fregnac Y. Orientation and direction selectivity of synaptic inputs in visual cortical neurons: a diversity of combinations produces spike tuning. Neuron 37:663-680, 2003.

Ohki K, Chung S, Ch'ng YH, Kara P, and Reid RC. Functional imaging with cellular resolution reveals precise micro-architecture in visual cortex. Nature 433:597-603, 2005.

Peterlin ZA, Kozloski J, Mao BQ, Tsiola A, and Yuste R. Optical probing of neuronal circuits with calcium indicators. Proc Natl Acad Sci USA 97:3619-3624, 2000.

Priebe NJ and Ferster D. Direction selectivity of excitation and inhibition in simple cells of the cat primary visual cortex. Neuron 45:133-145, 2005.

Read HL, Winer JA, and Schreiner CE. Modular organization of intrinsic connections associated with spectral tuning in cat auditory cortex. Proc Natl Acad Sci USA 98:8042-8047, 2001.

Schreiner CE, Sutter ML. Topography of excitatory bandwidth in cat primary auditory cortex: single-neuron versus multiple-neuron recordings. J Neurophysiol 68:1487-1502, 1992.

Schummers J, Marino J, and Sur M. Synaptic integration by V1 neurons depends on location within the orientation map. Neuron 36:969-978, 2002.

Segev I and London M. Untangling dendrites with quantitative models. Science 290:744-50, 2000.

Smetters D, Majewska A, Yuste R. Detecting action potentials in neuronal populations with calcium imaging. Methods 18:215-221, 1999.

Somers DC, Nelson SB, and Sur M. An emergent model of orientation selectivity in cat visual cortical simple cells. J Neurosci 15:5448-5465, 1995.

Sompolinsky H and Shapley R. New perspectives on the mechanisms for orientation selectivity. Curr Opin Neurobiol 7:514-522, 1997.

Stosiek C, Garaschuk O, Holthoff K, and Konnerth A. In vivo two-photon calcium imaging of neuronal networks. Proc Natl Acad Sci USA 100:7319-7324, 2003.

Swadlow HA and Gusev AG. The impact of 'bursting' thalamic impulses at a neocortical synapse. Nat Neurosci 4:402-408, 2001.

Sutter ML and Schreiner CE. Physiology and topography of neurons with multipeaked tuning curves in cat primary auditory cortex. J Neurophysiol 65:1207-1226, 1991.

Tan AYY, Atencio CA, Heiser MA, Teng C, Zhang LI, and Schreiner CE. Spectrotemporal receptive fields, static and dynamic nonlinearities in a frequency sweep direction selective network. Program No. 529.11. 2004 Abstract Viewer/Itinerary Planner. Washington, DC: Society for Neuroscience, 2004. Online.

Troyer TW, Krukowski AE, Priebe NJ, and Miller KD. Contrast-invariant orientation tuning in cat visual cortex: thalamocortical input tuning and correlation-based intracortical connectivity. J Neurosci 18:5908-5927, 1998.

Volkov IO and Galazyuk AV. Peculiarities of inhibition in cat auditory cortex neurons evoked by tonal stimuli of various durations. Exp Brain Res 91:115-120, 1992.

Wang X, Lu T, Snider RK, Liang L. Sustained firing in auditory cortex evoked by preferred stimuli. Nature 435:341-346, 2005.

Wehr M and Zador AM. Synaptic mechanisms of forward suppression in rat auditory cortex. Neuron 47:437-445, 2005.

Zemelman BV, Lee GA, Ng M, and Miesenbock G. Selective photostimulation of genetically chARGed neurons. Neuron 33:15-22, 2002.

Zemelman BV, Nesnas N, Lee GA, and Miesenbock G. Photochemical gating of heterologous ion channels: remote control over genetically designated populations of neurons. Proc Natl Acad Sci USA 100:1352-1357, 2003.